LIGHT SCATTERING STUDIES ON THE PATTERN OF THE SELF-ASSOCIATION OF BILE ACID SALTS

by

Yunik Chang

A dissertation submitted to the faculty of the
University of Utah in partial fulfillment of the requirements
for the degree of

Doctor of Philosophy

in

Pharmacy

Department of Applied Pharmaceutical Sciences

University of Utah

March 1977

UNIVERSITY OF UTAH GRADUATE SCHOOL

SUPERVISORY COMMITTEE APPROVAL

of a dissertation submitted by

Yunik Ch ng

I have read this dissertation and have found it to be of satisfactory quality for a doctoral degree.

Date

J.R. Cardinal, Ph.D.
Chairman, Supervisory Committee

I have read this dissertation and have found it to be of satisfactory quality for a doctoral degree.

2/18/77
Date

S.W. Kim, Ph.D.
Member, Supervisory Committee

I have read this dissertation and have found it to be of satisfactory quality for a doctoral degree.

'77
Date

R.V. Petersen, Ph.D.
Member, Supervisory Committee

I have read this dissertation and have found it to be of satisfactory quality for a doctoral degree.

Date

Member, Supervisory Committee

I have read this dissertation and have found it to be of satisfactory quality for a

Date

F.W. Ph.D.
Member, Supervisory Committee

THE UNIVERSITY OF UTAH GRADUATE SCHOOL

FINAL READING APPROVAL

To the Graduate Council of The University of Utah:

I have read the dissertation of Yunik Chang in its final form and have found that (1) its format, citations, and bibliographic style are consistent and acceptable; (2) its illustrative materials including figures, tables, and charts are in place; and (3) the final manuscript is satisfactory to the Supervisory Committee and is ready for submission to the Graduate School.

2/18/77
Date

J.R. Cardinal, Ph.D.
Member, Supervisory Committee

Approved for the Major Department

R.V. Petersen, Ph.D.
Chairman/Dean

Approved for the Graduate Council

ABSTRACT

This thesis is concerned with the study of the nature of self-association of the trihydroxy and dihydroxy bile salts in aqueous electrolyte solutions. Most often the pattern of this association has been described by using a monomer-micellar model borrowed from flexible chain surfactants. One of the characteristics of this model is the existence of the critical micelle concentration (CMC). Based on this model, it is assumed that there is no higher aggregate in the dilute concentrations somewhat below the CMC.

Utilizing the light scattering technique, the turbidity as a function of concentration was obtained for sodium cholate, sodium taurocholate and sodium glycocholate over the concentration range from 0-25 mg/ml. For the bile salt sodium cholate, the concentration of the supporting electrolyte, NaCl, was varied over the range from 0-0.5 M. For sodium glycocholate, the turbidity was determined in 0.15 M NaF, NaCl, and NaI and for sodium cholate and sodium taurocholate the turbidity was determined in the above systems plus NaBr.

Comparison of the light scattering data with the monomer-micelle equilibrium model shows qualitative agreement; however, quantitative agreement cannot be achieved. Further examination of the data has shown that the light scattering

results are in excellent agreement with a model which includes dimers, trimers and a higher aggregate containing an average of about 8 monomeric units.

For the dihydroxy bile salts, the turbidity as a function of concentrations was determined for sodium deoxycholate, sodium taurodeoxycholate and sodium glycodeoxycholate over the concentration range from 0-20 mg/ml. For sodium deoxycholate, the turbidity was obtained in 0.15 M NaCl. On comparison of the light scattering data obtained from these dihydroxy bile salts with the monomer-micelle model, qualitative agreement was again obtained; however, quantitative disagreement with this model is more significant than that observed in the trihydroxy bile salts. Qualitative as well as quantitative agreement with the experimental results was obtained for the above systems utilizing a model which assumes the existence of dimers, trimers, tetramers and a much higher aggregate. The average aggregation number for the higher aggregate was found to be 25 for sodium taurocholate, while values of 17.6 and 18 were found for sodium deoxycholate and sodium glycodeoxycholate.

From the study of the ionic strength effects on the self-association of sodium cholate, an increasing tendency in the values of the association constants for the small oligomers and in the aggregation numbers for the high aggregates was indicated. However, this effect is hard to confirm from the present results.

For the purpose of comparison of the model for the trihydroxy bile salts obtained from the light scattering results, the equilibrium solubility of naphthalene in 0.15 M NaCl was determined.

Based on the analysis, the light scattering results show excellent agreement with the naphthalene solubility data. This is a further proof of the validity of the model obtained from the light scattering results for the self-association of the trihydroxy bile salts.

ACKNOWLEDGEMENTS

Of the many individuals who have contributed to this work, I would especially like to acknowledge the following:

Dr. Sung Wan Kim, for his constant encouragement throughout my graduate career;

Mr. Stephen Kuwahara, for his technical assistance in the naphthalene solubility measurement;

Dr. John R. Cardinal, for his sincere interest in my development as a scientist and in my research project;

My wife, Unhee Chang, for her patience and constant encouragement throughout my graduate career;

The University of Utah Research Committee and the Utah Heart Association who have provided financial support, for which acknowledgement is gratefully made.

TABLE OF CONTENTS

LIST OF FIGURES

LIST OF TABLES

I. INTRODUCTION

Surfactant molecules in aqueous solution self-associate to form large spherical aggregates called micelles. The micelle is made up of perhaps 50 surfactant monomers arranged in such a fashion that the hydrocarbon chains are directed towards the center or core of the micelles. The core is effectively an oil droplet which is capable of solubilizing water insoluble species. This phenomena is utilized daily by everyone whenever surfactants such as soaps, detergents, etc., are used for the purpose of cleaning. Such surfacant actions are also important in the human today. The molecules primarily responsible for this are the bile salts (1).

Bile salts are produced by the liver and stored in the gall bladder. In terms of molecular structure, bile salts are kinked steroid nuclei possessing two or three hydrophilic hydroxyl groups on one side and a charged ionic group at one end of the molecule. The opposite side of the nucleus is hydrophobic.

The bile salts have important actions in regulation of cholesterol biosynthesis in the liver and in the small intestine. The bile salts also play an important role in the regulation of electrolytes and water transport in the large intestine and possibly the small intestine (2). These actions are not directly related to the surfacant properties of the bile salts. However, several important physiological actions are a direct consequence of these

surfactant properties. One of these actions is to facilitate fat absorption. Dietary triglycerides are hydrolyzed to 2-monoglycerides and fatty acids by pancreate lipase (3). These lipolytic products are insoluble or poorly soluble in water, but are readily solubilized by bile salts (4,5). The bile salts disperse lipolytic products into a homogeneous aqueous phase by the formation of a bile salt-fatty acid mixed micelle which enhances the absorption of the fatty acids by the mucosal cell (6).

Bile salts also play an important role in the solubilization of cholesterol. Cholesterol is virtually water insoluble. Large amounts of cholesterol are found in normal bile, approximately 500 mg per 100 ml of bile, which far exceeds its molecular solubility (7). For many years, it was thought that bile salts were responsible for solubilizing this cholesterol. However, it is now well known that the solubility of cholesterol in pure bile salt solutions is very low. During the last 15 years it has been shown conclusively that cholesterol is solubilized by bile salt-lecithin mixed micelles (8,9). The solubilization capacity of the bile salt lecithin micelle for cholesterol is limited. Under certain pathological conditions, this solubilization capacity can be exceeded which may eventually lead to cholesterol gallstone formation (7,10). In the United States over 15 million people have cholesterol gallstones, of which over one third are surgically removed, leading to total medical expenses of about $1 billion per year (11). Because of this, a great deal of effort has been directed toward

understanding the mechanism by which cholesterol is solubilized in the bile.

The above physiologically important actions of the bile salts have been well known for many years, but the physico-chemical properties of the bile salt-lecithin or bile salt-fatty acid mixed micelle are not well understood. However, it is clear that the formation of mixed micelles of bile salt with fatty acid and/or lecithin becomes possible due to the surfactant properties of bile salts. Since the surfacant properties are directly related to the physico-chemical properties of bile salts, much work has been done in this area. One question of particular interest has been the nature of the self-association of the bile salts in aqueous solution. It seems essential that this question be understood before a complete picture of the more complex mixed systems can be developed.

A. Review of Different Patterns of Self-Association

Previous investigators of the self-association of the bile salts have argued that the nature of this association is similar to that of normal long chain surfactants (12). Others have argued against this hypothesis in favor of other mechanisms of association. It seems appropriate, therefore, to review briefly the properties of typical long-chain surfactant molecules in aqueous solution. By way of contrast the pattern of the association of molecules which have markedly different molecular structures will be presented.

1. Self-association of Typical Long-Chain Hydrocarbon Surfacants

Surfactants are amphipathic molecules containing a hydrophobic hydrocarbon chain and hydrophylic polar head group at the end of the molecule. The hydrocarbon chain contains 8-18 carbon atoms and is flexible. The polar head group may be ionic, nonionic or zwitterionic. The molecular weight of the surfactant monomer is usually in the range of 100 to 500 (13). These molecules in aqueous solution form large aggregates called micelles. The association of monomers into a micelle is reversible. The micelle is usually composed of 20 - 100 monomer units (13). It is usually spherical but it may be rod-like when it is large. The hydrocarbon chains form the center or core of the spherical micelle while the polar head groups are located at the surface. Since the core of the micelle is made up mainly of hydrocarbon chains, micelles are capable of solubilizing many water-insoluble but oil-soluble species.

The surfactant concentration at which micellization begins is called the critical micelle concentration (CMC). The transition from monomers to micelles occurs over a narrow range of surfactant concentration rather than at a single concentration (13). Because of this, a plot of a certain physical property as a function of surfactant concentration usually shows a sharp change of slope around the CMC. The CMC is obtained by extrapolation of the pre-CMC and post-CMC branches of the curve (13). The CMC derived from the extrapolation will depend to a limited extent on the method of extrapolation; however, these variations are usually small. For example,

if the solubility of a slightly soluble dye is utilized to obtain an estimate of the CMC as was done by Williams, et al. (14), the variation in the CMC depending on the method of extrapolation is only about 1.5%.

Below the CMC the surfactant molecules seem to behave as unassociated monomers. Evidence has been suggested, however, that some dimerization of the surfactant ions may occur. This suggestion was made by Mukerjee, et al. (15) based on the analysis of the conductivity of dilute solutions of sodium lauryl sulfate (NaLS). These authors have shown that the equivalent conductance of dilute solutions of NaLS is very much greater than expected based on the limiting Onsager theory.(15). This deviation is in the opposite direction to that expected for simple ion-pair formation in the system. The value obtained for the dimerization constant was in the range of $1.0 - 3.5 \times 10^2$, which suggests that the dimerization of the lauryl sulfate anions is pronounced below the CMC. Mukerjee (13) also investigated the effects of chain length on the dimerization of fatty acids. For this purpose, he utilized the equilibrium partition data of Goodman (16) who had measured the partition of several long-chain fatty acids between water and n-heptane. From the above investigation, Mukerjee has shown that the dimerization constant increases from about 40 for decanoate to about 1.3×10^7 for stearate. The high values obtained for the C_{16} and C_{18} fatty acids would suggest that they are almost completely dimerized at concentrations as low as 10^{-6} M (13). In view of the significant dimerization of these surfacants below the CMC, it is curious to note that little

evidence is found for trimerization (13). This is probably due to the increased charge repulsion and the decreased hydrophobic effects in the trimer (13).

In much of the early literature in the micelle area it was argued that the concentration of the monomer above the CMC was constant (17). This argument was based on the assumption that micellization was represented as a phase separation. If the above assumption is correct, then the CMC should be a precise point. However, it has now been well established by several methods (15, 18) that distinct curvature exists in the CMC region. The degree of curvature increases as the aggregation number of the micelle decreases (21). One of the major objectives of the above work was to show that micellization is, in fact, best represented by the law of mass action. This point is now well accepted (13, 20). One implication of the law of mass action is that the monomer concentration must increase above the CMC. This phenomena has been shown conclusively by Mysels, et al. (19, 20) based on equilibrium dialysis and surface tension experiments. The extent to which the monomer concentration increases with increases in total concentration depends upon the aggregation number of micelles. Mukerjee (21) has shown this fact clearly by model calculations on ideal uncharged micellar systems which have aggregation numbers of 100 and 20. Based on the above calculations, he indicated that the increase in monomer concentration above the CMC is negligible with respect to the increase in total concentration in the case of aggregation number of 100, while it is

significant if the aggregation number is 20. This implies that the contribution of a varying monomer concentration to the total concentration above the CMC must be taken into account when the micellar aggregation number is much smaller than 20.

The net forces responsible for micelle formation arise from the hydrophobic attraction and polar group repulsion. The hydrophobic force results from a favorable entropy change upon the transfer of a surfactant monomer from the aqueous phase to the micelle (22). Forces opposing micelle formation arise from electrostatic repulsive forces between the ionic head groups at the micellar surface for the case of ionic surfactants (23). In the case of nonionic surfactants, the repulsive forces arise from the self interactions of the hydrophilic head groups of the monomers at the micellar surface (13). Consequently, micelle formation is the result of a balance between hydrophobic and polar interactions.

2. Self Association of Aromatic Ring Compounds

In contrast to the micellar association of hydrocarbon surfactants, some aromatic ring compounds are capable of a "stacking" type association (21). One such molecule which undergoes a stacking type association is methylene blue. Methylene blue has a planar aromatic ring structure. Because of this, the molecule is roughly symmetrical with respect to the hydrophobicity on both sides of the flat structure. The cationic charge is dispersed in the molecule through resonance. The molecules, therefore, do not possess a particularly polar or non-polar end. These molecular characteristics

allow methylene blue to associate by stacking interactions as a result of face to face association (24-27). Mukerjee and Ghosh (24) have discussed in detail the self-association of methylene blue and suggested that cooperative interactions occur in the early stages of association. Thus, in spite of the greater charge repulsion involved in the trimer, the formation of trimer was suggested to be more favorable than dimer formation due to increased hydrophobic interactions. As the result of this, the contribution of low aggregates to the total concentration in the stacking type of association becomes important. In addition, the increase in monomer concentration with increases in the total concentration is significant. Mukerjee and Ghosh also suggested that high association constants in the self association of methylene blue decrease in a mild sequence, which is in agreement with the expected build-up of the charge repulsion. However, it was indicated that the decrease in the association constants was not very large.

As the compounds possessing similar characteristics to methylene blue, the derivatives of pyrimidine and purine can be examples. Broom, et al. (56) and Plesiewica, et al. (57) investigated the nature of self association of these molecules utilizing osmometry and showed that these molecules associate by a continuous stepwise fashion with all association constants being equal. More detailed analysis of the equilibrium and of the differences between the various association constants of the type done by Mukerjee and Ghosh (24) is not possible in these systems due to the limitations of the method.

Another type of molecule which undergoes self-association is the rigid but non-planar aromatic ring compounds like the phenothiazine derivatives. In this molecule the ring structure is kinked due to the lack of aromaticity in the central ring. A charge group is located on the side chain of the molecule. The association arises from the interaction between the concave side of one molecule and the convex side of the other. The cationic charged groups would be arranged in such a fashion as to minimize the charge repulsive interactions. The dimers in this configuration still have a concave and convex side open for further association. Therefore, this self-association pattern can continue indefinitely (21). Florence and Parfitt (28, 29) have studied the self-association of these molecules utilizing N.M.R. In the plots obtained from the chemical shifts of various identifiable protons as a function of reciprocal concentration, a break at a certain concentration could be identified in each of these plots. This break was interpreted to indicate the existence of a CMC which led these authors to suggest that the pattern of the self-association of the phenothiazines was best represented by a monomer-micelle equilibrium model. However, in a recent article, Mukerjee (21) has argued that breaks suggesting the existence of a CMC can be found even in a continuous stepwise association system. Thus, the mere existence of a break in the plots made by Florence and Parfitt (28, 29) is not sufficient evidence to suggest the monomer-micellar model. Further evidence against this model for the association of the phenothiazines was presented by Cardinal (30). He argued that

the degree of curvature of the plots varies depending on the identifiable proton used in the plot. As an example, the results for promethazine HCl were considered. The plot of chemical shifts due to the aromatic protons versus reciprocal concentration shows marked curvature throughout the concentration range while the plot of chemical shifts due to $N\text{-}CH_3$ or $C\text{-}CH_3$ protons versus reciprocal concentration shows fairly sharp breaks over a narrow range of concentrations. Cardinal (30) indicated that interpretation of the shifts for the $N\text{-}CH_3$ and $C\text{-}CH_3$ is made more difficult because of the observed change in the degree of dissociation of the amine function as the concentration increases. Thus, the shifts due to the aromatic protons may be more reliable. However, these shifts as a function of reciprocal concentration show marked curvature throughout the concentration range studied. Based on the above arguments, Cardinal also indicated that the results obtained by Florence and Parfitt (28, 29) would appear to be insufficient to discriminate between the micellar model and the stepwise association model.

Finally, another type of molecular structure which can undergo self-association are the diphenyl methane derivatives. Diphenyl methane derivatives contain two aromatic phenyl rings and polar chain groups. These molecules are aromatic but non-planar and flexible. Attwood and Udeala (31, 32) studied the self-association of these compounds. From this study, they suggested that the diphenyl methane derivatives form micelles as in the case of long-chain hydrocarbon surfactants even if the molecules contain aromatic rings. In support of this model, these authors suggested that the

rotational motion of the diphenyl rings around the central carbon atom hinders the stacking type of interactions between the molecules.

Attwood and Udeala (33, 34) also studied the self-association of pyridine derivatibes. Most of the pyridine derivatives contain an aromatic phenyl ring and a polar side chain as well as the pyridine nucleus. From this study, they suggested that some derivatives form micelles while others aggregate by a stepwise association process. The reasons for the different mode of aggregation of these compounds was not clearly stated. However, they indicated that the difficulty in differentiating the systems between micellar and stepwise self-association arises from the low aggregation number of the system.

From the above discussions, it is clear that the pattern of self-association can be different depending on the molecular structure of solute. When the molecules possess rigid aromatic rings, and they are roughly symmetrical with respect to the hydrophobicity on both sides of the rings, the stacking type of association between these molecules is possible. On the other hand, if the molecules possess flexible hydrocarbon chains and the hydrophobic and hydrophilic portions in the molecule are well separated, typical micellar association is favored.

In the molecular structure of bile salts, one side of the molecule includes hydrophilic hydroxyl groups while the opposite side is hydrophobic due to hydrocarbon rings. It is not symmetrical with

respect to the hydrophobicity. Also, these molecules are inflexible and non-planar. The molecular structure of bile salts, therefore, belongs to neither of the above classes.

B. General Background of the Nature of Self-Association of Bile Salts

1. Molecular Structure of Bile Salts

Bile salts are derivatives of cholanic acid. Cholanic acid is a cyclopentenophenanthrene nucleus containing 24 carbon atoms as shown in the following figure. The A and B ring juncture of the steroid nucleus has a 5β-hydrogen, which causes the steroid nucleus to be kinked rather than flat at this juncture. The cross section of the nucleus is about 6 or 7 $\mathring{A}$ at the narrowest and widest diameters. This gives a cross sectional area of 42 $\mathring{A}^2$ (figured as a rectangle) 38.6 $\mathring{A}^2$ (figured as a circle with a radius of 3.5 $\mathring{A}$) (12). This length corresponds to the conjugated bile salts. The length of unconjugated bile salts is about 18 $\mathring{A}$. Then, the area of longitudinal sections of cholanic acid becomes about 108 $\mathring{A}$ (figured as a rectangle). Ekwall, et al. (35, 36) have measured the area of surface monolayer of cholanic acid in 3M NaCl solution and suggested that the maximum surface area per molecule lying flat on the surface is about 190 $\mathring{A}^2$ and the maximum is about 105 $\mathring{A}^2$.

Cholic acid (Mw = 408.56) has three alpha hydroxyl groups at the 3.7 and 12 positions of the steroid nucleus (3α, 7α, 12α - trihydroxy - 5β-cholanic acid). The distance between each of the three hydroxy groups measured by Stuart-Breigleb Model, is about 5 $\mathring{A}$. They form a rough triangle on one side of the steroid nucleus.

This side and the charged carboxylate group at one end of the molecule are the hydrophilic portions of the structure. The opposite side of the nucleus is hydrophobic.

Deoxycholic acid (M_W = 392.56) has two hydroxyl groups at the 3α and 12α positions (3α, 12α-dihydroxy-5β-cholanic acid).

Bile salts in human bile are usually conjugated with glycine or taurine by peptide bonds at the carboxylate side chain of the steroid nucleus. The pKa value of free cholic acid is about 5 while the pKa of glycine conjugate is about 4 and the pKa of taurine conjugate is about 1.9 (12).

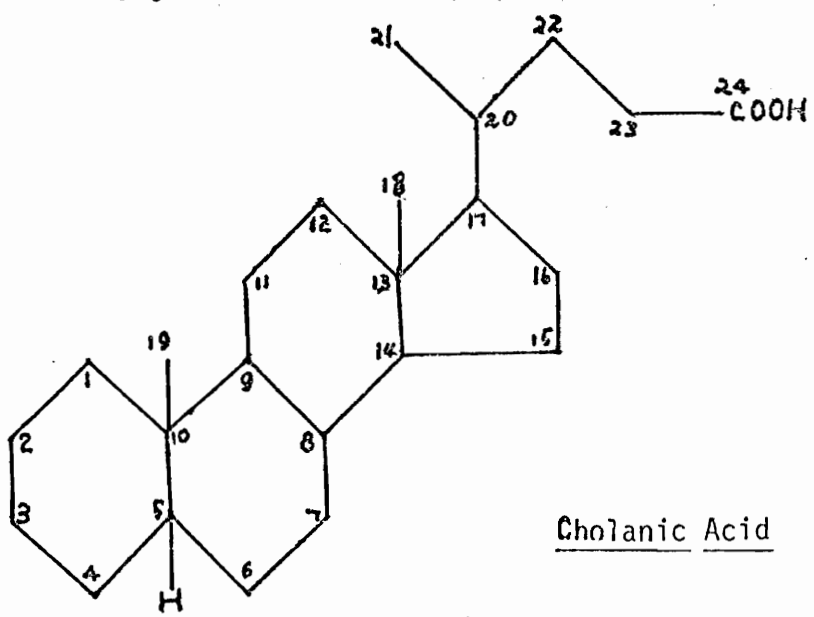

Cholanic Acid

2. Review of Previous Work

One of the pioneering works was that of Roepke and Mason who measured the equivalent conductance and the osmotic coefficient as a function of bile salt concentration (37). From this study, they suggested that the bile salts form typical micelles. This suggestion was based on comparison of some similarities between the curves obtained for the bile salts and those obtained for typical

long-chain surfactants. Since their suggestion, many workers have studied the nature of bile salt self-association utilizing various techniques like light scattering (38-43), solubilization (4, 44-48), viscosity (49), N.M.R. (50 - 51), surface tension (39), x-ray scattering (52), ultracentrifugation (38), as well as conductivity (49), and osmotic coefficient measurements (53). Most of the previous workers have interpreted the nature of the self-association of the bile salts as a monomer-micelle equilibrium model. However, remarkable variations occur in the CMC values obtained by different workers: for example, reported CMC values of sodium taurocholate in 0.15 M NaCl at 20° - 25°C, pH 9±1 vary from 2.7 mM/l (47) to 7.3 mM/l (43). These variations in the CMC may arise from experimental errors. More possibly, the variations may result from the different methods or concentration ranges used in the extrapolation to estimate the CMC. This fact has already been indicated by Mukerjee and Cardinal (44) who suggested that CMC values differing by at least a factor of two could be obtained from the same data depending only on the range of concentrations used in the extrapolation. In the case of typical micellar systems like sodium lauryl sulfate, due to the abrupt monomer-micellar transition (14) such variations are less than 1 or 2%.

Similar variations have also been found in the aggregation number. For example, the aggregation numbers of sodium glycocholate under the same conditions were found to be 19.4 (38) and 26.0 (40).

Carey and Small (48) and Small (38) studied the effects of bile salt structure, counter ion concentration and temperature on the size of aggregates. They suggested that the aggregation number

of trihydroxy bile salts is less than 10 while dihydroxy bile salts form small aggregates at low concentrations and large aggregates at higher concentrations. It was also suggested that the conjugated bile salts behave in a way similar to their unconjugated homologs. The aggregation number was suggested to increase with the increase in the counter ion concentration. The size of aggregates was shown to be affected little by temperatures between 4° - 36°C., when the aggregation number is less than 10. However, the size of aggregates of dihydroxy bile salts having aggregation numbers greater than 10 was suggested to decrease with an increase in temperature.

In contrast to the monodispersed micellar assumption, Ekwall, Fontell and Sten (54) and Fontell (42, 47, 49, 52, 55) argued that the nature of bile salt self-association must be a concentration limit system, that is, the size of aggregates changes in a stepwise fashion as a function of concentration. They suggested three concentration limits for trihydroxy bile salts and another three for dihydroxy bile salts. These concentration limits seem to be independent of conjugation of the bile salts. They indicated that there is no association below the first concentration limit and the aggregates are small between the first and second limits and somewhat large between the second and the third limits. Above the third limit, the aggregates were suggested to be of colloidal dimensions. Vitello (43) argued against the concentration limit theory based on the results obtained by light scattering techniques. He suggested that the CMC is well defined and the slope above this concentration remains constant beyond the concentration identified as the second limit in Fontell's work.

Recently, Cardinal and Mukerjee (44) discussed the nature of self-association of sodium cholate in the absence of added electrolyte. They determined the variation in the solubility of naphthalene as a function of the total concentration of bile salts. Naphthalene is practically insoluble in water. The solubility was shown to increase in a very smooth fashion with the increase in the sodium cholate concentration. From this study, they indicated that the nature of association of bile salts is neither a monomer-micelle nor the concentration limit model. However, their conclusion was that the model of bile salt self-association should include monomer, dimer, and high oligomers.

3. Aim and Scope of This Research

Many workers have investigated the nature of self-association of bile salts in aqueous solution. Most of the previous works suggested that the nature of bile salt self association follows a monomer-micelle equilibrium model. On the other hand, some authors suggested different models such as a stepwise association and a system containing dimer and high oligomers.

It was the aim of this research to test the above models based on the analysis of the variation in turbidity as a function of bile salt concentration obtained by the light scattering technique.

For the analysis of the light scattering data, it was the hope to make a comparison between the experimental values and the results obtained by calculation according to the above models.

II. EXPERIMENTAL

A. Materials

Sodium chloride (J. T. Baker Co.), sodium bromide (J. T. Baker Co.), and sodium iodide (Mallincrodt), were all used as received. Sodium fluoride (Fischer Scientific Co.) was dissolved in deionized water, filtered through a 0.22μ millipore filter (Millipore Co.) and recrystallized. Deionized water was prepared by passing the laboratory distilled water through an ion-exchange column (Corning-Model LD-2a). This water was double distilled from an all-glass distillation system before use. Cholic acid (J. T. Baker Co.) was purified by the method of Hofmann (58). Deoxycholic acid (Aldrich Chemical Co.) was purified by the method of Sobotka, et al. (59). Sodium cholate and sodium deoxycholate were prepared by neutralizing the acids with sodium hydroxide (J. T. Baker Co.) to pH 10.0 $\pm$ 0.2. Sodium glycocholate, sodium taurocholate, sodium taurodeoxycholate and sodium glycodeoxycholate were all synthesized according to the method of Lack, et al. (60).

All the prepared bile salts were dried in the vacuum oven at 40 $\pm$ 2°C until constant weight was obtained. The existence of other bile salts as an impurity was checked by a thin layer chromatographic method (61) using about a 100 μgm spot.

Glycine and taurine contamination in conjugated bile salts was also checked by the same chromatographic procedure, except ninhydrin was utilized for development. All the bile salts studied showed no indication of impurities by the above tests. Naphthalene (J. T. Baker Co.) was used for the solubility measurement.

B. Apparatus

All turbidity measurements were made with the Light Scattering Photometer (The Virtis Co. Model BP-2000) at incident light wavelength 436 nm. The photometer output was measured on a Digimeter Model DMR-300 (Phoenix Precision Instrument Co.).

The refractive index was measured by a Brice-Phoenix Differential Refractometer Model BP-2000-V (The Virtis Co.) at 25 $\pm$ 0.1°C. The light scattering cell for the turbidity measurements was a small semioctagonal type (The Virtis Co., Cat. No. T-105) requiring 10 ml of sample. The cell was splashed with freshly condensed acetone in a device similar to the one described by Shipmann and Farber (62). The pH of the sample solutions was measured with a Digital 110 Expanded Scale pH Meter (Corning Co.), equipped with a Corning Series 500 Combination pH electrode (Cat. No. 476110). A U.V. Spectrophotometer (Gilford Model 240) was used for naphthelene solubility measurements.

C. Measurements

1. Calibration of Light Scattering Photometer

The light scattering instrument calibration was performed by the method of Huisman (18) using double distilled, deionized water

filtered through a 0.22μm millipore filter. The literature turbidity value for water, 4.79×10^{-5}, at 436 nm obtained by Huisman (18) was accepted as a standard. The apparatus constant L_{436} has been calculated by Equation (1):

$$L_{436} = \frac{4.79 \times 10^{-5}}{1.34^2 \times F \left(\frac{G_{90}}{G_0}\right)} \qquad (1)$$

where G_{90}/G_0 is the ratio of galvanometer deflections when viewing scattered radiation at 90° to that for the transmitted radiation at 0°. 1.34 is the refractive index for water, and F is the transmittance of the combination of neutral filters used to determine the scattering ratio. In order to confirm the calibration constant, the turbidities of carbon tetrachloride and benzene were measured. The values obtained were 2.502×10^{-4} for carbon tetrachloride and 7.710×10^{-4} for benzene. These values are in agreement with the literature values of carbon tetrachloride (2.497×10^{-4} - 2.508×10^{-4}) (63) and benzene (7.790×10^{-4}) (64). The calibration constant was checked at the beginning of each set of experiments.

2. Sample Preparation for Turbidity Measurement

The sample cell was cleaned with potassium dichromate cleaning solution and rinsed thoroughly with distilled water. Finally the cell was splashed with freshly condensed acetone in the cell cleaning apparatus (62). The pH of the sample solution was adjusted to 10.0 ± 0.2 with NaOH. The major difficulty in preparing the sample for light scattering measurement was to remove dust particles from

the solution. The methods employed for the removal of particulate matter from solutions such as repeat filtration or ultracentrifugation provided largely scattered values which are not adequate for the purpose of this investigation. It was found, however, that the following procedure yields better particulate free solutions than other methods. A syringe was filled with 50 ml of the solution for measurement. Approximately 25 ml of this solution was filtered through a millipore filter (0.22 μm pore diameter), and saved for future use; then without removing the applied pressure, the final portion of the solution was filtered directly into the light scattering cell. Using this technique, scattering ratios which are reproducible within the ability to read the galvanometer deflection are obtained. This is true for both repeat measurements of the same sample and for successive portions of a sample of a given concentration.

3. Refractive Index Measurement

The differential refractometer was calibrated with sodium chloride or potassium chloride at 25 $\pm$ 0.1°C. The refractive index of each sample solution was followed by turbidity measurement of the sample.

4. Dissymmetry and Depolarization Measurements

When the particles in solution are larger than about one-tenth of the wavelength of the incident light, scattering will not be symmetrical about 90° due to the geometry of the particles. In this event, the scattered light intensity should be corrected for

this dissymmetry. The main purpose of dissymmetry measurement for our sample solution is to check the clarification of the sample solution. The dissymmetry ratio (45°/135°) Z, was measured for each sample solution by Equation (2)*.

$$Z = \frac{i^{45°}_{\text{solution}} - i^{45°}_{\text{solvent}}}{i^{135}_{\text{solution}} - i^{135}_{\text{solvent}}} \qquad (2)$$

where i is the scattered intensity from solution and solvent at the specified direction.

When the particles in solution are anisotropic, a correction must be made to the turbidity for the depolarization arising from the anisotropic property. The depolarization ρ_μ is defined by Equation (3).

$$\rho_u = (i^h_{\text{solution}} - i^h_{\text{solvent}})/(i^v_{\text{solution}} - i^v_{\text{solvent}}) \qquad (3)$$

where i^v and i^h are the scattered intensity of the vertical and horizontal component of the light from solution and solvent when the incident light beam is unpolarized. The final correction factor for total turbidity, so called Cabannes Correction, is $(6+6\rho_\mu)/(6-7\rho_\mu)$. The correction factor for our system was found to be unity, which means that the depolarization effect on our system is negligible.

* Taken from Virtis Co., Manual OM-2000.

5. Fluorescence Measurement

When appreciable fluorescence is present in the scattering solution, turbidity will be too high due to the intensity of fluorescence. Fluorescence from our system was found to be negligible utilizing the small auxiliary filter (The Virtis Co.-Cat. No. K-CF-343).

6. Turbidity Measurement

Turbidity measurements at 90° were done from the higher concentration to the lower by the dilution method. The light scattering cell was placed at the same place on the cell table reproducibly by using four polymer plugs having the same width. Whenever a new sample solution is made, the reproducibility of the measurement was checked with the previous measurement. Very low concentrations of solution were made independently. After all the measurements of a set of experiments, the reproducibility of our data was checked with a few extra measurements.

7. Naphthalene Solubility Measurement

The highest concentration of sodium cholate stock solution was made with 0.15 M- NaCl. The pH of this stock solution was adjusted to 10 $\pm$ 0.1 with NaOH. The different concentrations of sodium cholate solution were made by volumetric dilution of the stock solution. About 5 ml of each sample solution was placed in a 2 dram vial to which an excess of naphthalene crystals was added. These vials were capped and sealed with parafilm and rotated in a water bath at 25 $\pm$ 0.1°C for three days. Then, an appropriate

volume was withdrawn from each vial with a pipet whose tip had been covered with glass wool to filter excess crystals of naphthalene remaining in the solution. These solutions containing solubilized naphthalene were quickly diluted with distilled water to obtain reasonable naphthalene concentrations for U.V. measurements at the wavelength of 276 nm. The solubilized naphthalene concentration was measured according to the Beer's law plot. In order to measure the extinction coefficient of naphthalene, a 2.64^{-2}M solution of naphthalene in methanol was made. 10 ml of this solution was diluted to 1000 ml with 0.15M-NaCl, which gives the naphthalene concentration of 2.64×10^{-4}M. With this concentration, the molar extiction coefficient of naphthalene was obtained by dilution as 4.96×10^{3}. This value is in agreement with the values in the literature (44).

III. METHOD FOR THE ANALYSIS OF LIGHT SCATTERING DATA

The light scattered by small uncharged particles is measured as the Rayleigh ratio (R_θ) given by Equation (4).

$$R_\theta = \frac{i_\theta r^2}{I_o} \tag{4}$$

where I_o is the intensity of the unpolarized incident beam, i_θ is the scattered intensity per unit volume at angle θ, and r is the distance between the medium and the photomultiplier tube. Usually, the Rayleigh ratio is measured in the 90° direction. The Rayleigh ratio (R_{90}) and the turbidity, τ, in the case of unpolarized light and small isotropic particles are related by Equation (5).

$$\tau = \frac{16\pi}{3} R_{90} \tag{5}$$

The turbidity of a solution arises from inhomogeneities in the refractive index of the system due to the random motion of the particles and is dependent on the small scale density and concentration fluctuations (65). For the measurement of molecular weight of colloidal particles in a two component system containing a solute and a pure solvent, Debye derived the equation (6).

$$\frac{Hc}{\tau-\tau_o} = \frac{1}{M} + 2Bc \tag{6}$$

where

$$H = \frac{32\Pi^3 n^2 (\partial n/\partial c)^2}{3\lambda^4 N_o},$$

τ and τ_o are the turbidity of solution and solvent respectively. M is the molecular weight of the particle, B is the second virial coefficient, c is the concentration in gm/ml of the colloidal particle, n is the refractive index, $(\partial n/\partial c)$ is the refractive index increment, λ is the wavelength of incident light and N_o is Avogadro's number. From the intercept of plot $[Hc/(\tau-\tau_o)]$ versus c, the molecular weight of colloidal particle can be obtained.

Equation (6) is not directly applicable to micellar systems because of the presence of unassociated monomeric units and charge effects. In the following section, the mathematical treatment of light scattering data based on the micellar model will be discussed. This discussion is followed by the treatment of light scattering data based on the stepwise association model.

A. Monomer-Micelle Equilibrium Model

In a micellar system, the monomer concentration is assumed to increase linearly up to the CMC. Above the CMC it is assumed to be nearly constant and equal to the CMC. Based on this assumption, Equation (6) can be modified as Equation (7), which considers the presence of unassociated monomeric units and for the existence of a CMC.

$$\frac{H(c-c_o)}{\tau - \tau_o} = \frac{1}{M} + 2B\,(c-c_o) \qquad (7)$$

where τ_o is the turbidity at the CMC which is taken as c_o.

When the solution is a three component system containing charged micelles and a supporting electrolyte, Equation (7) is not applicable due to the negative adsorption of co-ions. The necessary corrections have been developed by Vrij and Overbeek (66). In the above three component systems, there will be an attractive force between the charged micelles and the counter ions as well as a repulsive force between the charged micelle and the co-ions. As a result of these interactions, excess counter ions adsorb on micelle and fluctuate with the micelle while the co-ions are repelled from the micelle. Because of this negative adsorption, the molecular weight of the micelle obtained by Equation (7) is not a true molecular weight but rather an apparent molecular weight. In order to obtain the true micellar molecular weight corrected for the effects due to the negative adsorption of co-ions, Vrij and Overbeek derived Equation (8).

$$\frac{H'(c-c_o)}{\tau-\tau_o} = \frac{1}{M} + 2B(c-c_o) \qquad (8)$$

where

$$H' = H \frac{(\partial n/\partial c_1)^2_{\mu_s}}{(\partial n/\partial c_1)^2_{c_2}}$$

c_1 and c_2 are the concentration of solute and supporting electrolyte, M is the true molecular weight of the micelle, B is the second virial coefficient, $(\partial n/\partial c_1)_{\mu_s}$ is the refractive index increment of solute at constant chemical potential of the supporting electrolyte,

and $(\partial n/\partial c_1)_{\mu_s}$ is the refractive index increment of solute at constant electrolyte concentration. For comparison purposes, Equation (7) can be rewritten as Equation (9).

$$\frac{H(c-c_o)}{\tau-\tau_o} = \frac{1}{M^*} + 2B^*(c-c_o) \tag{9}$$

where M* and B* are the apparent molecular weight and apparent second virial coefficient of the micelle in a supporting electrolyte solution. From the comparison between Equation (8) and (9), it can be seen that the only difference between the true and the apparent values arises from the difference between H' and H.

In order to solve the relationship between H' and H, Vrij and Overbeek (66) developed Equation (10), which is similar to the equation used by Ooi (67) in the discussion of the adsorption from a mixed solvent to uncharged polymers.

$$(\partial_n/\partial c_1)_{\mu_s} = (\partial n/\partial c_1)_{c_2}\left[1 + \frac{(\partial n/\partial c_2)_{c_1}}{(\partial n/\partial c_1)_{c_2}}, (\partial c_2/\partial c_1)_{\mu_s}\right] \tag{10}$$

where $(\partial n/\partial c_2)_{c_1}$ is the refractive increment of supporting electrolytes at constant solute concentration. By comparing Equation (10) with Equation (8), H' is related to H by Equation (11).

$$H' = H\cdot\left[1 + \frac{(\partial n/\partial c_2)_{c_1}}{(\partial n/\partial c_1)_{c_2}}\cdot(\partial c_2/\partial c_1)_{\mu_s}\right]^2 \tag{11}$$

From Equations (8), (9), and (11), the apparent values are related to the true values by Equations (12) and (13).

$$M^* = M\left[1 + \frac{(\partial n/\partial c_2)_{c_1}}{(\partial n/\partial c_1)_{c_2}} \cdot (\partial c_2/\partial c_1)_{\mu_s}\right]^2 \tag{12}$$

$$B^* = B\left[1 + \frac{(\partial n/\partial c_2)_{c_1}}{(\partial n/\partial c_1)_{c_2}} \cdot (\partial c_2/\partial c_1)_{\mu_s}\right]^{-2} \tag{13}$$

The quantities of M* and B* for the micelle in different sodium halide solutions can be determined from a Debye plot based on Equation (9). The values of $(\partial n/\partial c_1)_{c_2}$ for all sodium halide solutions are equal within experimental error. Then, under the assumption that the negative adsorption $(\partial c_2/\partial c_1)_{\mu_s}$ of supporting electrolytes on the micelle is independent on a change in co-ions, the plots of $\sqrt{M^*}$ versus $(\partial n/\partial c_2)_{c_1}$ and $\frac{1}{\sqrt{B^*}}$ versus $(\partial n/\partial c_2)_{c_1}$ can be made. From the intercepts of the plots, $\frac{1}{\sqrt{B^*}}$, the true molecular weight, M, and the true second virial coefficient, B, of the micelle can be obtained. The aggregation number of micelles are obtained from the molecular weight of micelle.

In order to determine the degree of agreement between the experimental values and the results obtained by calculations based on the described models, a method for the calculation of the turbidity as a function of concentration is necessary. Based on the above analysis, this method will be discussed.

As mentioned previously, a micellar system is an equilibrium state between the monomers and the micelles. According to the law of mass action, the equilibrium between monomeric units and micelles can be represented by Equation (14).

$$n[A_1] \underset{}{\overset{K_m}{\rightleftharpoons}} [c_m] \tag{14}$$

where $[A_1]$ is the monomer concentration and $[c_m]$ is the concentration of micelle containing n monomers. The corresponding equilibrium constant, K_m, is represented as Equation (15).

$$K_m = \frac{[c_m]}{[A_1]^n} \tag{15}$$

In the above equation, it is assumed that the activity coefficient of monomer and micelle are constant. Also, the above equation is ideal in the sense that counter-ion terms in the equilibrium expression are neglected. However, these terms become part of the equilibrium constant in the present study since the concentration of the counter ions is effectively constant. Based on Equations (14) and (15), the total concentration, c_T, and the total turbidity, τ_T, of the micellar system are represented by Equations (16) and (17).

$$c_T = [A_1] + nK_m [A_1]^n \tag{16}$$

$$\tau_T = \tau_o + \tau_{mo} + \tau_{mic} \tag{17}$$

where τ_o, τ_{mo} and τ_{mic} are the turbidity due to solvent, monomer and micelle. Debye (68) assumed that τ_o for a pure solvent arises from the density fluctuations of the solvent. Later, Vrij and Overbeek (66) proved that for τ_o in electrolyte solutions, the electrolytes can be regarded as a part of solvent. Also, they showed that the contribution of the solvent and electrolyte to the total turbidity is the same regardless of the presence of colloidal particles. At a certain total concentration, the value of K_m can be obtained by using the CMC as $[A_1]$ and the aggregation number, n. Practically, K_m is obtained by fitting the experimental curve at a given c_T. Then, by Equation (16) the total concentration for any monomer concentration can be calculated.

In the calculation of total turbidity, it is necessary to add up the measured τ_o with the values of τ_{mo} and τ_{mic} which are calculated according to Equations (18) and (19).

$$\frac{Hc_i}{\tau_i} = \frac{1}{M_i} \tag{18}$$

$$\frac{Hc_{mic}}{\tau_{mic}} = \frac{1}{M_{mic}} + 2Bc_{mic} \tag{19}$$

where τ_i is the turbidity due to i-mer, c_i and c_{mic} are the concentrations of the i-mer and the micelle and M_i and M_{mic} are the molecular weights of i-mer and micelle. As can be seen from Equation (18), the turbidity due to monomer is calculated assuming the second virial coefficient, B, to be zero, which seems to be reasonable for the low concentration of solute in electrolyte solutions.

B. Stepwise Association Model

One of the characteristics of a typical micelle-forming system is that the first detectable aggregates (micelle) above the CMC may be already quite large. This implies that the intermediate species have little stability.

In contrast to the micellar system, the stability of the intermediate sized aggregates in stepwise association system is significant. Therefore, the contribution of these low aggregates to the total concentration is significant. The simplest association is dimerization, as shown in Equation (20).

$$2\,A_1 \underset{}{\overset{K_2}{\rightleftharpoons}} A_2 \qquad (20)$$

$$K_2 = \frac{[A_2]}{[A_1]^2}$$

where A_1 is the monomer, A_2 is the dimer and K_2 is the association constant for the dimer. As stepwise association continues, larger multimers form.

$$\begin{aligned} A_2 + A_1 &\overset{K_3}{\rightleftharpoons} A_3 \\ A_3 + A_1 &\overset{K_4}{\rightleftharpoons} A_4 \\ &\vdots \\ A_{n-1} + A_1 &\overset{K_n}{\rightleftharpoons} A_n \end{aligned} \qquad (21)$$

where A_3, A_4, and A_n are the concentrations of trimer, tetramer

and n-mer, and K_3, K_4, and K_n are the association constant values for the trimer, tetramer and n-mer. Based on the above equations, the total concentration c_T and total turbidity τ_T can be represented by Equations (22) and (23).

$$c_T = A_1 + 2A_2 + 3A_3 + \cdots nA_n$$
$$= A_1 + 2K_2[A_1]^2 + 3K_2 \cdot K_3 \cdot [A_1]^3 + \cdots n \prod_{i=2}^{n} K_i[A_1]^n \qquad (22)$$

$$\tau_T = \tau_o + \tau_{mo} + \tau_{di} + \tau_{tri} + \cdots \tau_n \qquad (23)$$

where $\tau_o, \tau_{mo}, \tau_{di}, \tau_{tri}, \tau_n$ are the turbidity due to solvent, monomer, dimer, trimer and n-mer. If all association constant values are the same, the total concentration can be expressed as Equation (24).

$$c_T = nK_i^{n-1} [A_1]^n \qquad (24)$$

For the analysis of the system, the method developed by Steiner (69) will be utilized. This method has been used by Attwood, et al. (31-34) in the investigation of the self association of various antihistamines. In this method, the weight average molecular weight, M_w, is related to weight concentration, c(gm/ml) by Equation (25).

$$\frac{M}{M_w} = 1 + \frac{d \ln x}{d \ln c} \qquad (25)$$

where x is the weight fraction of compound of molecular weight, M, existing as the monomer. Consequently,

$$\ln x = \int_0^c [(M/M_w) - 1] d \ln c$$

or

$$\ln x = \int_0^c \left[\frac{(M/M_w) - 1}{c}\right] dc \qquad (26)$$

M_w can be obtained by Equation (18). From the graphical integration of the plot of $\frac{(M/M_w)-1}{c}$ versus c, x can be obtained at any concentration, c. Based on the values of x at certain concentrations, the equilibrium constants, K_i, can be estimated by Equation (27).

$$\left[(\frac{M_w}{xM} - 1)/ \frac{xc}{M}\right] = 4K_2 + 9K_2 \cdot K_3 \cdot (\frac{xc}{M}) + \cdots n^2\left(\prod_{i=2}^{n} K_i\right) (\frac{xc}{M})^{n-2} \qquad (27)$$

K_2 and K_3 can be obtained from the intercept and limiting slope of plot $\left[(\frac{M_w}{xM} - 1)/ (\frac{xc}{M})\right]$ versus $(\frac{xc}{M})$. The value of K_4 can be found from the slope of the plot of

$$\left[(\frac{M_w}{xM} - 1)/ (\frac{xc}{M})^2\right] - \left[\frac{4K_2}{(\frac{xc}{M})}\right] \text{ versus } (\frac{xc}{M}) .$$

In a similar manner, high equilibrium constants can be estimated until a linear slope of the plot is obtained. Once the equilibrium constant values are obtained, the total concentration for any monomer concentration can be calculated by Equations (22)

or (24). Also, the total turbidity can be calculated by adding the experimentally measured solvent turbidity with the turbidity of aggregates calculated according to Equation (18).

IV. RESULTS

The turbidity, τ, cm^{-1} of sodium cholate, sodium taurocholate, sodium glycocholate and sodium deoxycholate in various 0.15 M sodium halide solutions as a function of concentration has been shown in Figures 1-4. The turbidity versus concentration of sodium taurodeoxycholate and sodium glycodeoxycholate in 0.5M NaCl has been shown in Figure 5. In Figure 6, the turbidity of sodium cholate in the absence of added electrolytes and in Figure 7, the turbidity of sodium cholate in 0.3 M NaCl and 0.5 M NaCl have been plotted as a function of concentration.

Since all the plots of refractive index versus concentration were linear, the plots of sodium cholate and sodium deoxycholate in 0.15 M NaCl are shown in Figures 8 and 9. The refractive index increments $(dn/dc_1)_{c_2}$ at constant electrolyte concentration for the above systems are given in Table 1, together with the values obtained by others. Refractive index increments of various sodium halides in aqueous solution are given in Table 2.

In Table 3, the naphthalene solubility as a function of sodium cholate in 0.15 M NaCl is listed. The solubility data has been plotted as a function of concentration in Figure 10.

Table 1. Refractive Index Increments for Bile Salts at 25°C

	$(\partial n/\partial c_2)_{c_1}$ at 436 nm								
Electrolyte	NaC	NaTC		NaGC	NaDC	NaGDC		NaTDC	
0.15M NaF	0.191[1]	0.167[1]	0.168[2]	0.189[1]	0.193[1]				
0.15M NaCl	0.193	0.166	0.172	0.184	0.193	0.193[1]	0.2[3]	0.171[1]	0.171[3]
0.15M NaBr	0.194	0.164	0.172	--	0.193				
0.15M NaI	0.193	0.173	0.165	0.189					
0.3M NaCl	0.196								
0.5M NaCl	0.198								

[1]Present work

[2]Reference (49)

[3]Reference (46)

Table 2. Refractive Index Increments for Sodium Halides at 25°C

Electrolyte	$(\partial n/\partial c_2)_{c_1}$ at 436 nm	
0.15M NaF	0.121[1]	0.132[2]
0.15M NaCl	0.180	0.184
0.15M NaBr	0.142	0.142
0.15M NaI	0.153	0.156

[1]Present work

[2]Reference (49)

Table 3. Naphthalene Solubility as a Function of Concentration of Sodium Cholate in 0.15M NaCl

c_T(mol/l)	$N_T \times 10^4$ (mol/l)
0	2.36
.004	2.40
.005	2.415
.006	2.44
.008	2.538
.01	2.808
.015	4.27
.015	4.38
.028	5.53
.02	6.586
.02	6.613
.023	8.256
.0251	9.39
.03	12.439
.04	19.317
.06	33.985

Plot of turbidity, τ, vs. concentration, c, mg/ml of NaC in 0.15 M Sodium halides. For τ, each division represents 5 x 10^{-5} cm^{-1}. The intercepts for NaF(▽), NaCl(△), NaBr(□) and NaI(○) are 4.83 x 10^{-5}, 5.07 x 10^{-5}, 5,32 x 10^{-5} and 5.93 x 10^{-5} respectively.

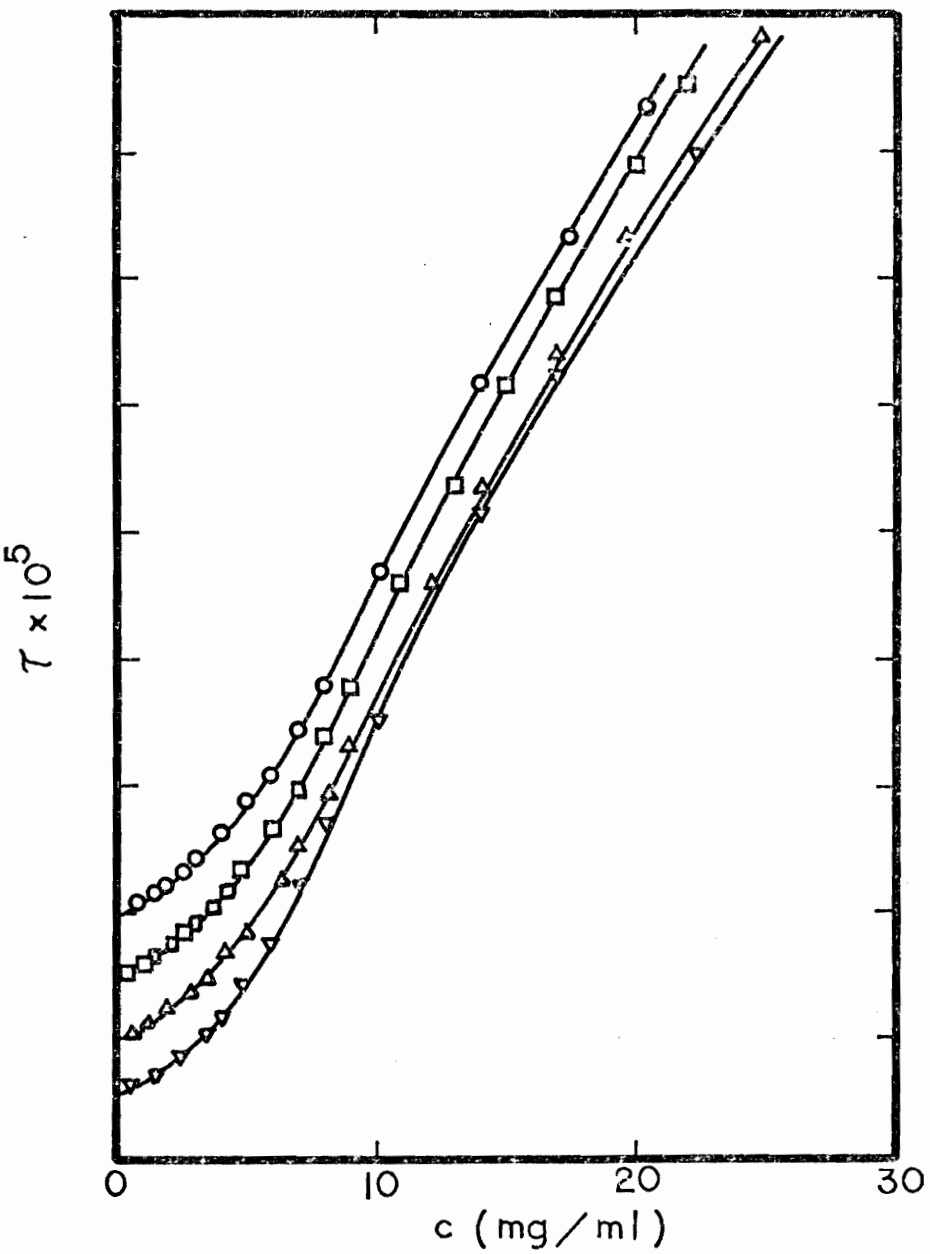

Figure 1. Turbidity vs. Concentration Plots of NaC in 0.15M Nax.

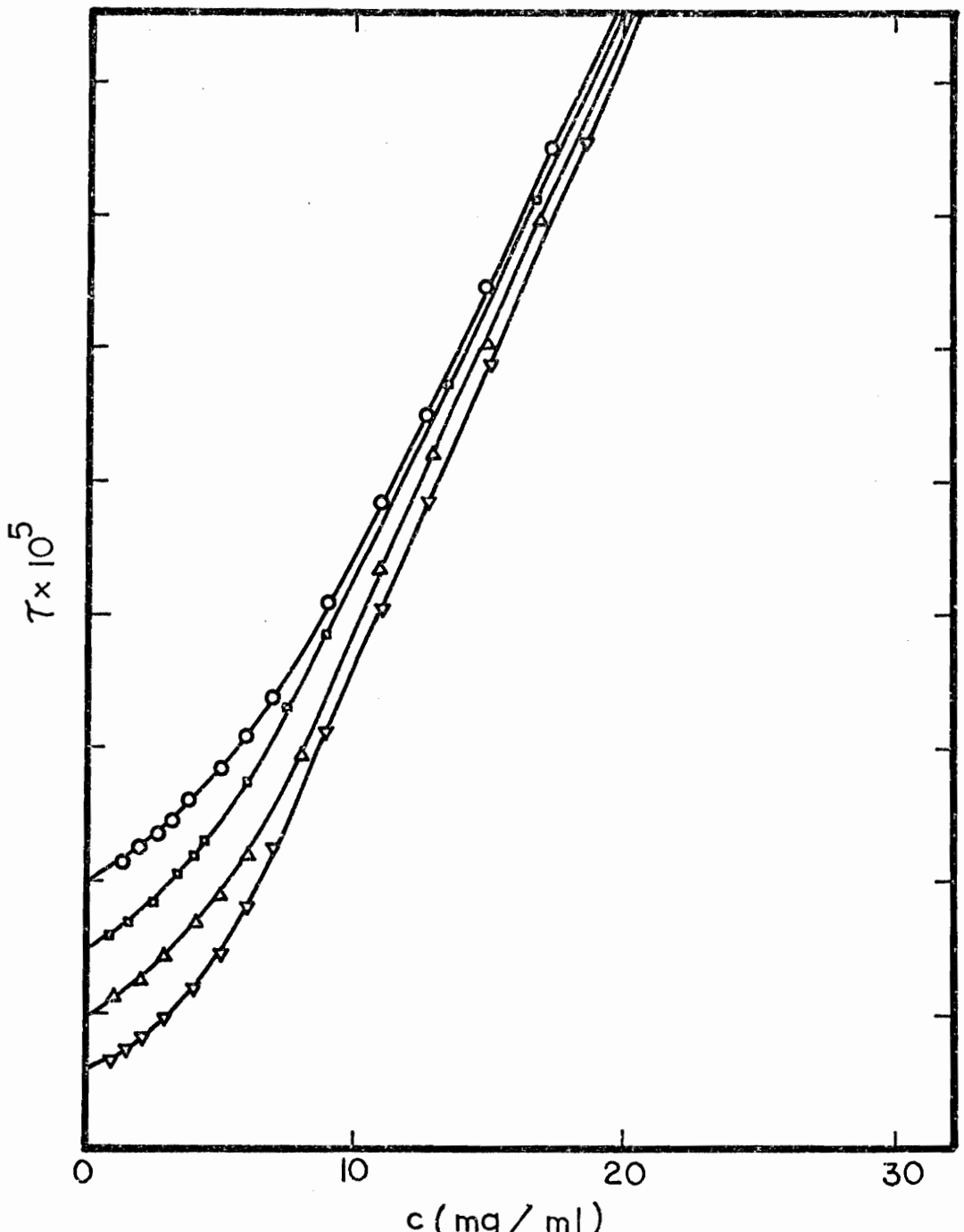

Plot vs. turbidity, τ, vs. concentration, c, mg/ml of NaTC in 0.15M Sodium halides. The division intercepts and symbols are the same as Figure 1.

Figure 2. Turbidity vs. Concentration Plots of NaTC in 0.15M NaX.

Plot of turbidity, τ, vs. concentration, c, mg/ml of NaGC in 0.15M Sodium halides. The division intercepts and symbols are the same as Figure 1.

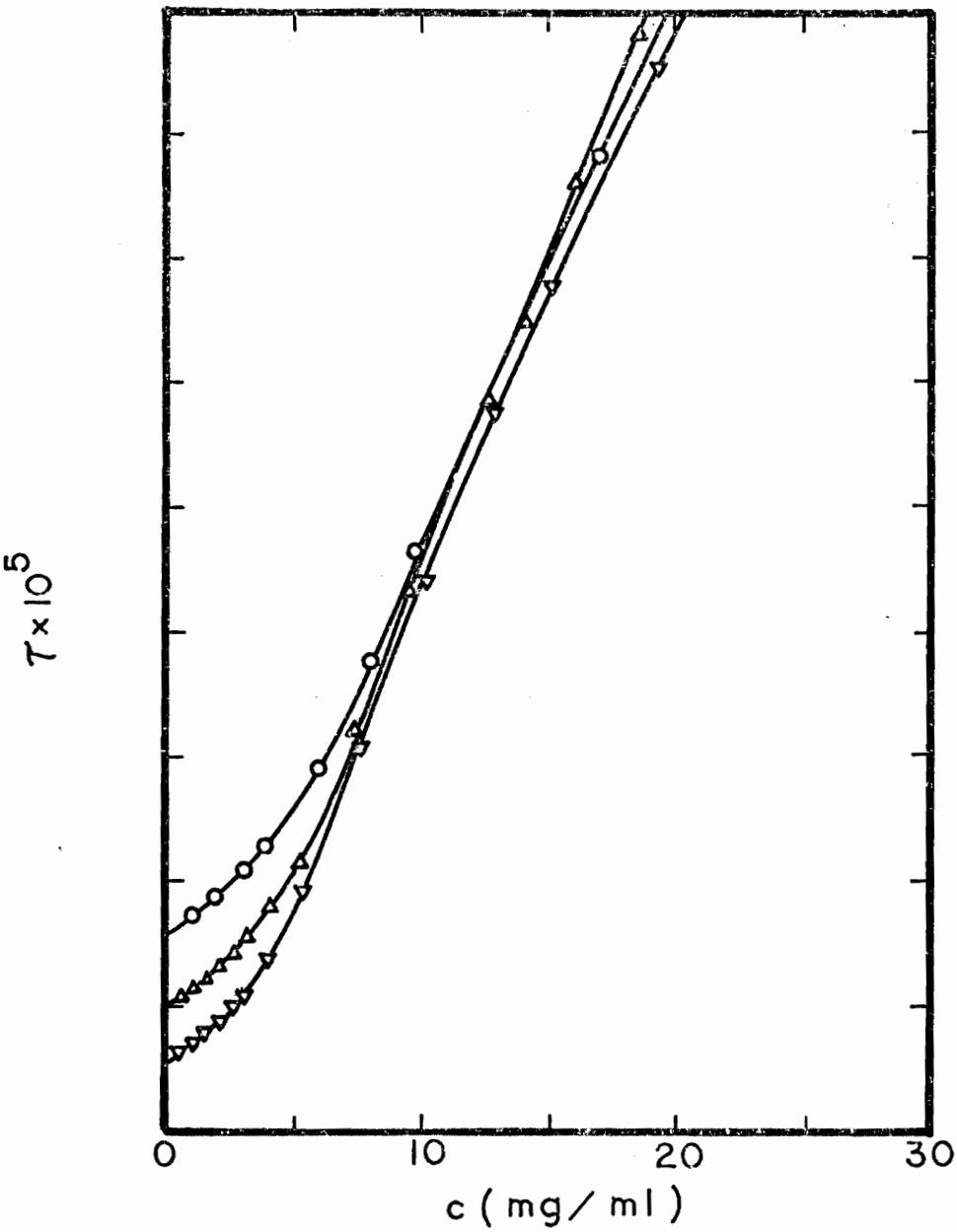

Figure 3. Turbidity vs. Concentration Plots of NaGC in 0.15M NaX.

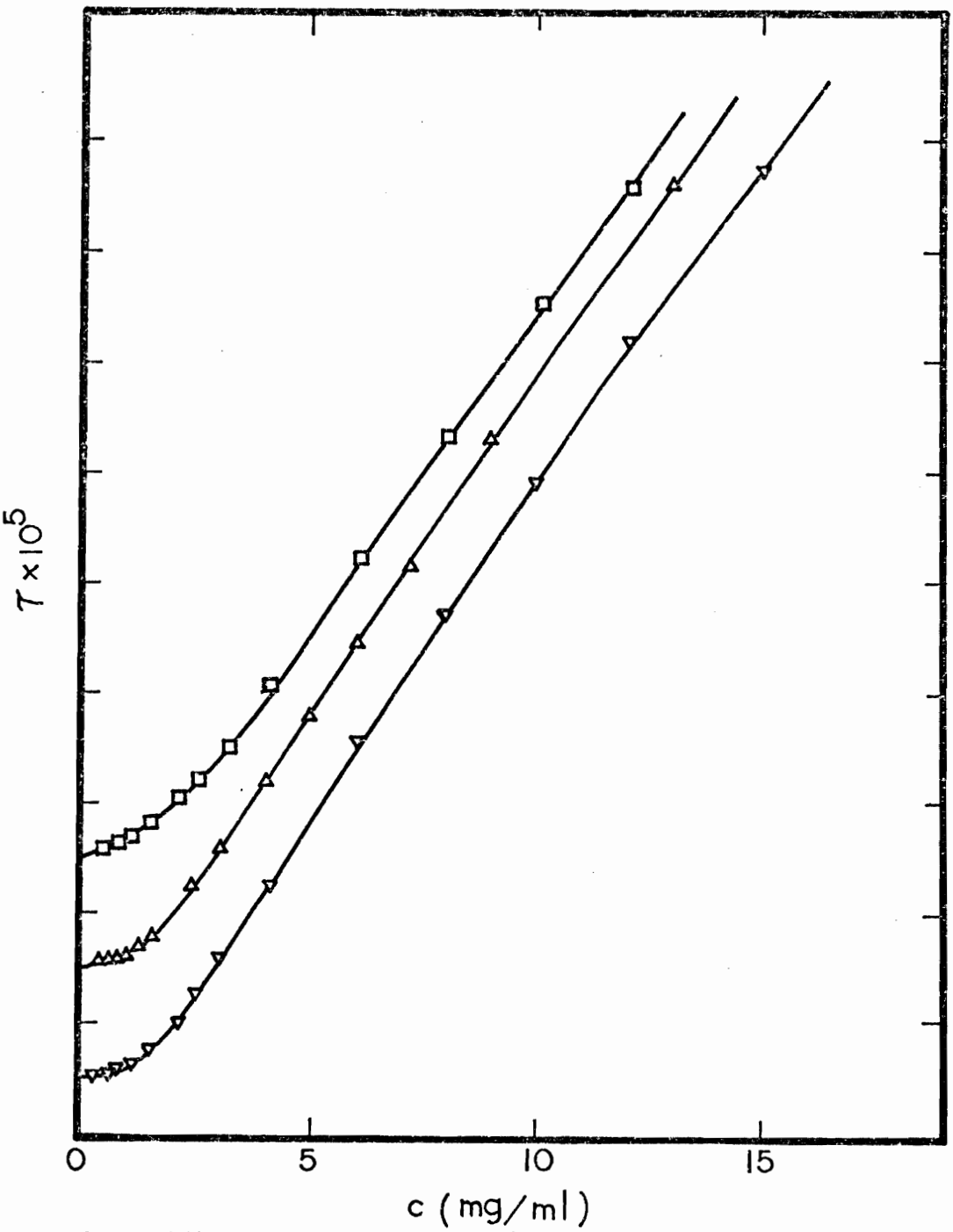

Plot of turbidity, τ, vs. concentration, c, mg/ml of NaDC in 0.15M sodium halides. For τ, each division represents 10 x 10^{-5} cm^{-1}. The intercepts and symbols are the same as Figure 1.

Figure 4. Turbidity vs. Concentration Plots of NaDC in 0.15M NaX.

Plot of turbidity, τ, vs. concentration, c, mg/ml of NaTDC and NaGDC in 0.15M NaCl. The division and intercepts are the same as Figure 4.

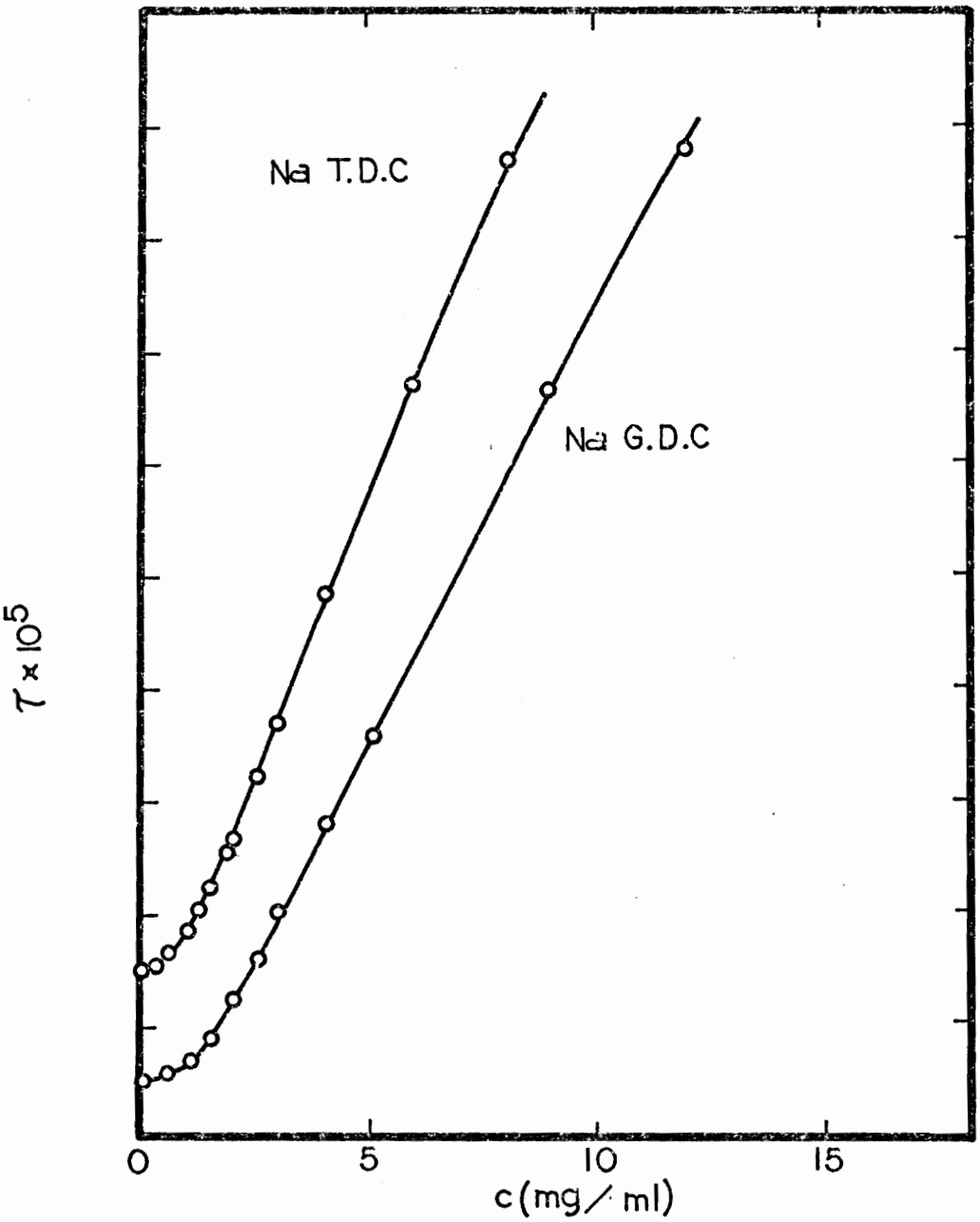

Figure 5. Turbidity vs. Concentration Plots of NaTDC and NaGDC in 0.15M NaCl.

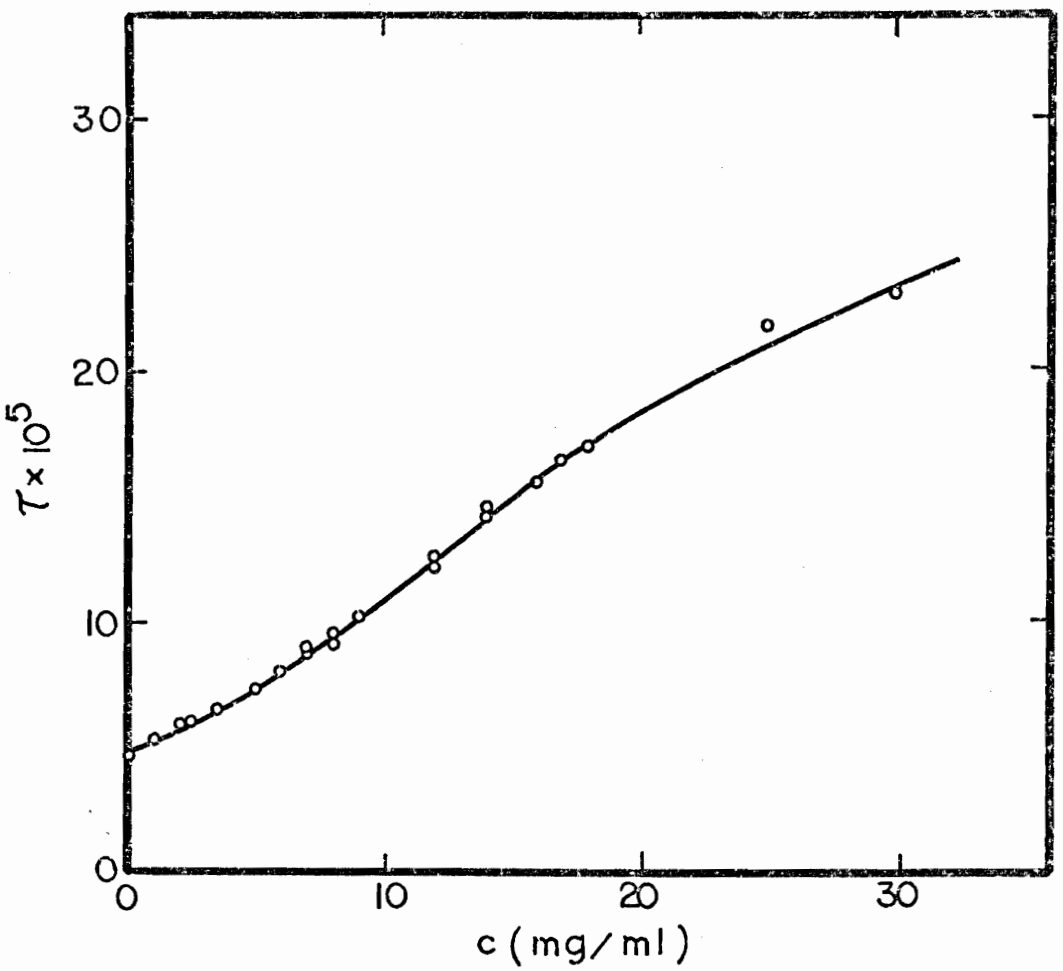

Plot of turbidity, τ, vs. concentration, c, mg/ml of NaC in the absence of salt. The intercept for water is 4.79×10^{-5}.

Figure 6. Turbidity vs. Concentration Plots of NaC in the Absence of Salt.

Plot of turbidity, τ, vs. concentration, c, mg/ml of NaC in 0.3M and 0.5M NaCl. The intercepts for 0.3M NaCl and 0.5M NaCl are 5.34×10^{-5} and 5.79×10^{-5} respectively.

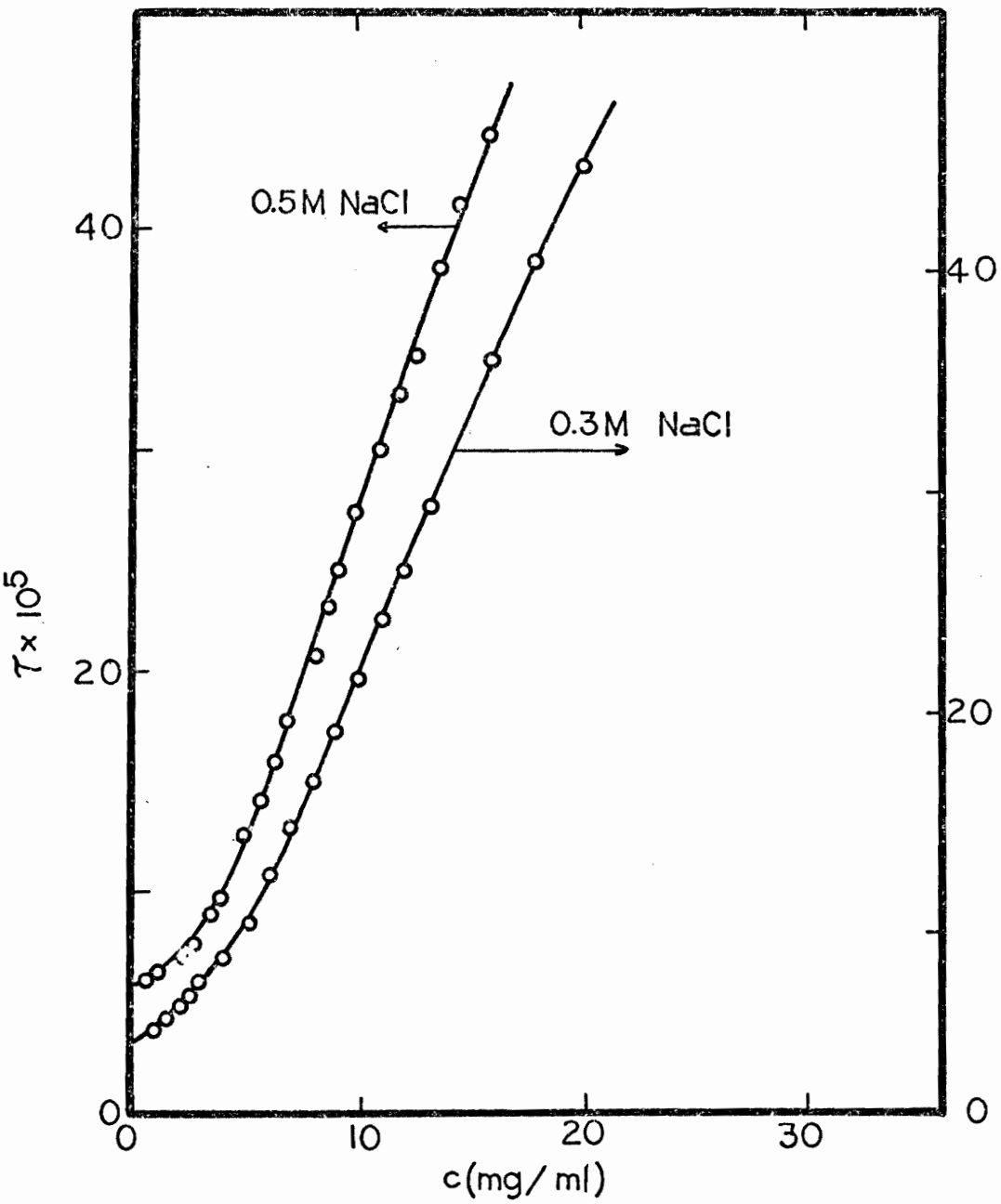

Figure 7. Turbidity vs. Concentration Plots of NaC in 0.3M NaCl in 0.5M NaCl.

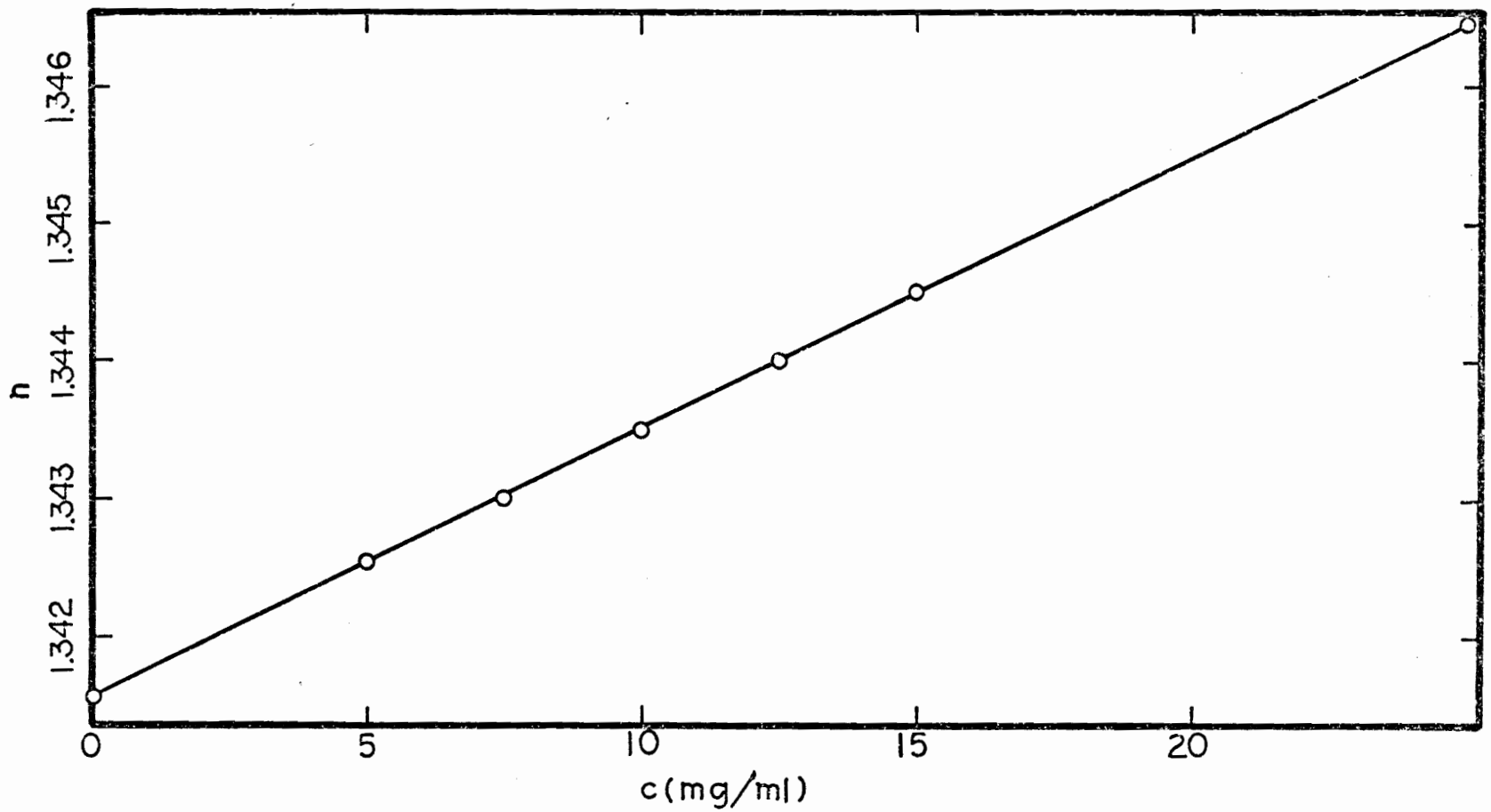

Plot of refractive index, n, vs. concentration of NaDC in 0.15M NaCl.

Figure 8. Refractive Index vs. Concentration Plot of NaDC in 0.5M NaCl.

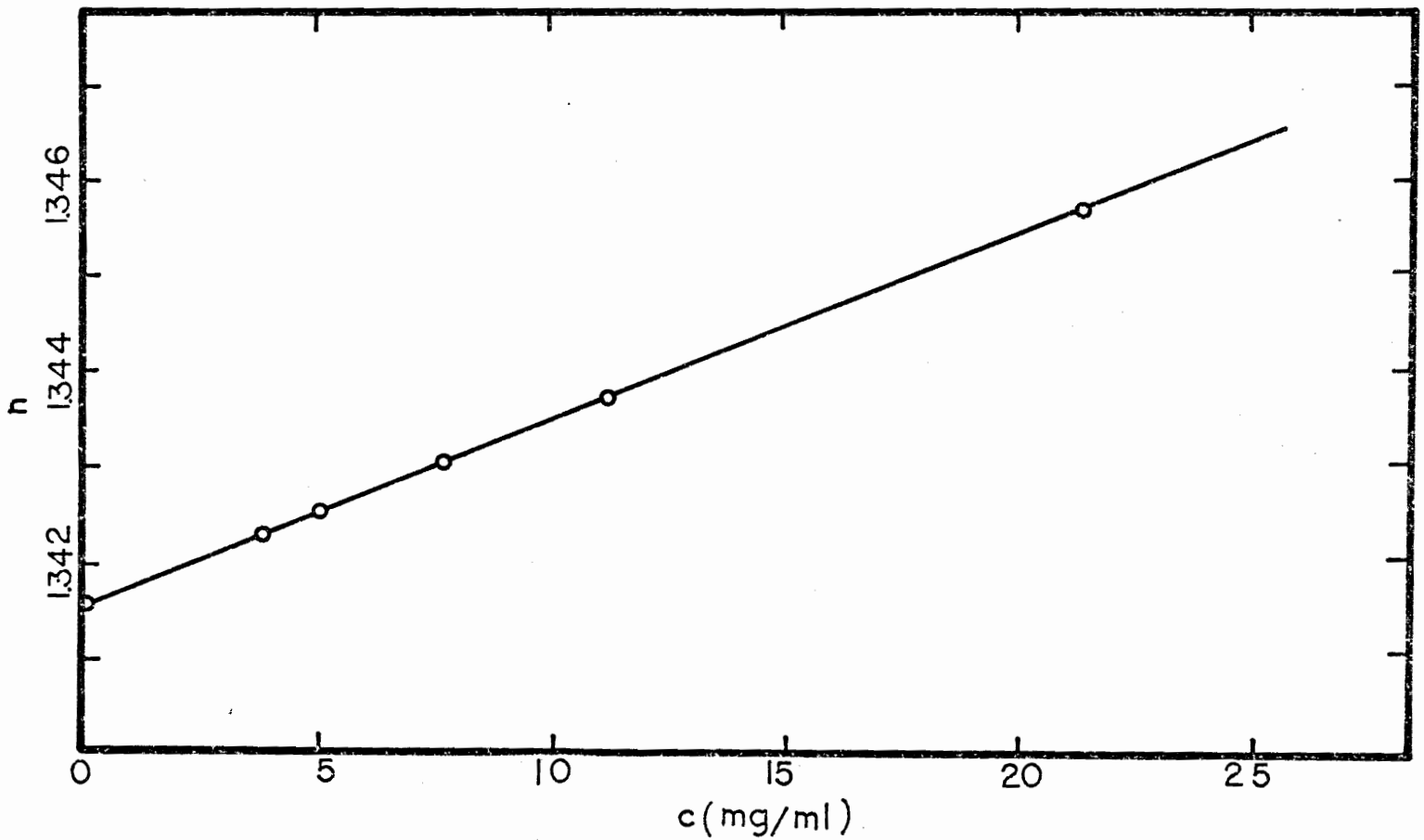

Plot of refractive index, n, vs. concentration, c, mg/ml of NaC in 0.15M NaCl.

Figure 9. Refractive Index vs. Concentration Plot of NaC in 0.15M NaCl.

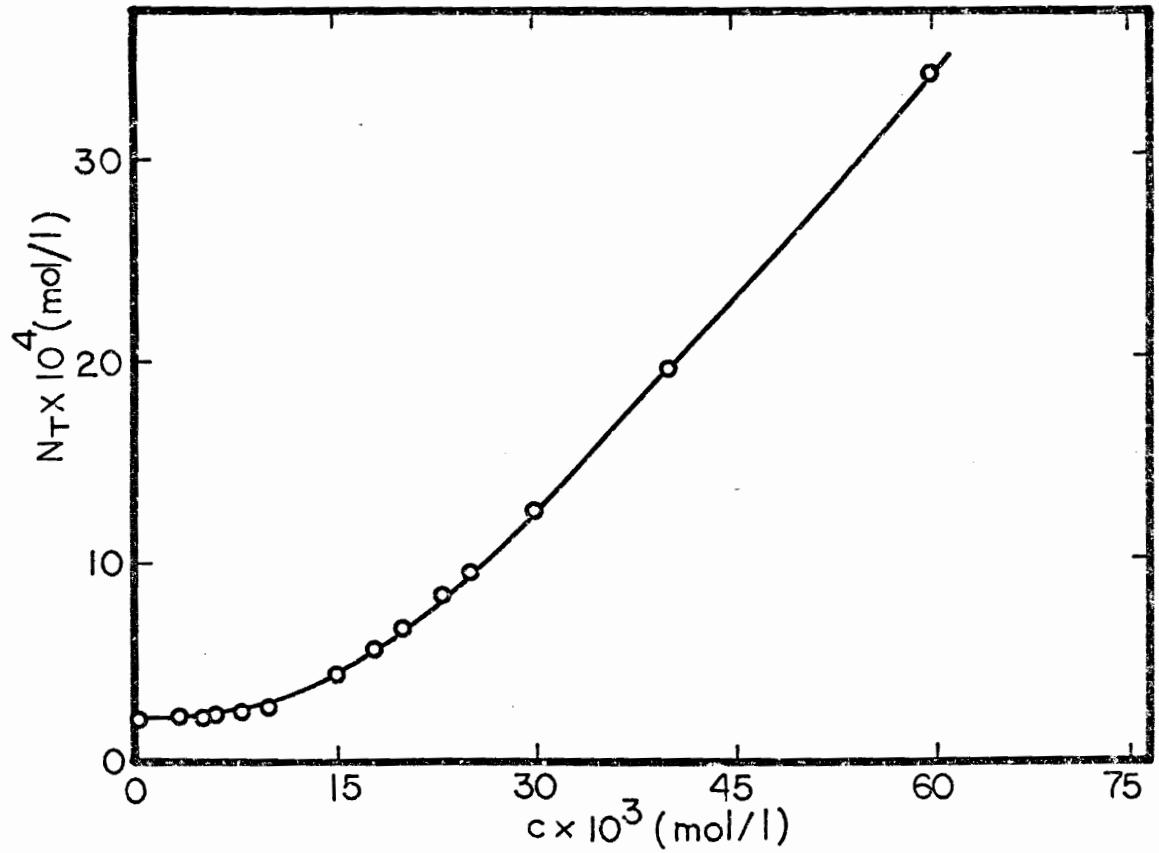

Plot of the equilibrium naphthalene solubility, N_T, mol/l, vs. the model concentration, c, of NaC.

Figure 10. Plot of the Naphthalene Solubility vs. the Concentration of NaC in 0.15M NaCl.

V. DISCUSSION

The turbidity versus concentration plots obtained from various trihydroxy and dihydroxy bile salts are in qualitative agreement with previous light scattering work (40, 43, 52). The turbidity increases slowly at low concentrations followed by a rapid increase in turbidity at high concentrations. This abrupt increase is usually attributed to micelle formation.

Some important quantitative differences exist, however, between the present results and those of previous investigators. Vittelo (43) suggested that the plot of turbidity versus concentration of bile salts shows a sudden change of slope at a concentration corresponding to the CMC. The data obtained in this work would appear to be inconsistent with his assumption. Vitello also indicated that it is most difficult to obtain a reliable value of turbidity in the vicinity of the CMC due to high experimental error in this region. Because of this, Vitello developed an iterative procedure to obtain a self consistent value for the CMC. In order to accomplish this, it was assumed that the second virial coefficient for the micelles is zero. However, this might be a severe assumption in view of the fact that the micelles are charged and the salt concentration is relatively low.

On the other hand, Fontell (52) suggested that there are three stages or concentration limits over which micellization occurs. For trihydroxy bile salts, these limiting concentrations are:

limit 1, 1.0-1.5 x 10^{-2}M; limit 2, 4-5 x 10^{-2}M; and limit 3, 1.1-1.2 x 10^{-1}M. For dihydroxy bile salts these limiting concentrations are: limit 1, 4-5 x 10^{-3}M; limit 2, 9-10 x 10^{-3}M; and limit 3, 4-5 x 10^{-2}M. These concentration limits are presumed to be independent of salt concentration. The above model implies that the plot of turbidity versus concentration should show abrupt changes in slope at these concentration limits due to the sudden increase in the size of aggregates. Examination of Figures 1-7 for the various bile salts show that there is no indication of these abrupt changes. All the plots show a smooth curvature especially in low concentration ranges. That this transition region is continuous has been made very clear in the plots showing the low concentration regions. Similar conclusions concerning this point have been reached by Vitello (43) based on light scattering work and by Mukerjee and Cardinal (44) based on the variation of naphthalene solubility as a function of sodium cholate concentration. Therefore, the concentration limit model appears to be an unreasonable model for bile salts self-association.

Based on the above discussion and the points mentioned in the introduction of this thesis, it seems appropriate to consider the nature of bile salt self-association according to the two models; the monomer-micelle equilibrium model and a stepwise association model (44).

For the present work, the light scattering data are analyzed based on these two models in the following sections.

A. Monomer-Micelle Equilibrium Model

Traditionally, the analysis of light scattering data obtained from micellar systems has been based on Equation (7) as derived by Debye (18). This Equation is known to be valid for a two component system containing solvent and uncharged colloidal particles. For systems containing added electrolytes and charged particles, corrections must be made for the effects due to negative adsorption (66). In the area of bile salt self-association, both methods of analysis have been utilized previously. For the purposes of comparison, the present light scattering data will be analyzed utilizing both methods.

In the analysis, the results obtained from sodium taurocholate in 0.15 M NaCl are discussed in detail, as the results for other systems are qualitatively the same.

As mentioned previously, one of the characteristics of a monomer-micelle equilibrium system is the existence of a CMC. Commonly, the CMC in light scattering work is estimated by extrapolation of the pre- and post-CMC branches of the plot of turbidity versus concentration. In a typical micellar system the CMC appears clearly as a "break" on such a plot. However, as shown in Figures 1-7 and Figure 11, a high degree of curvature exists in the CMC region in these plots for the bile salt solutions. This causes significant variations in the value of the CMC depending on the method fo extrapolation. For example, if the extrapolation of the data in Figure 11 is made utilizing the data obtained in the concentration region below 4.5×10^{-3} (gm/ml), then the value

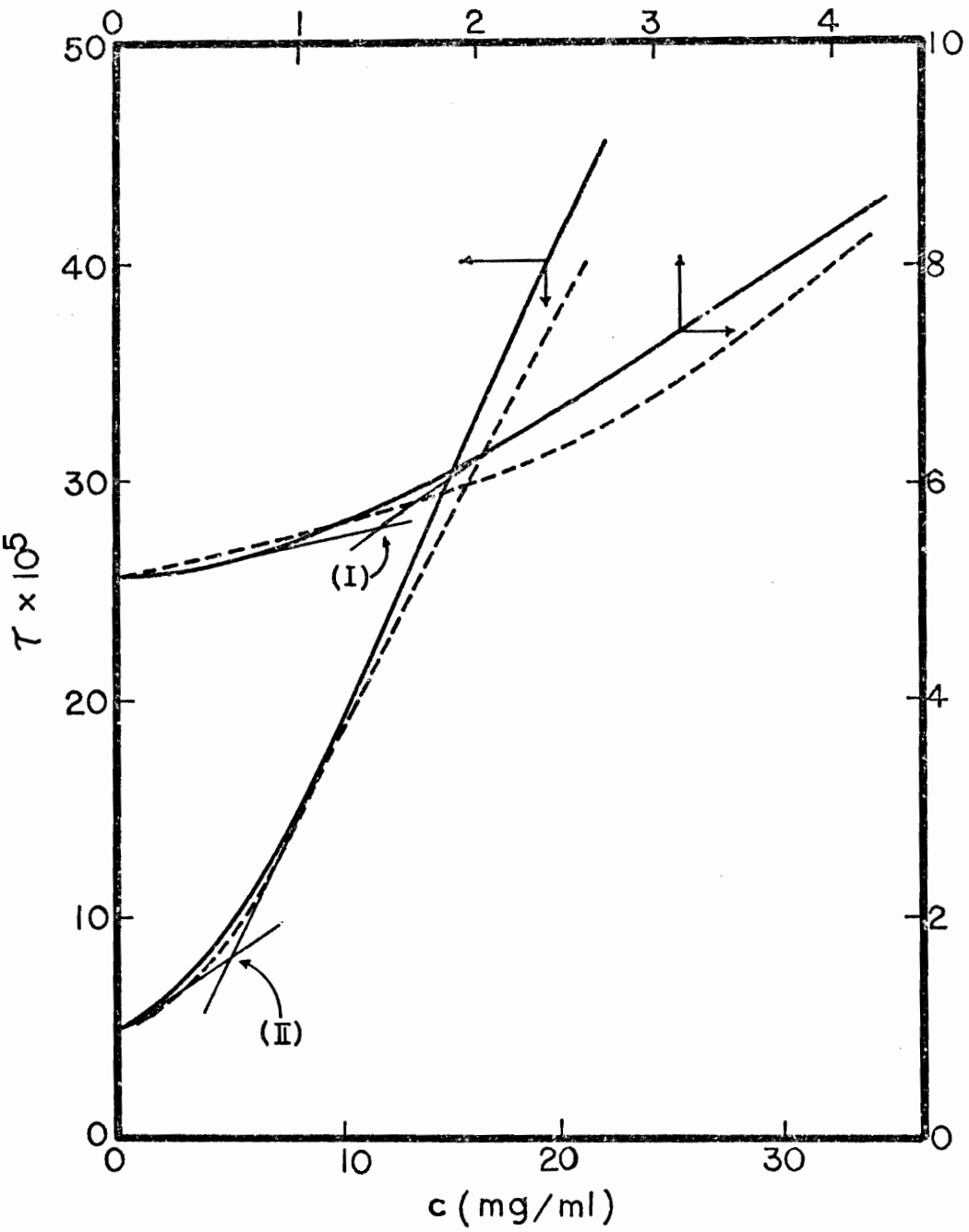

Plot of turbidity, τ, vs. concentration, c, mg/ml of NaTC in 0.15M NaCl. (I) and (II) represent different values of the CMC. Solid lines are experimental values and broken lines represent the results calculated based on monomer-micelle model.

Figure 11. Turbidity vs. Concentration of NaTC in 0.15M NaCl.

of CMC is 1.5×10^{-3} (gm/ml), while a value CMC II of 4.82×10^{-3} (gm/ml) is obtained from the extrapolation of the data of the whole concentration range is utilized in the extrapolation. Similar variations in the CMC have been noted previously in the review article by Small (12) and from the solubility data of Mukerjee and Cardinal (44). For the present calculation, the value of 4.82×10^{-3} (gm/ml) was accepted for the CMC. This was obtained by extrapolation of very low concentration range and the concentration range higher than 8.0×10^{-3} (gm/ml) as shown in Figure 11. This value is consistent with most literature values (43, 48). The turbidity at the CMC is 7.45×10^{-5} cm^{-1}.

Using these values of the turbidity and the CMC, the micelle molecular weight can be obtained according to Equation (7). This plot has been shown in Figure 12. From the intercept of this plot, the micelle molecular weight of sodium taurocholate in 0.15 M NaCl was found to be 3.07×10^{3}, which corresponds to an aggregation number of 5.7. From the slope of the plot, the second virial coefficient was found to be 8.1×10^{-4} mol·ml/gm^2.

To determine the extent to which the monomer micelle model gives a true representation of the nature of the self-association of sodium taurocholate, a comparison between the experimental curves and those obtained by calculation according to Equations (16-19) will be made. In order to calculate total turbidity at any concentration c, it is necessary to combine the turbidity due to monomer and micelle calculated by Equations (18, 19) with the experimentally measured turbidity of solvent. The value of equilibrium constant

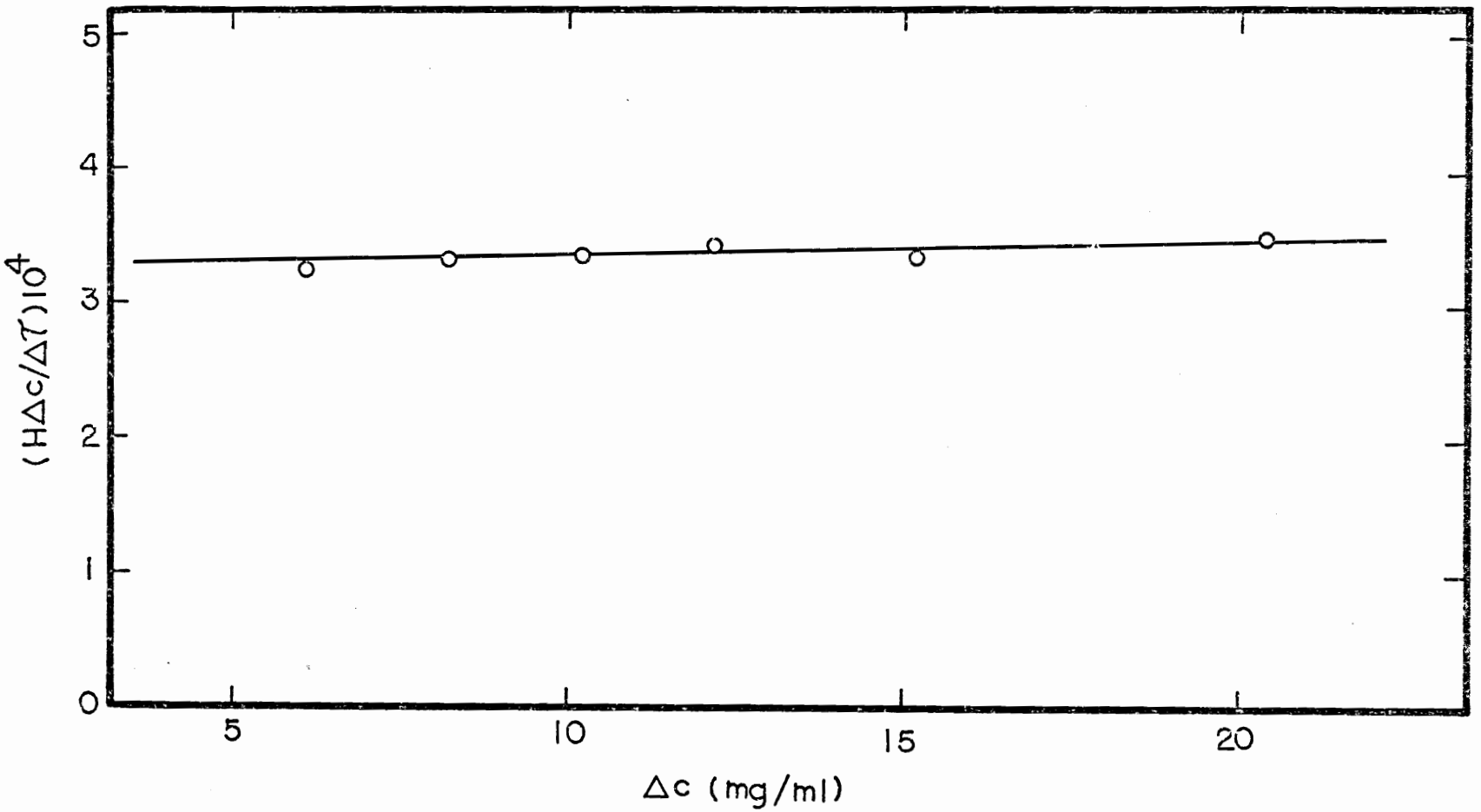

Plot of $H\Delta C/\Delta\tau$ vs. ΔC of NaTC

Figure 12. Plot of $H\Delta c/\Delta\tau$ vs. Δc of NaTC Based on the Monomer-Micelle Model.

shown in Equation (16) is obtained by fitting the experimental curve. This value varies with the concentration used for the fitting. If the concentration of 10 mg/ml is used for the fitting, the equilibrium constant, 7.92×10^8 is obtained, while the fitting at 22 mg/ml, gives 4.91×10^{10} for the equilibrium constant. For the purposes of comparison, the total turbidity as a function of concentration was calculated by utilizing the above two values of equilibrium constant.

Figure 11 gives a comparison of experimental curves and calculated results using the equilibrium constant, 7.92×10^8, which is obtained at an experimental concentration of 10 mg/ml. As can be seen from this plot, the calculated turbidity curve shows reasonable agreement with the experimental curve in the low concentration region. At higher concentrations, the calculated curve shows significant disagreement from the experimental curve. Figure 13 shows the comparison between the experimental curve and the curve calculated by using the equilibrium constant, 4.91×10^{10}. In contrast to the results shown in Figure 11, reasonable agreement between the experimental curve and the calculated curve is found only in the high concentration region.

Based on similar procedures, the light scattering data obtained from sodium cholate and sodium deoxycholate in 0.15 M NaCl have also been analyzed according to the Debye method. As shown in Table 4, the aggregation numbers for these systems are also in agreement with the values in the literature. However, these systems also showed a similar trend of disagreement from the experimental

Table 4. Summary of Aggregation Numbers for NaC, NaDC, and NaTC Micelles in 0.15M NaCl

Bile Salt	pH	Aggregation Number	Reference
Sodium Cholate	10 ± 0.2	5.57	Present work
	8-9	4.80	(44)
	?	4.00	(104)
	?	8.00	(105)
Sodium Deoxycholate	10 ± 0.2	15.65	Present work
	8-9	15.20	(44)
	?	13.0	(104)
Sodium Taurocholate	10 ± 0.2	5.70	Present work
	8-9	4.60	(44)
	?	7.0	(105)
	?	7.1	(49)

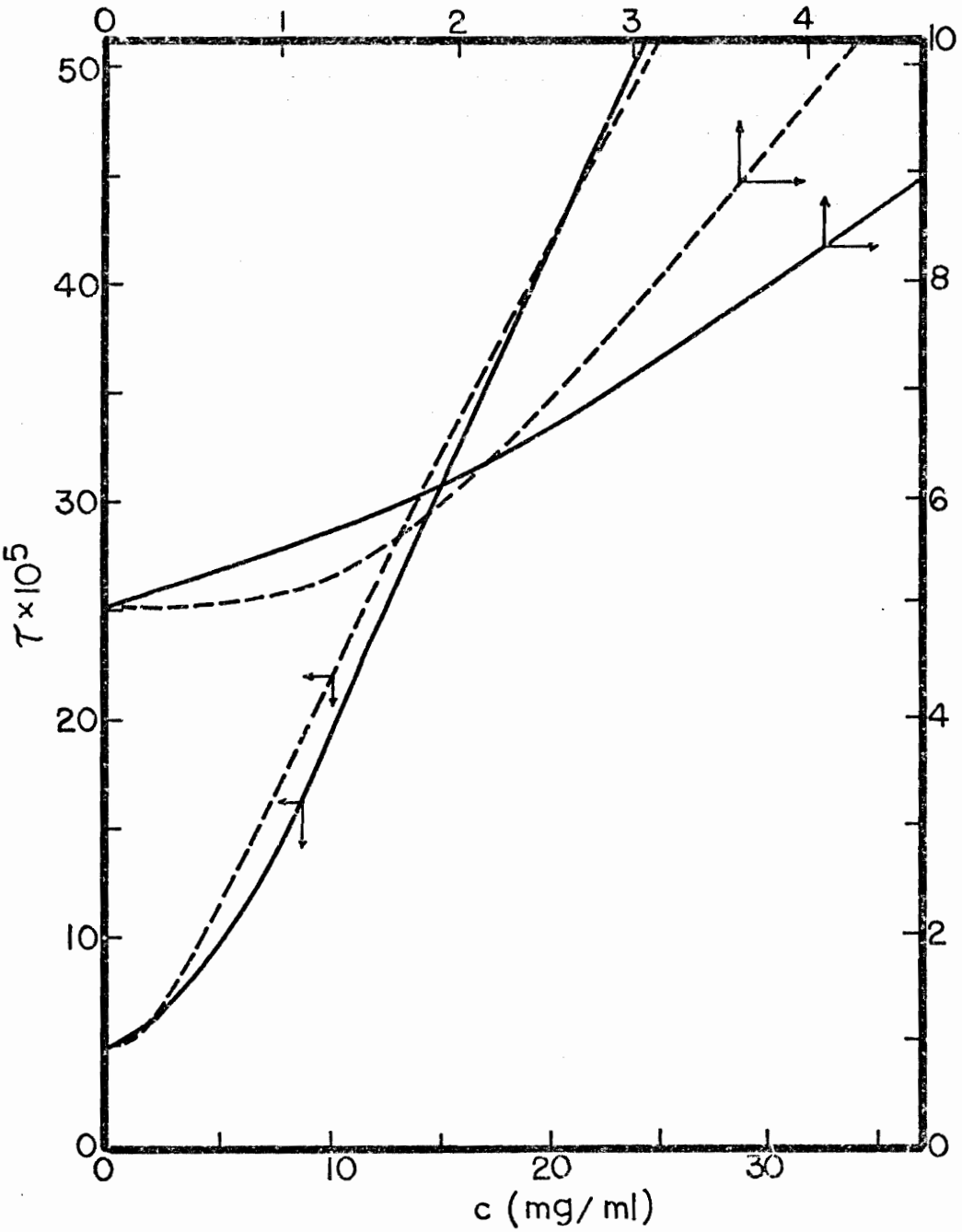

Comparison of the experimental turbidity of NaTC in 0.15M NaCl with the calculated values obtained by experiments as a function of concentration.

Figure 13. Comparison of the Experimental Turbidity of NaTC with the Results Calculated Based on Monomer-Micelle Model.

results as observed in sodium taurocholate when compared with the calculated curves. Such disagreement may be due to the assumption of a monomer-micelle equilibrium model. In order to investigate this point in further detail, these data were analyzed according to the monomer-micelle equilibrium model by the method of Vrij and Overbeek (66).

In the analysis of sodium taurycholate in 0.15 M sodium halides based on the Vrij and Overbeek approach, apparent micelle molecular weights were obtained according to Equation (7). These apparent micelle molecular weights are plotted according to Equation (12) to obtain the true micelle molecular weight as shown in Figure 14. Based on Equation (12), the apparent micelle molecular weight is to be plotted against $(\partial n/\partial c_2)_{c_1}$. However, as Huisman (18) pointed out, it is more appropriate to make the plot $\sqrt{M^*}$ versus $M_2(\partial n/\partial c_2)_{c_1}$. The micelle molecular weight was found to be 3490 which corresponds to an aggregation number of 6.5. The apparent micelle molecular weights and the values of $M_2(\partial n/\partial c_2)_{c_1}$ necessary for plotting, according to Equation (12), are shown in Table 5.

In order to compare the experimental results with the calculated curves, the turbidity as a function of concentration was obtained by the same procedure mentioned above. In the calculation, the equilibrium constant, 1.23×10^{11}, was used. This value was obtained by fitting the experimental curve for sodium iodide at a concentration of 15 mg/ml. The second virial coefficient, $7.5 \times 10^{-4} \frac{\text{mol.ml}}{\text{gm}^2}$, was used, which is the average value obtained

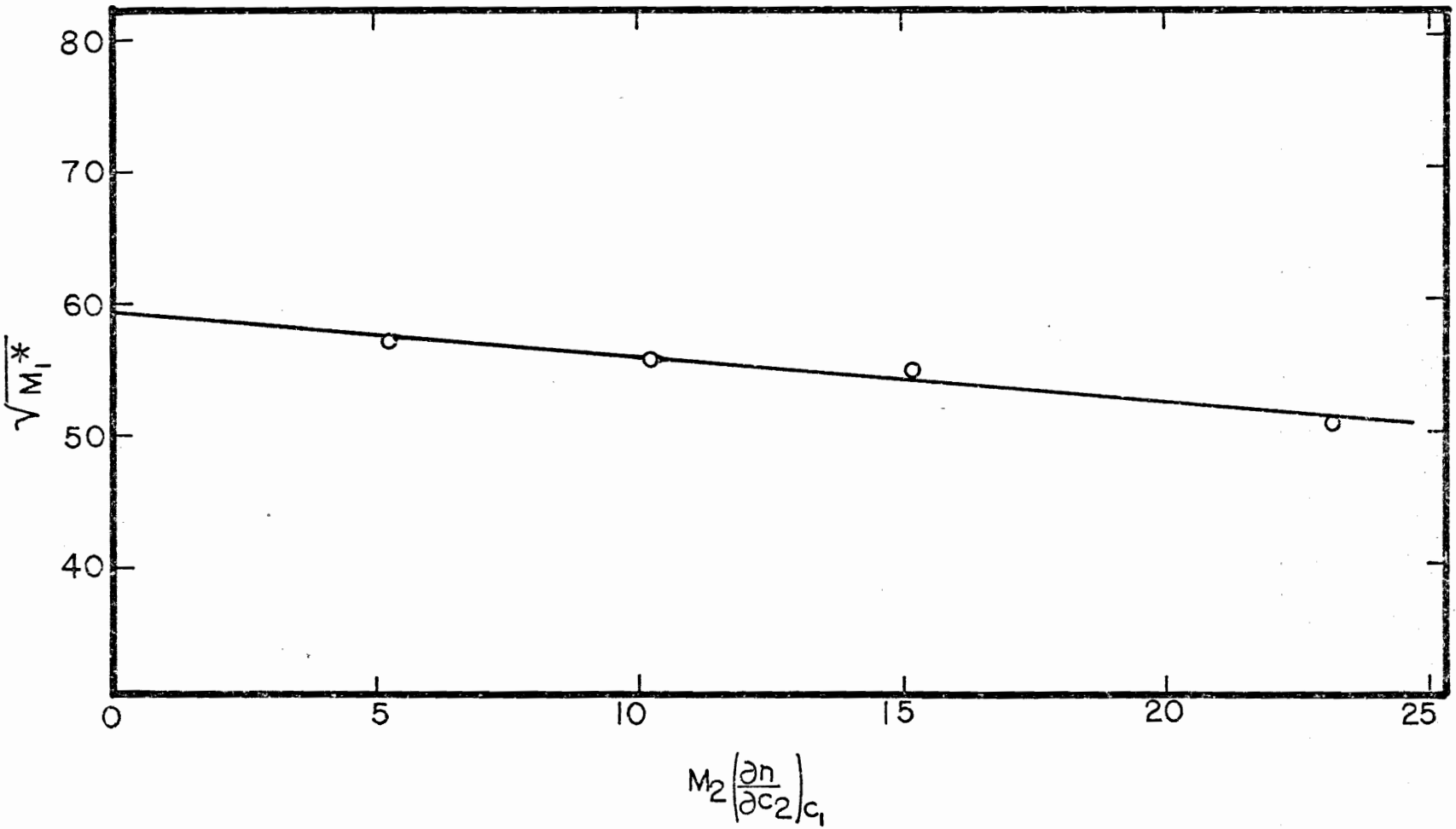

Figure 14. Plot of $\sqrt{M_1^*}$ vs. $M_2(\partial n/\partial c_2)_{c_1}$ of NaTC.

Table 5. Sodium Taurocholate Results from the Vrij-Overbeek-Huisman Treatment

0.15M Salt	$M_2(\partial n/\partial c_2)_{c_1}$	$\sqrt{M^*}$	Agg. #	C.M.C.(gm/ml)	H'
NaF	5.6	56.65	5.97	4.75×10^{-3}	7.2×10^{-6}
NaCl	10.35	55.36	5.70	4.82×10^{-3}	6.8×10^{-6}
NaBr	15.20	54.86	5.60	4.35×10^{-3}	6.4×10^{-6}
NaI	23.0	50.38	4.72	4.70×10^{-3}	5.8×10^{-6}

Table 6. Sodium Cholate Results from the Vrij-Overbeek-Huisman Treatment

0.15M Salt	$M_2(\partial n/\partial c_2)_{c_1}$	$\sqrt{M^*}$	Agg. #	C.M.C.(gm/ml)	H'
NaF	5.6	46.60	5.0	4.1×10^{-3}	9.91×10^{-6}
NaCl	10.35	46.57	5.0	4.3×10^{-3}	9.75×10^{-6}
NaBr	15.20	44.71	4.6	4.5×10^{-3}	9.57×10^{-6}
NaI	23.0	45.32	4.8	4.45×10^{-3}	9.28×10^{-6}

Table 7. Sodium Deoxycholate Results from the Vrij-Overbeek-Huisman Treatment

0.15M Salt	$M_2(\partial n/\partial c_2)_{c_1}$	$\sqrt{M^*}$	Agg. #	C.M.C.(gm/ml)	H'
NaF	5.6	81.2	15.9	1.70×10^{-3}	9.67×10^{-6}
NaCl	10.35	80.3	15.6	1.73×10^{-3}	9.23×10^{-6}
NaBr	15.20	77.3	14.4	1.86×10^{-3}	8.78×10^{-6}

from four systems. For the calculation of turbidity due to the micelle, the value of H' for each sodium halide solution was obtained by Equations (8) and (10). This value can then be utilized together with Equations (8), (16) and (17) to calculate the turbidity versus concentration curves. As can be seen from the above treatment, all the parameters for each halide are the same except for the value of H'.

In Figures 15 and 16, comparisons between the calculated and the experimental results for the four different sodium halides are made. As can be seen from Figures 15 and 16, at low concentration the calculated turbidity is lower than the experimental values, while at intermediate range of concentration the calculated turbidity is higher than the experimental values. At high concentrations, the calculated turbidity shows the tendency to be lower than the experimental turbidity. If other consistent values are chosen for the second virial coefficient, the aggregation number and the equilibrium constant, the region of disagreement between the calculated and experimental curves will be different. However, it is impossible to obtain a consistent set of parameters to fit the experimental curves.

This type of comparison between the experimental results and the calculated curves is also made for sodium cholate and sodium deoxycholate. From the analysis of the sodium cholate data in 0.15 M-sodium halides, the aggregation number of 5.1, average second virial coefficient, $1.28 \times 10^{-3} \frac{\text{mol.ml}}{\text{gm}^2}$, and association constant,

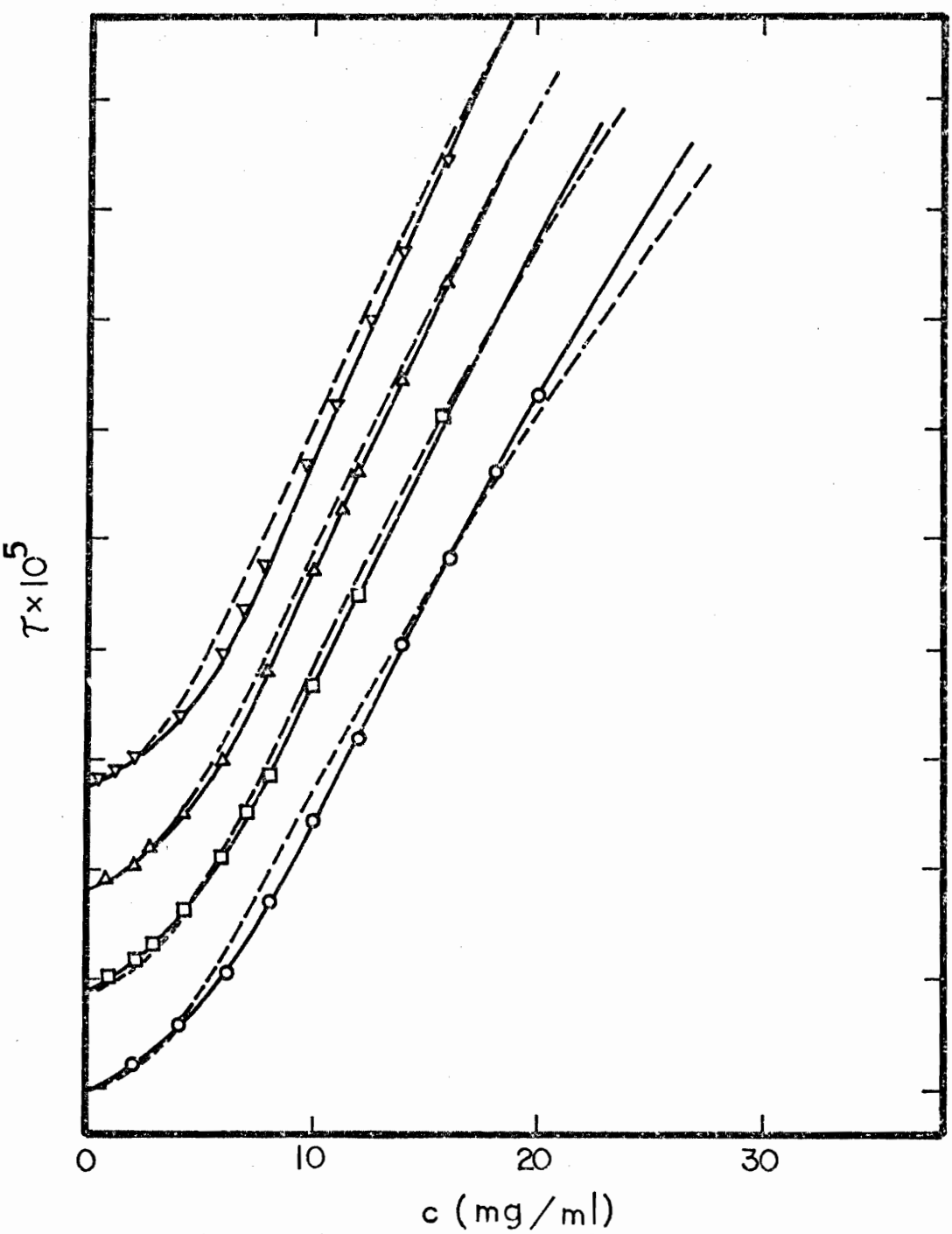

Comparison of the experimental turbidity with the results calculated from monomer-micelle model as a function of concentration of NaTC in 0.15M NaX. The division, intercepts and symbols are the same as Figure 1. Solid lines represent the experimental values and broken lines are calculated results.

Figure 15. Comparison of the Experimental Turbidity of NaTC with the Results Calculated by Vrij-Overbeek-Huisman Treatment of the Monomer-Micelle Model.

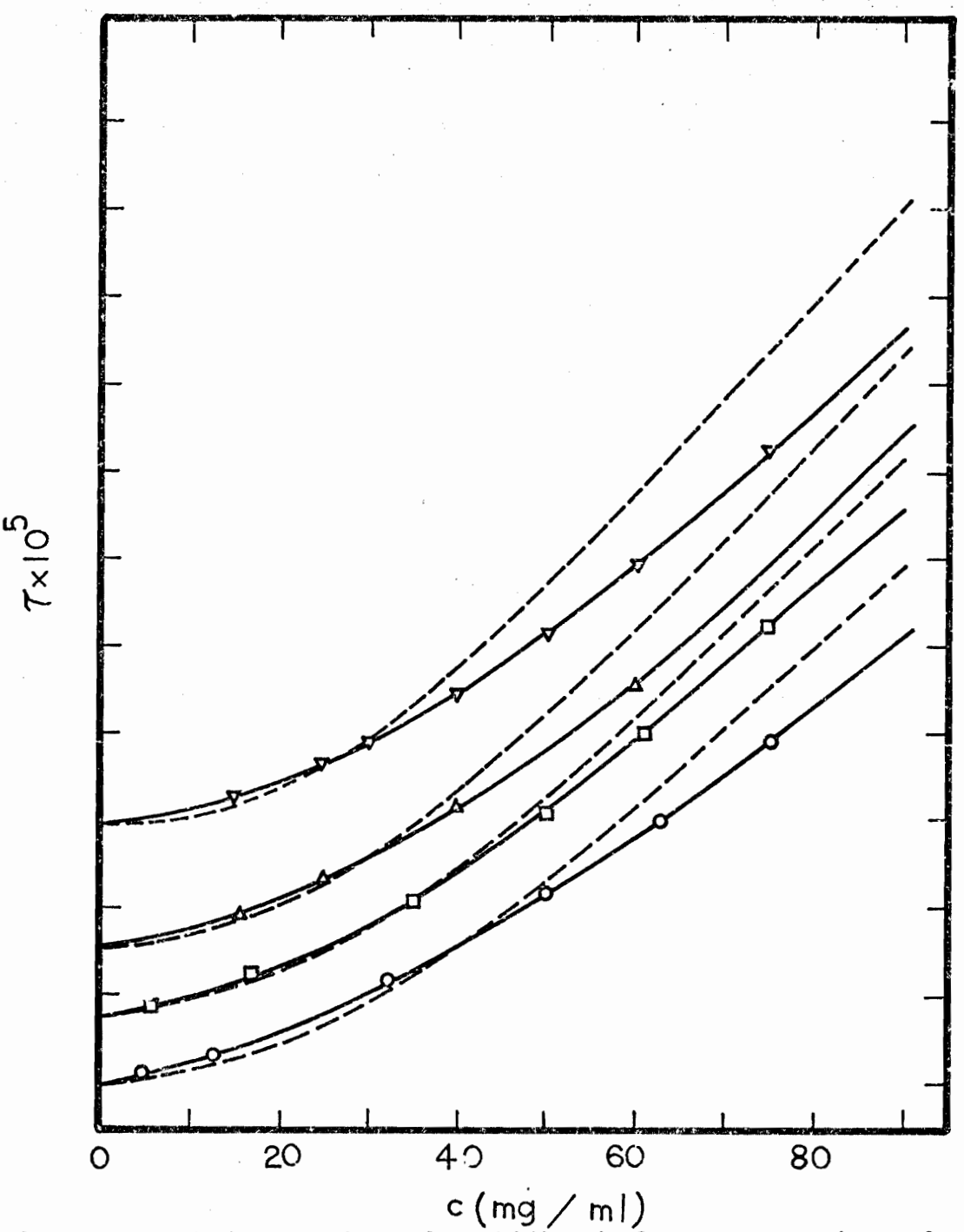

Comparison of the experimental turbidity in low concentrations of NaTC in 0.15M NaX with the results calculated from monomer-micelle model. For τ, each division represents 2 x 10^{-5} cm^{-1}. All the symbols and the intercepts are the same as Figure 15.

Figure 16. Comparison of the Experimental Turbidity in Low Concentrations of NaTC with the Results Calculated by Vrij-Overbeek-Huisman Treatment of the Monomer-Micelle Model.

4.9×10^{7} were obtained. The association constant was obtained by fitting at the experimental curve of sodium iodide at a concentration, 10 mg/ml. From the analysis of sodium deoxycholate systems, the aggregation number, 17, average second virial coefficient, $6.36 \times 10^{-4} \frac{mol.ml}{gm^2}$, and association constant, 2.216×10^{37}, were found. This association constant value was obtained by fitting the experimental curve of sodium bromide at a concentration of 10 mg/ml.

The results of these analyses are summarized in Tables 6 and 7. Figures 17-20 show the comparisons between the calculated results and the experimental values. It can be seen from Figures 17-20 that the calculated curves again show qualitative agreement with the experimental curves but quantitative agreement could not be obtained. Such disagreement in sodium deoxycholate appears to be much greater than in the case of the trihydroxy bile salts.

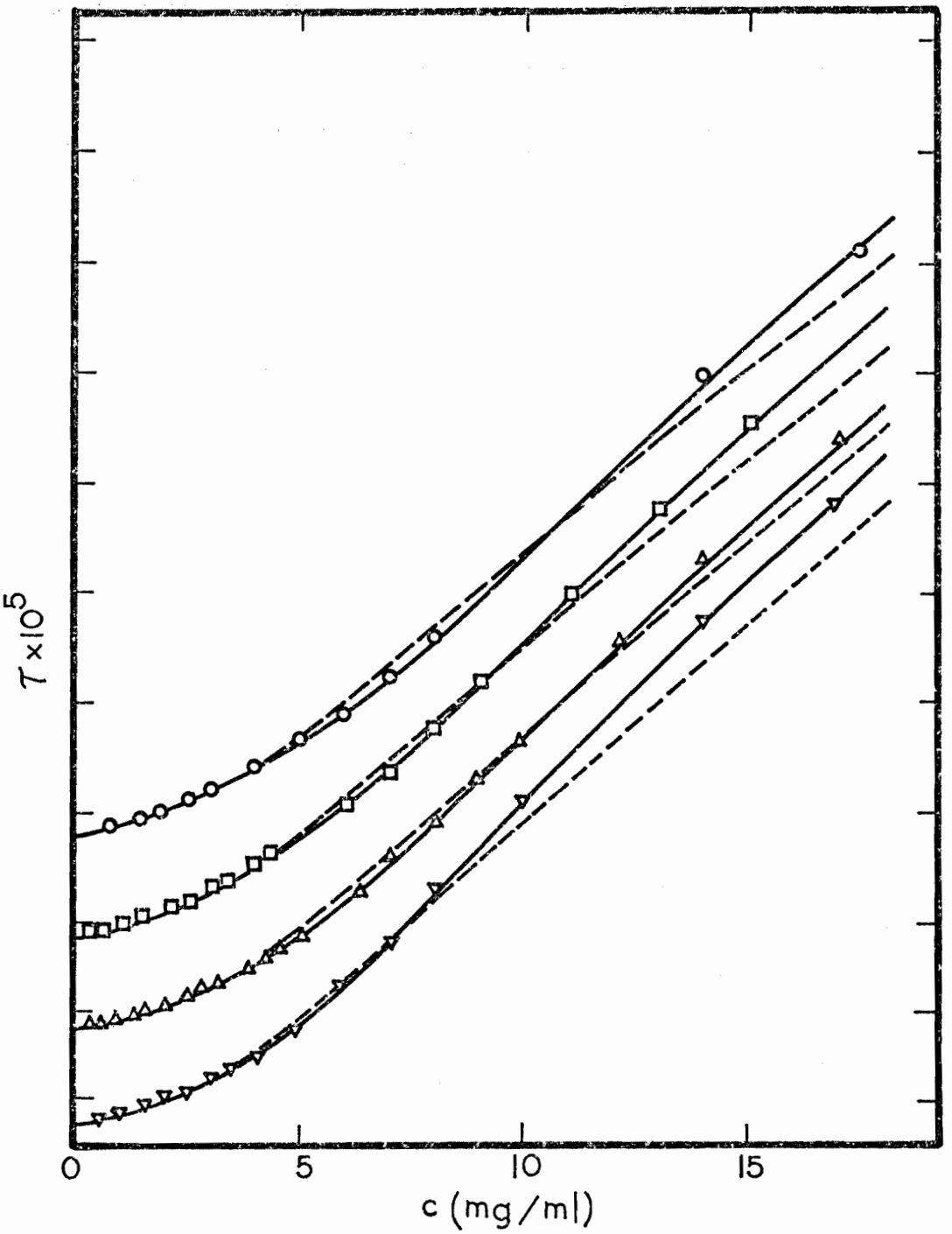

Comparison of the experimental turbidity of NaC in 0.15M NaX with the results calculated from monomer-micelle model. Each division, the intercepts and symbols are the same as Figure 1.

Figure 17. Comparison of the Experimental Turbidity of NaC with the Results Calculated by Vrij-Overbeek-Huisman Treatment of the Monomer-Micelle Model.

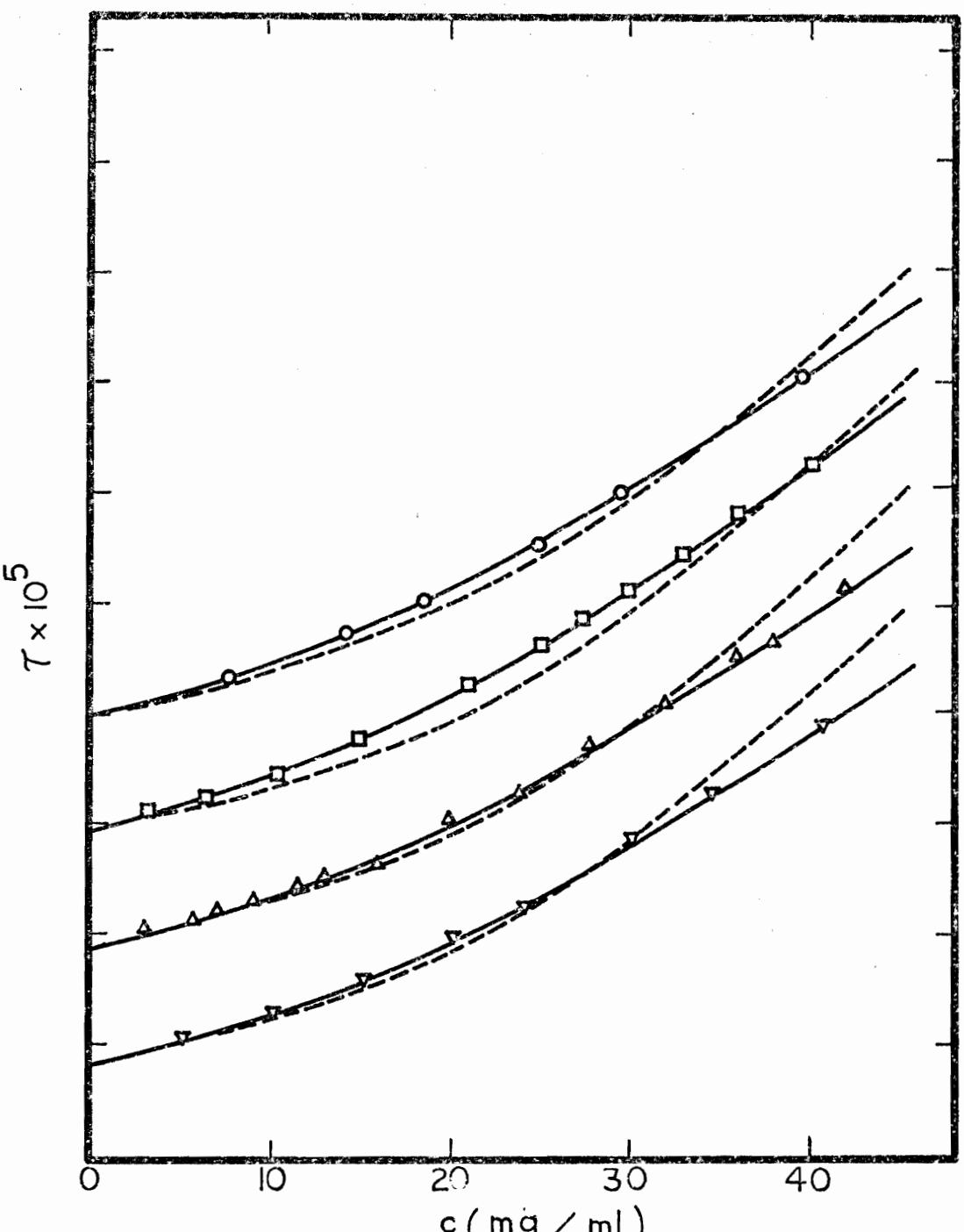

Comparison of the experimental turbidity of NaC in a 0.15M NaX with the results calculated from monomer-micelle model. For τ, each division represents 1 x 10^{-5} cm^{-1}. The symbols and intercepts are the same as Figure 1.

Figure 18. Comparison of the Experimental Turbidity in Low Concentrations of NaC with the Results Calculated by Vrij-Overbeek-Huisman Treatment of the Monomer-Micellar Model.

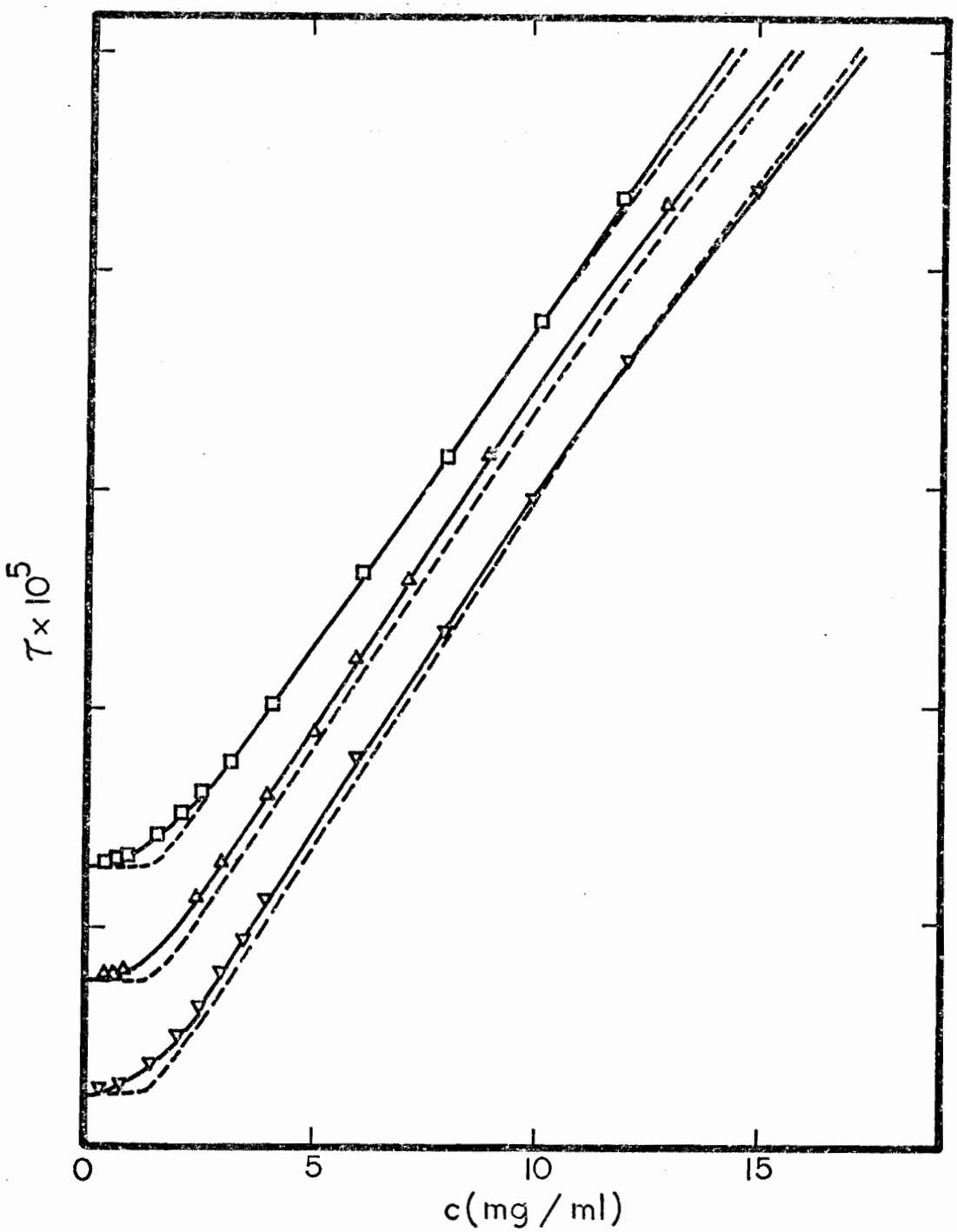

Comparison of the experimental turbidity of NaDC in 0.15M NaX with the results calculated from monomer-micelle model. The division, intercepts and symbols are the same as Figure 4.

Figure 19. Comparison of the Experimental Turbidity of NaDC with the Results Calculated by Vrij-Overbeek-Huisman Treatment of the Monomer-Micellar Model.

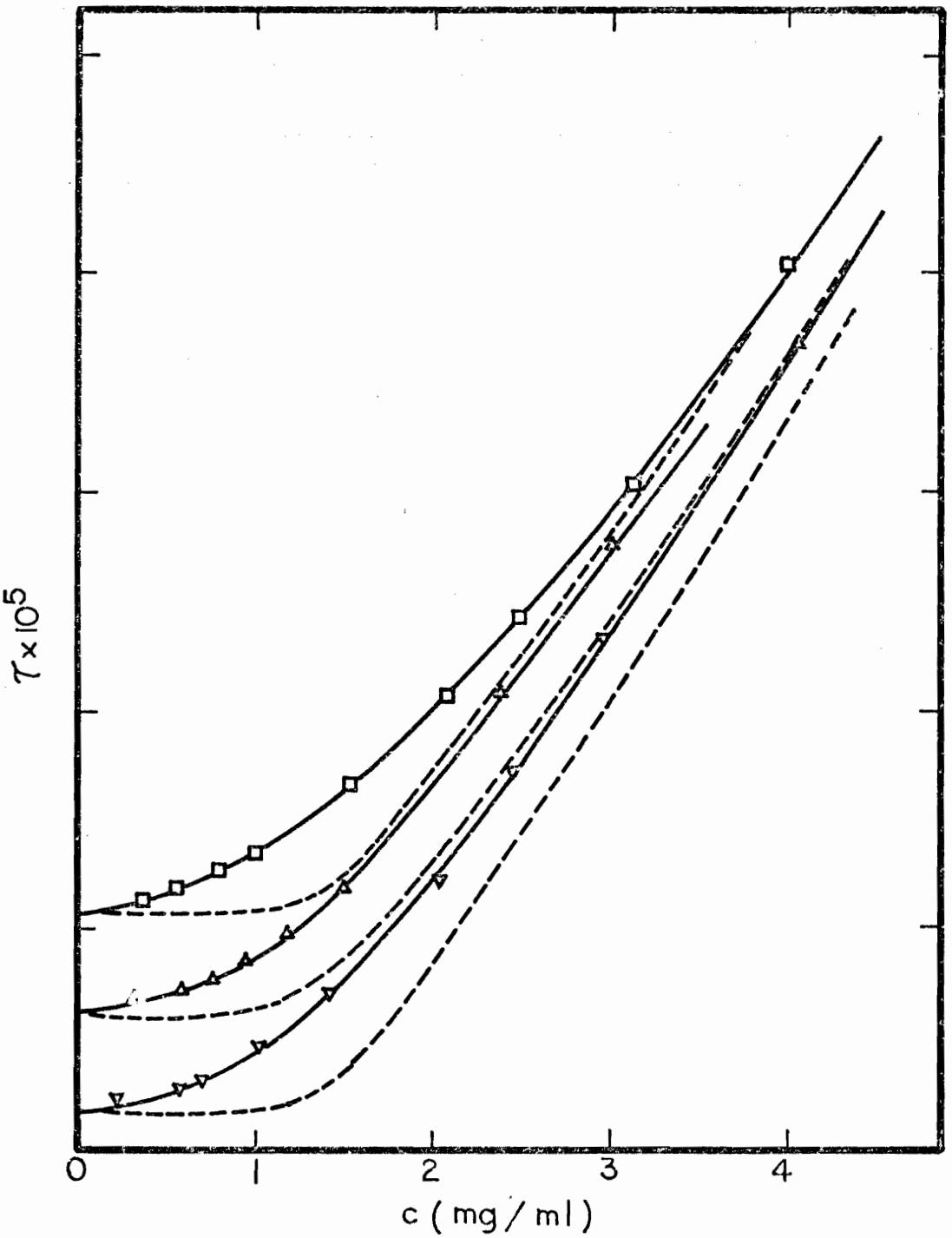

Comparison of the experimental turbidity of NaDC in 0.15M NaX with the results calculated from monomer-micelle model. For τ, each division represents 5 x 10^{-5} cm^{-1}. The intercepts and symbols are the same as Figure 4.

Figure 20. Comparison of the Experimental Turbidity in the Concentrations of NaDC with the Results Calculated by Vrij-Overbeek-Huisman Treatment on the Monomer-Micellar Model.

B. Stepwise Association Model

In order to examine the light scattering data according to the stepwise association model, the method of Steiner (69), as described previously, will be utilized. The experimental data are the same as used previously in the analysis of the monomer-micelle equilibrium model. Since the method of analysis for all bile salts followed the same procedure, only the data for sodium taurocholate is 0.15M NaCl will be discussed in detail. For the other bile salts, only the modifications from this procedure will be described.

According to Equation (26), the values of the monomer fraction, x, can be obtained from graphical integration as shown in Figure 21. Based on Equation (27), the association constants, K_2 and K_3, were obtained as 35 and 312, respectively. Figure 22 shows the plot used to obtain these values. As can be seen from Figure 22, the limiting slope of the plot increases linearly while at higher values of $(\frac{XC}{M})$ the plot shows an increasing curvature. This curvature of the plot is due to the existence of higher aggregates in the system. The next plot for the association constant of K_4 was made as shown in Figure 23. Normally, the values of K_3 and K_4 can be obtained from the intercept and the slope of the plot as explained before. As can be seen from Figure 23, the value of K_3 is reproduced from the intercept. However, the limiting slope of the plot is near zero, which means that the value of K_4 is nearly zero or relatively small with respect to K_2 and K_3. On the other hand, it can also be seen on the same plot that the slope at higher values of $(\frac{XC}{M})$ increases abruptly.

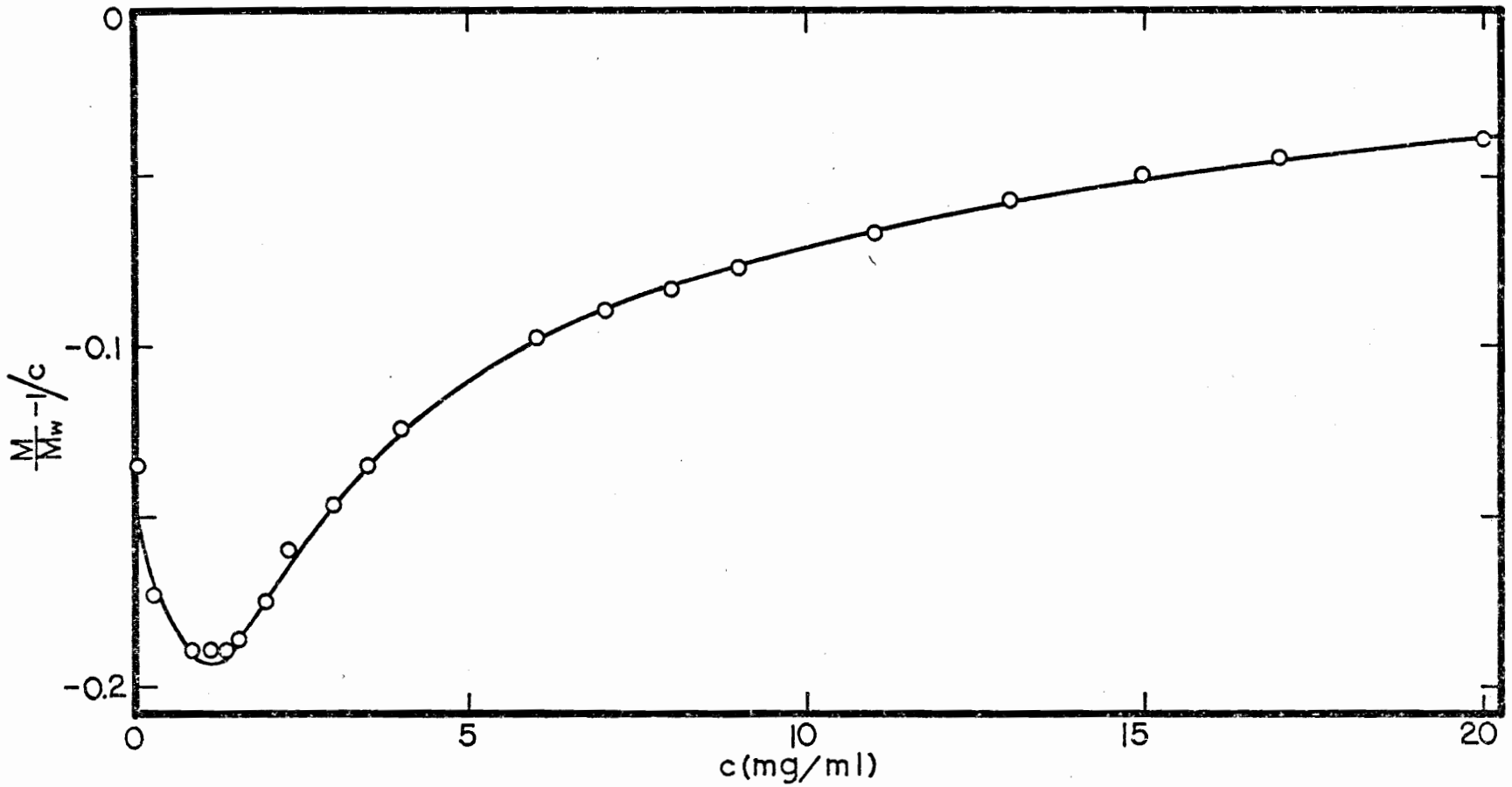

Figure 21. Plot of $[(M/M_w)-1]/c$ vs. c for NaTC.

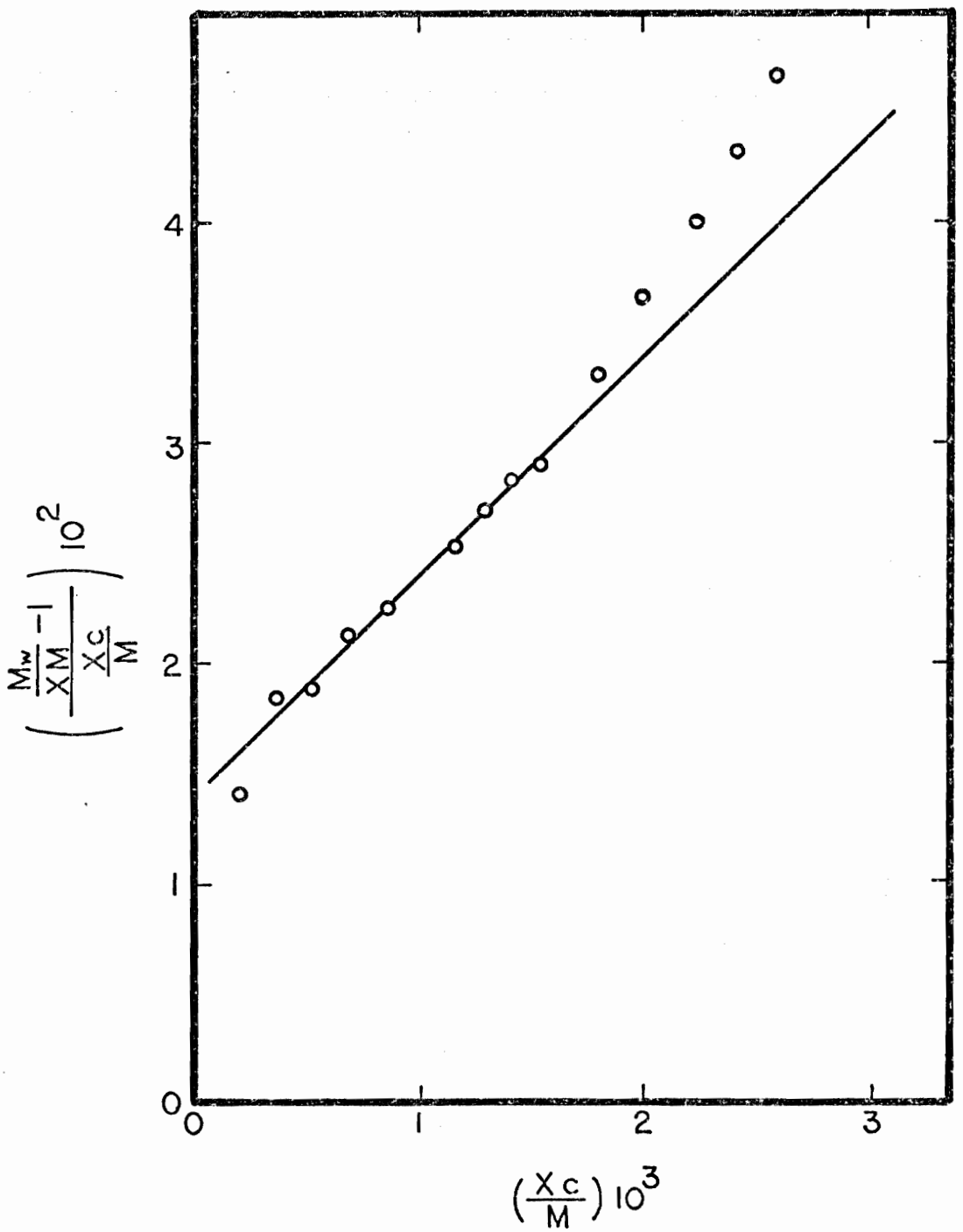

Plot of $(M_w/xM-1)/xc/M$ vs. xc/M for NaTC in 0.15M NaCl.

Figure 22. Plot of $[(M_w/xM-1)/xc/M$ vs. xc/M for NaTC..

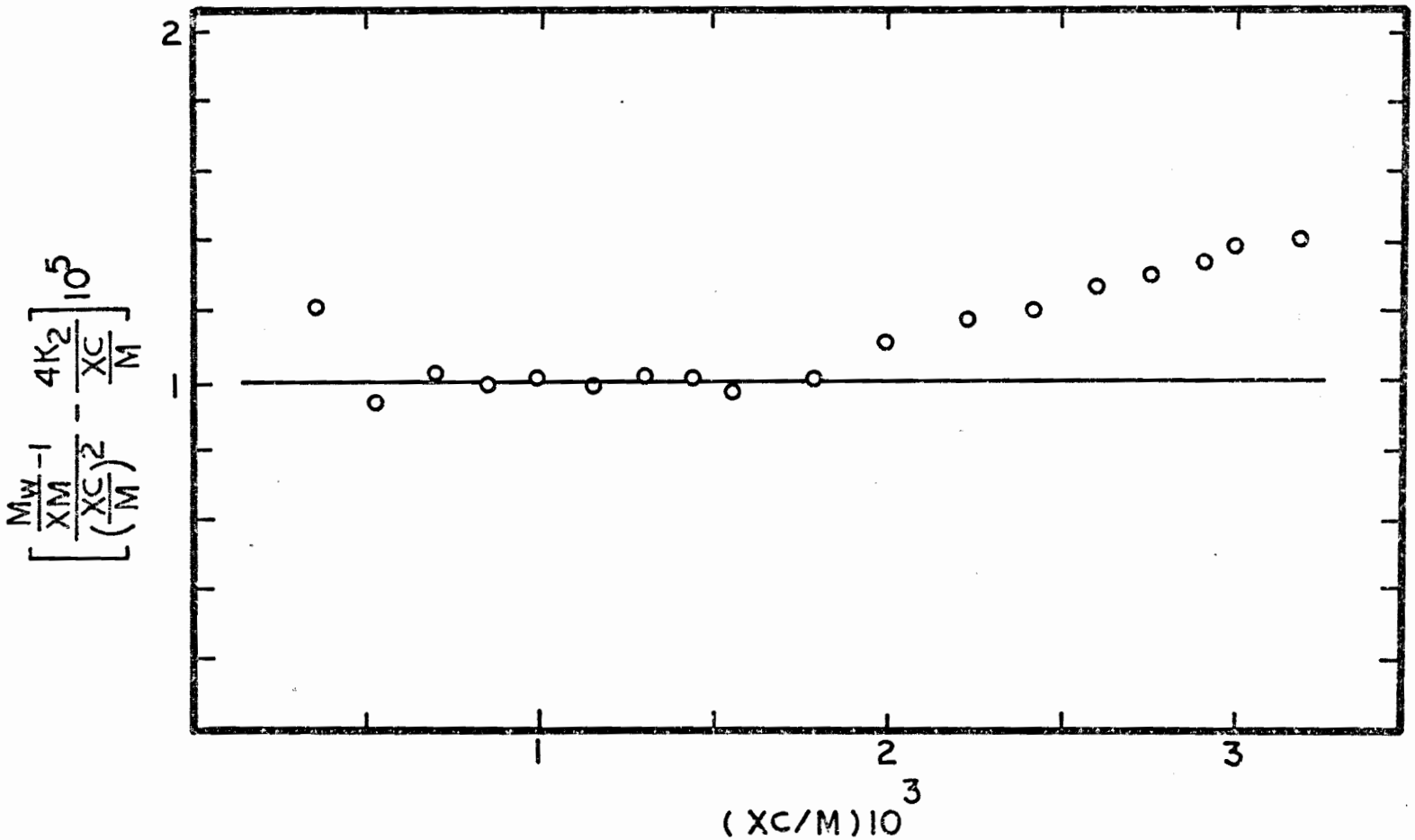

Plot of $[(M_w/xM-1)/xc/M)^2] - 4K_2/xc/M$ vs. xc/M for NaTC in 0.15M NaCl.

Figure 72, Plot of $[(M_w/xM-1)/(xc/M)^2] - [4K_2/(xc/M)]$ vs. xc/M for NaTC.

This rapid increase of the slope at higher values of $(\frac{xc}{M})$ suggests that aggregates larger than the tetramer must exist in solution.

To determine the size and association constants for these higher aggregates, the procedure as outlined above is not applicable since reliable estimates of K_4 cannot be obtained. However, based on the qualitative agreement between the experimental results and the monomer-micellar model discussed previously, as well as the results mentioned above, it seems reasonable to assume the possible existence of higher aggregates. This suggests that the total equivalent concentration c_T for sodium taurocholate in 0.15 M NaCl may follow a model given by Equation (28).

$$\begin{aligned} c_T &= [A_1] + 2[A_2] + 3[A_3] + q[A_q] \\ &= [A_1] + 2K_2[A_1]^2 + 3 \cdot K_2 \cdot K_3[A_1]^3 + q \cdot K_\beta[A_1]^q \end{aligned} \qquad (28)$$

where q is the aggregation number of large aggregates and K_β is the overall association constant for q-mer. The concentration of intermediate sized aggregates is assumed to be small.

In order to test this model against the experimental results, it was necessary to develop a method by which the average size of this higher aggregate could be determined.

In the literature, Mysels and Princen (73) discussed a similar problem in the investigation of the micellar size of sodium lauryl sulfate (NaLS). As discussed in the introduction of this thesis, it was suggested that monomeric ions of NaLS exist in

equilibrium with lauryl sulfate dimers below the CMC (17). Based on the above suggestion, Mysels and Princen (73) argued that the turbidity at the CMC of NaLS should be the sum of the turbidities due to solvent, monomer and dimer of NaLS. However, they could not measure the turbidity at the CMC because of experimental difficulties. Therefore, they used the calculated turbidity due to monomer, dimer and trimer in making the Debye plot to find out the size of the NaLS micelle.

In the analysis of the light scattering data for the present system according to the model depicted by Equation (28), a procedure similar to that of Mysels and Princen (73) has been followed; that is, the concentration of monomer, dimer and trimer was used as C_o, and the turbidity due to solvent, monomer, dimer and trimer was used as τ_o in Equation (9). C_o was obtained by Equation (22). τ_o was obtained by adding the experimentally measured solvent turbidity to the turbidity due to monomer, dimer and trimer calculated according to Equation (18).

It is important to mention that for any given value of c_T, the monomer fraction at that c_T is known from Equation (26). This means that the quantity $(C-C_o)$ and the $(\tau-\tau_o)$ in Equation (9) correctly represent the concentration and excess turbidity of the higher aggregates. Based on the above treatment of data, the plot of $\frac{H\Delta c}{\Delta\tau}$ versus Δc was made according to Equation (9) as shown in Figure 24. From the intercept of the plot, the molecular weight of the large aggregate formed by sodium taurocholate in 0.15M NaCl was

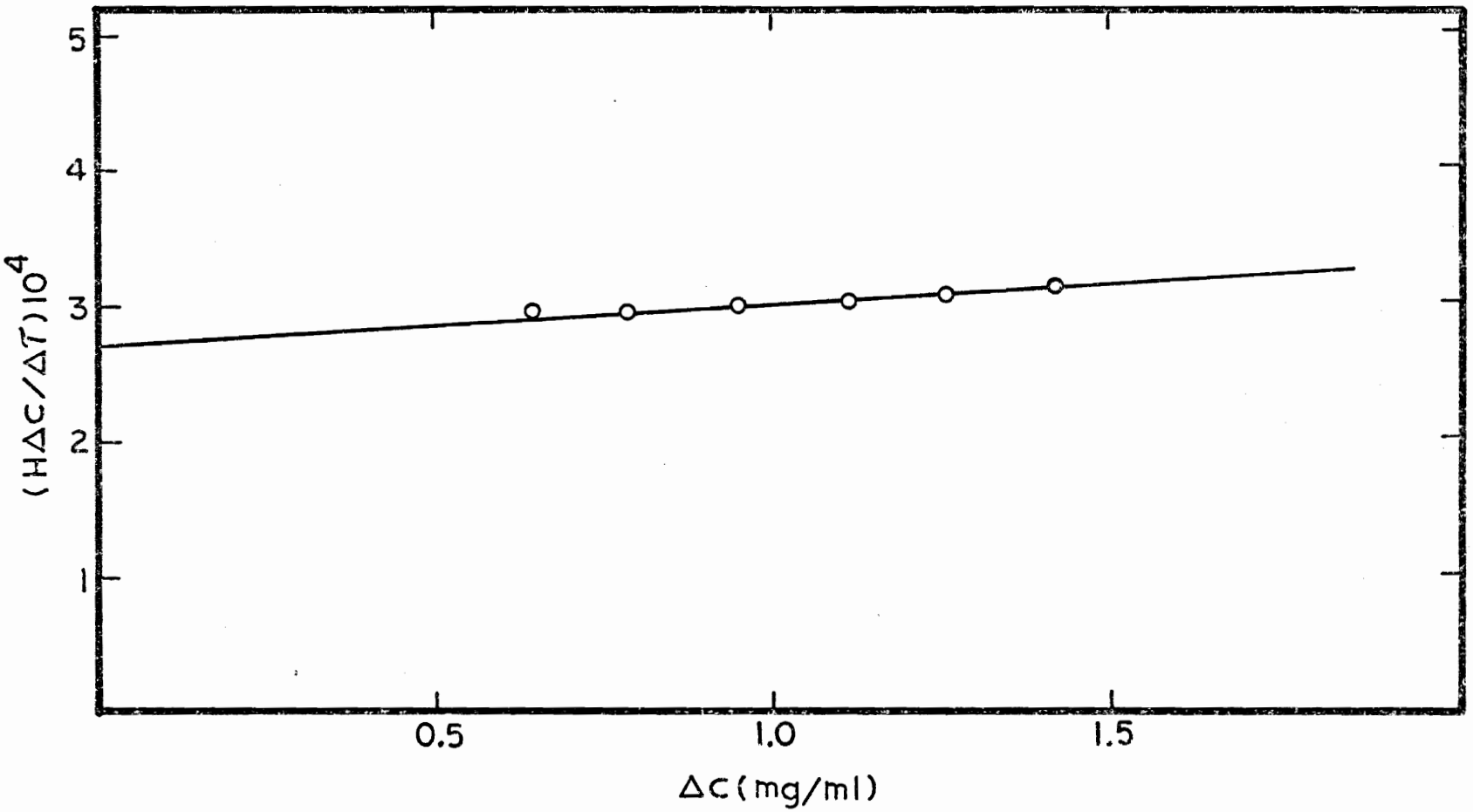

Plot of $H\Delta c/\Delta\tau$ vs. Δc for NaTC in 0.15M NaCl obtained from stepwise association model.

Figure 24. Plot of the Experimental Turbidity of NaTC with the Results Calculated Based on Stepwise Association Model.

found to be 3617, which corresponds to the aggregation number 6.7. From the slope of the plot, the second virial coefficient was obtained as $1.2 \times 10^{-3} \frac{\text{mol.ml}}{\text{gm}^2}$.

Based on the above analysis, a comparison between the experimental turbidity curve and the curve obtained by calculation according to Equations (18, 19, 26, 28) can be made to determine the extent of agreement between these two curves. In the calculation, the equilibrium constant was obtained by fitting the experimental curve. In contrast to the monomer-micelle equilibrium model, this value did not vary significantly with the value of c_T used in fitting.

Figure 25 shows the comparison between calculated results and the experimental curve. For the present calculation, the equilibrium constant for the formation of the high aggregates, K_β, was found to be 7×10^{12}. As can be seen from Figure 25, these two curves show excellent agreement with no systemic deviation as was observed with the monomer-micelle equilibrium model.

Based on the same procedure described above, the light scattering data obtained from sodium cholate and sodium glycocholate in 0.15M-NaCl were analyzed. In the calculations of turbidity as a function of concentration, the equilibrium constants, 5.19×10^{11}, for sodium cholate and 1.37×10^{16} for sodium glycocholate were obtained by fitting the experimental values at a c_T of 10 mg/ml.

Table 8 shows the results obtained from the above systems. As can be seen from Table 8, the size of large aggregates is not significantly changed by the conjugation of the bile salts. However, the association constants for dimerization seem to be higher for

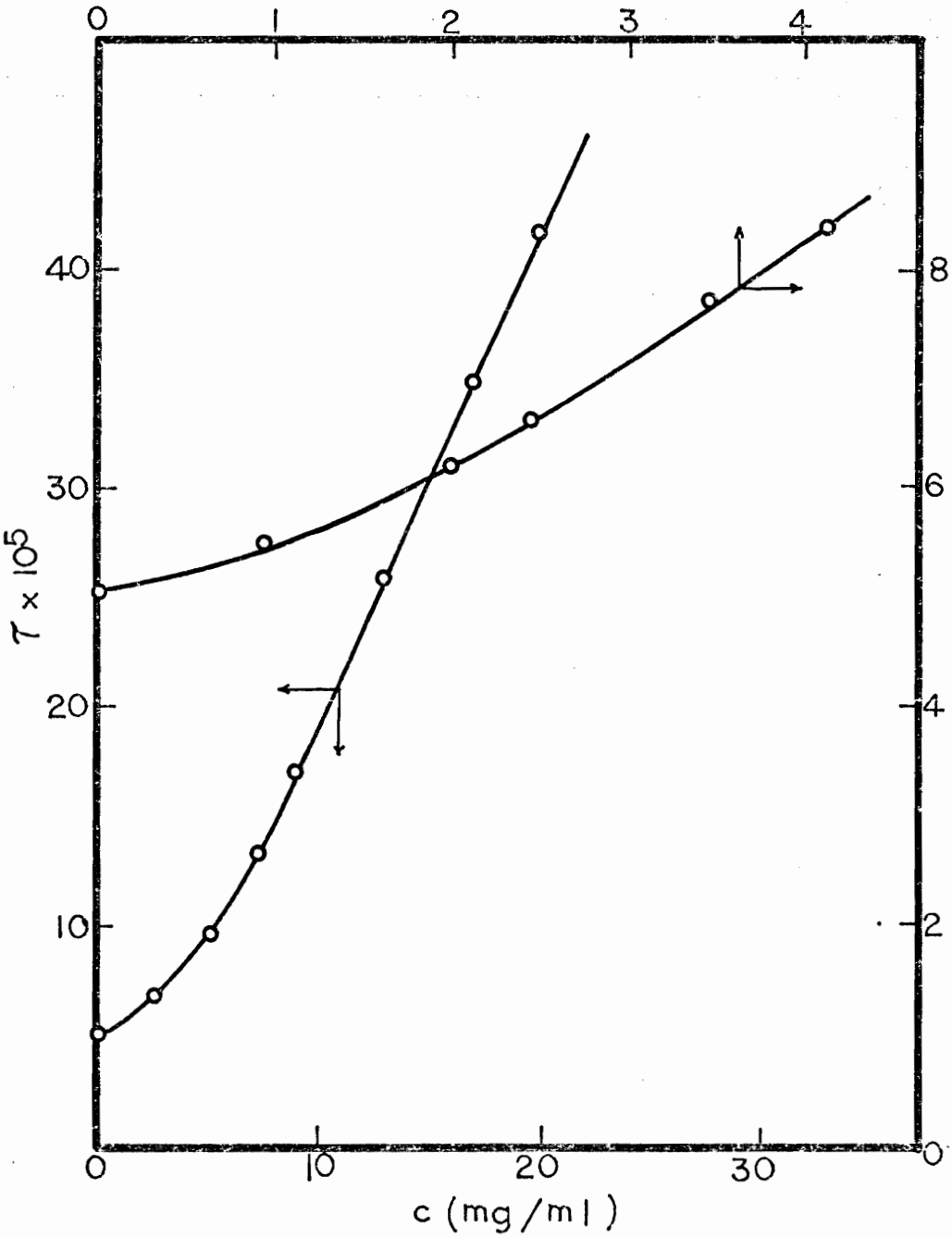

Comparison of the experimental turbidity of NaTC in 0.15M NaCl with the results calculated from stepwise association model. Solid lines are experimental values and curcles are calculated results.

Figure 25. Comparison of the Experimental Turbidity of NaTC with the Results Calculated Based on Stepwise Association Model.

Table 8. Results Obtained from Bile Salts in 0.15M NaCl Analyzed Based on Stepwise Association Model

Bile Salt in 0.15M NaCl	K_2	K_3	K_4	B	M_w^*	Agg.#
Sodium Taurocholate	35	312	0	1.18×10^{-3}	3616	6.7
Sodium Cholate	6.9	256	0	5.39×10^{-3}	3113	7.2
Sodium Glycocholate	34	200	0	2.15×10^{-3}	3490	7.2
Sodium Deoxycholate	313	871	1286	7.82×10^{-3}	6940	16.7
Sodium Taurodeoxycholate	6825	7163	2.94×10^{4}	1.23×10^{-4}	1.3×10^{4}	25.0
Sodium Glycodeoxycholate	500	778	1366	3.32×10^{-4}	8498	18.0

the conjugated bile salts. This increased dimerization of the conjugated bile salts compared with the free bile salts may be due to the reduced charge repulsive interactions between the monomers as a result of elongation of the side chain. The origin and consequences of these charge repulsions on the dimerization constant have been discussed in detail by Mukerjee and Cardinal (44). Figures 26 and 27 show the comparisons between the calculated results and the experimental values for the above systems. As can be seen from these figures, the calculated results also show excellent agreement with experimental curves throughout the concentration range studied.

The light scattering data on the dihydroxy bile salts such as sodium deoxycholate, sodium glycodeoxycholate and sodium taurodeoxycholate in 0.15M-NaCl have also been analyzed according to the method of Steiner. As can be seen from Figures 4 and 5, the turbidity of these systems increases very rapidly with concentration. Because of this, reliable values of monomer fraction x, and the molecular weight, M_w, in the low concentration range necessary for the analysis could not be obtained. Plotting of the experimental data according to the method of Steiner gives a fair amount of scatter in the points.

Therefore, it was necessary to develop a new analysis technique to obtain a consistent set of association constants. Utilizing approximate values of x and M_w, the approximate value of K_2 can be obtained from the intercept of the same type of plot as Figure 28. Using this value of K_2, the same type of plot as Figure 29 can be made. Since x and M_w are approximate values, the data in the range

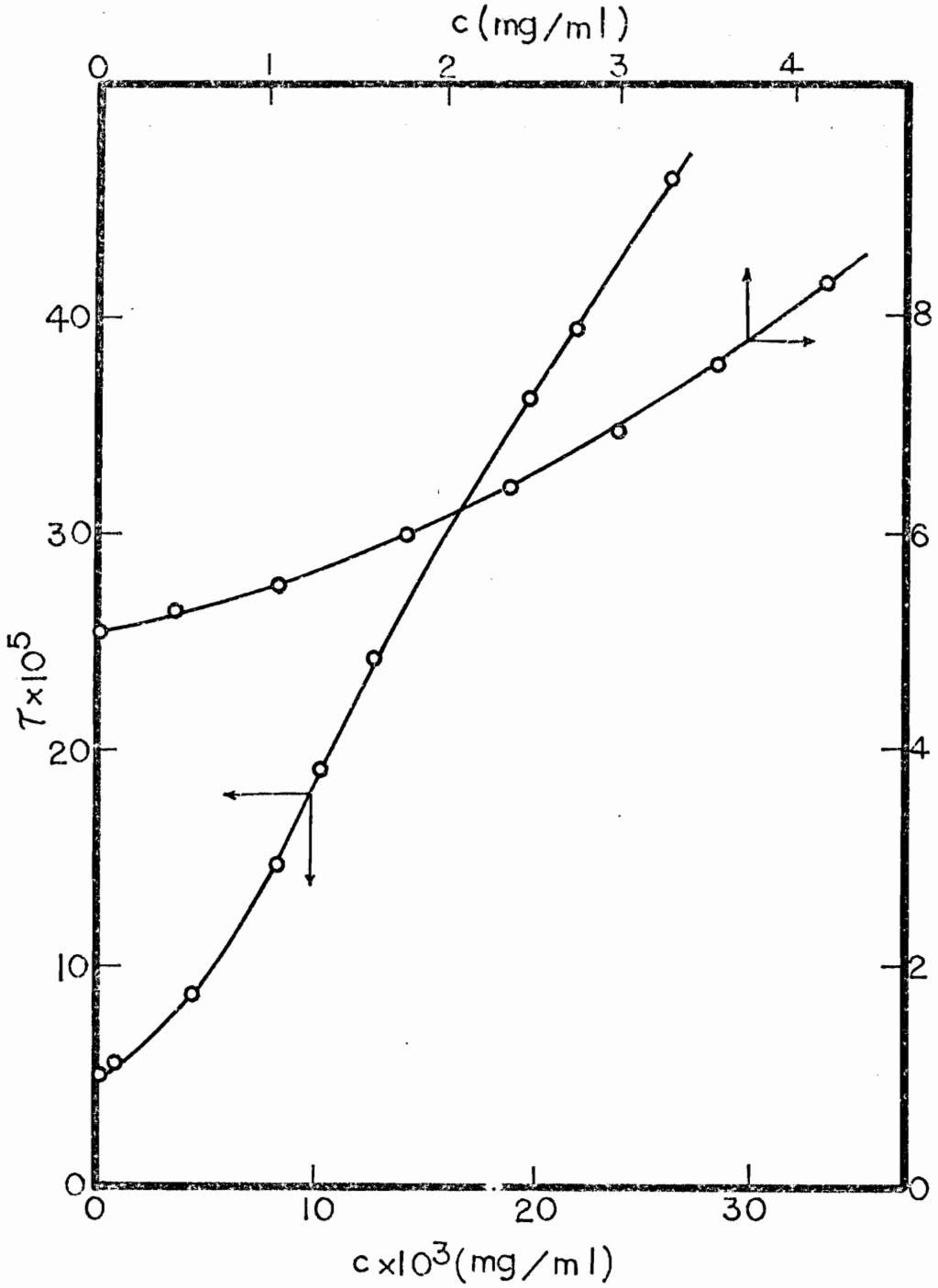

Comparison of the experimental turbidity of NaC in 0.15M NaCl with the results calculated from stepwise association model. The symbols are the same as Figure 25.

Figure 26. Comparison of the Experimental Turbidity of NaC with the Results Calculated Based on Stepwise Association Model.

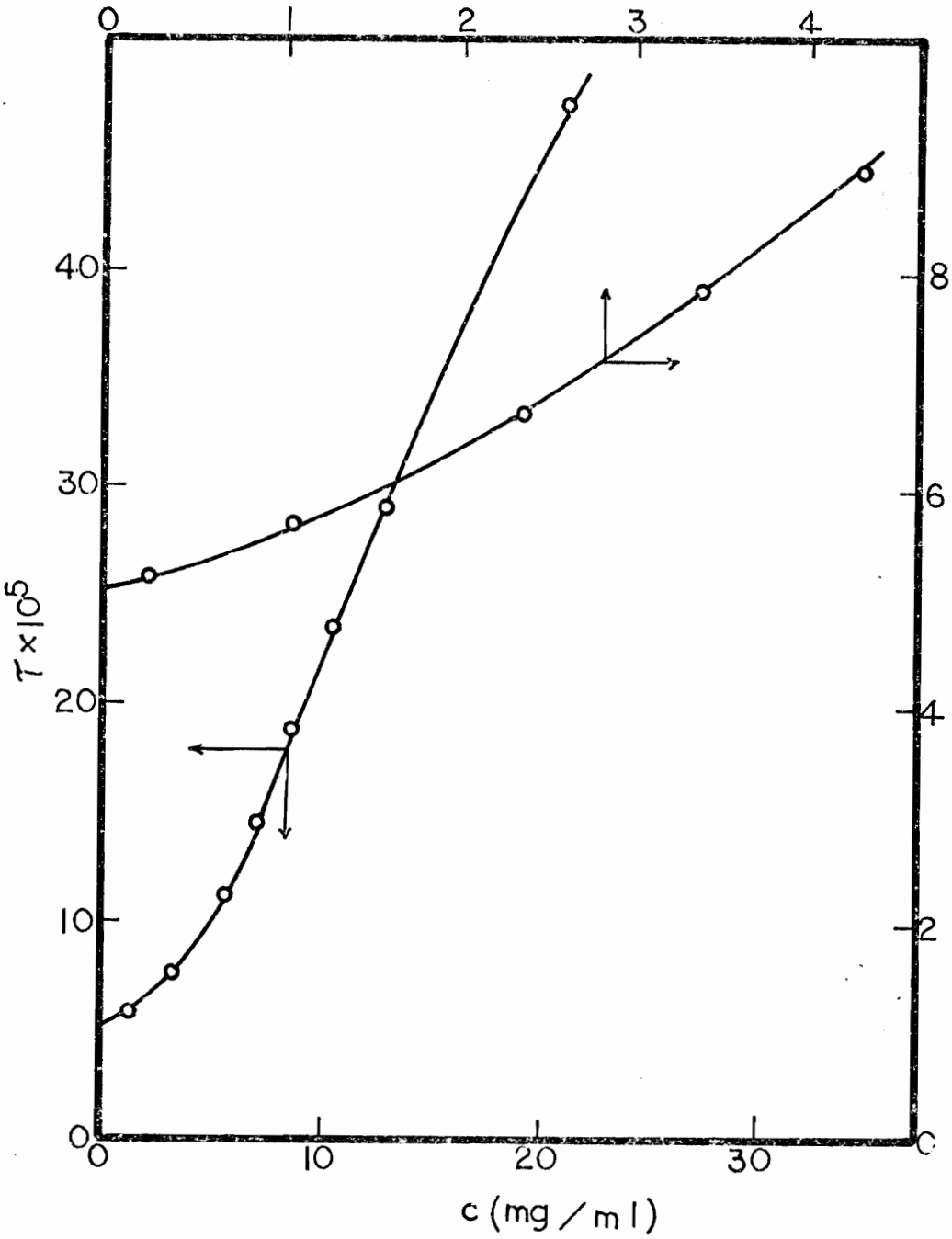

Comparison of the experimental turbidity of NaGC in 0.15M NaCl with the results calculated from stepwise association model. The symbols are the same as Figure 25.

Figure 27. Comparison of the Experimental Turbidity of NaGC with the Results Calculated Based on Stepwise Association Model.

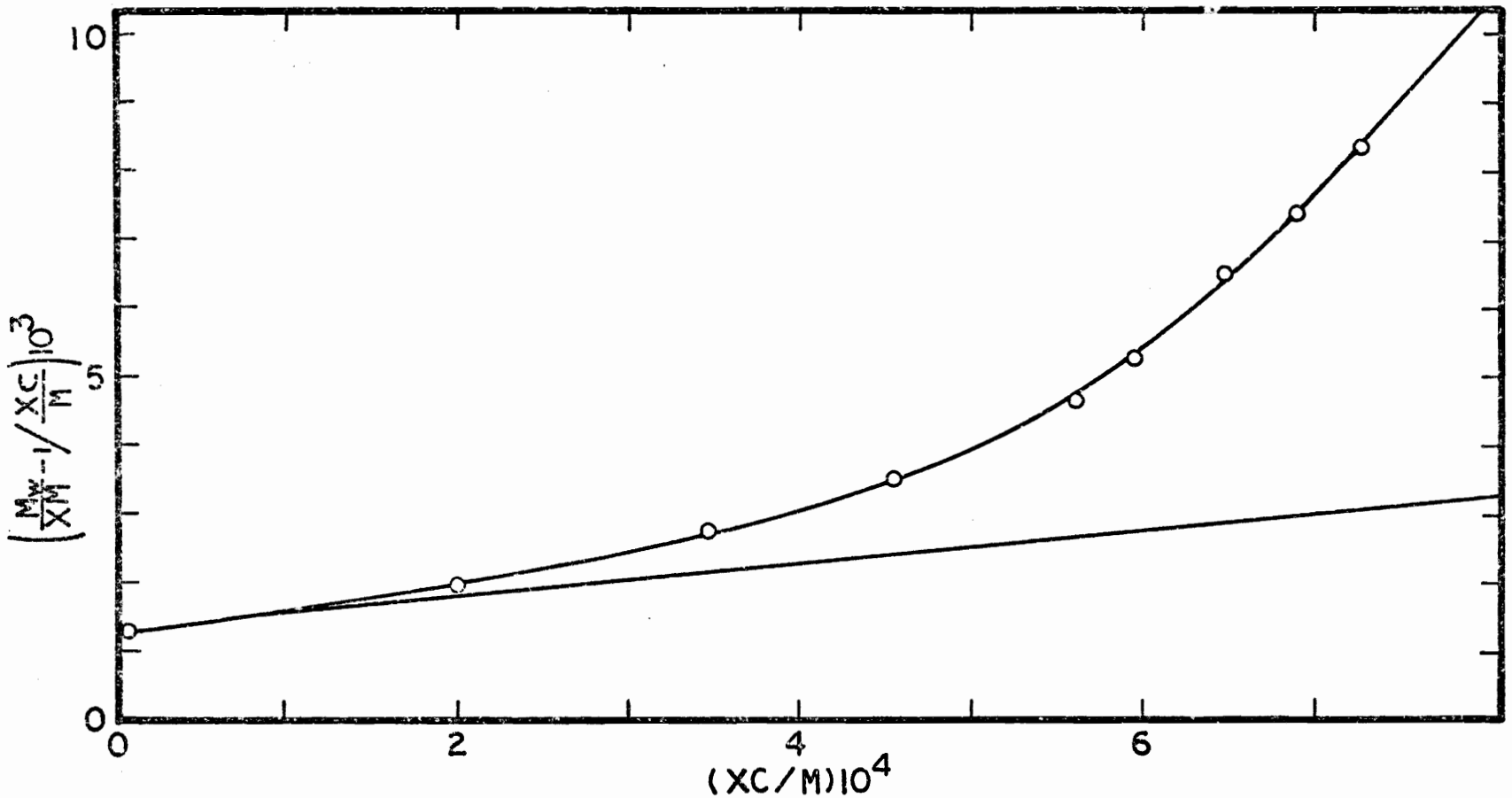

Plot of $\left[(M_w/xM)-1\right]/xc/M$ vs. xc/M for NaDC in 0.15M NaCl

Figure 28. Plot of $\left[(M_w/xM)-1\right]/xc/M$ vs. (xc/M) for NaDC.

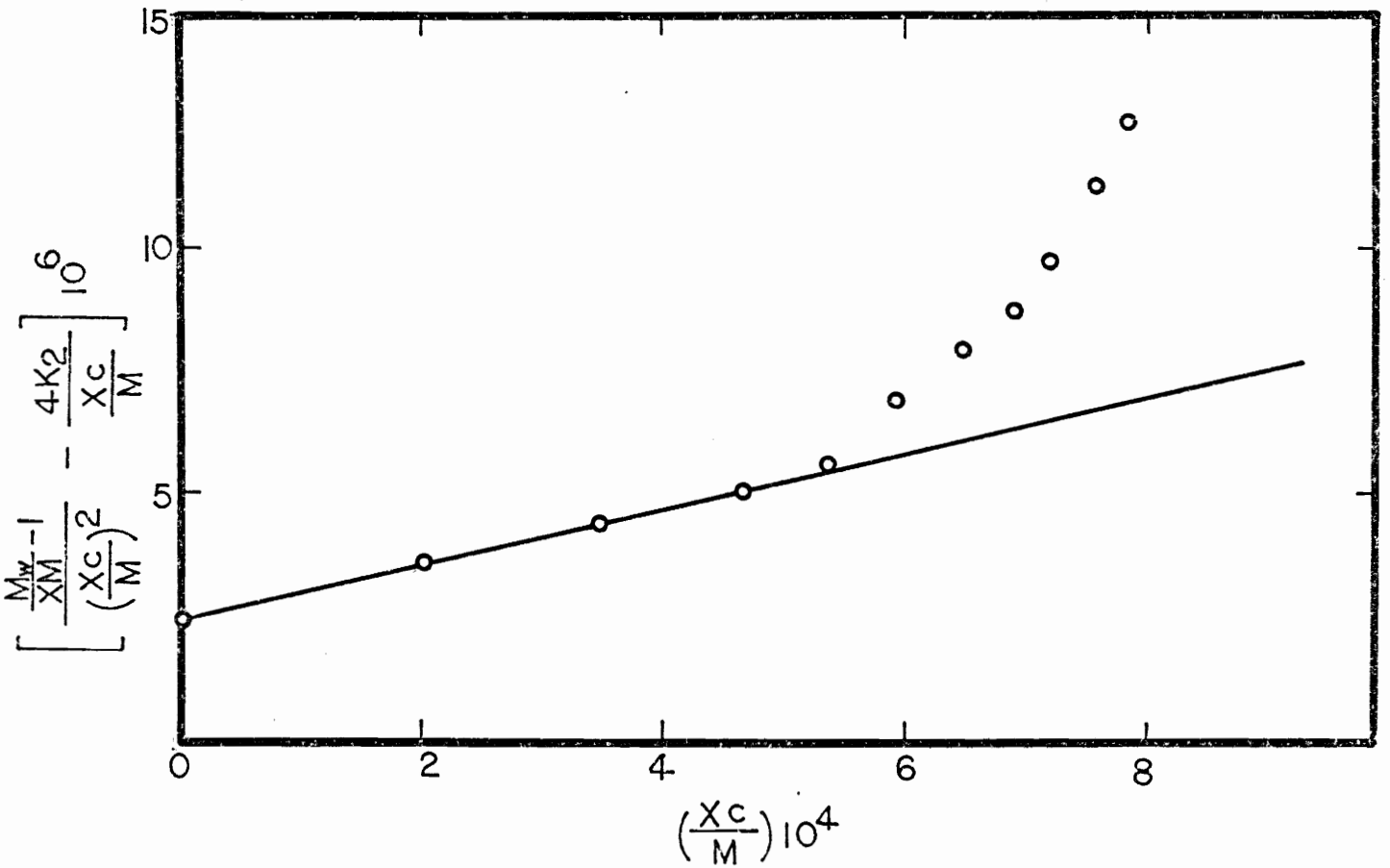

Plot of $[(M_w/xM - 1)/(xc/M)^2] - 4K_2/xc/M$ vs. xc/M for NaDC in 0.15M NaCl

Figure 29. Plot of $[(M_w/xM - 1)/(xc/M)^2] - [4K_2/(xc/M)]$ vs. (xc/M) for NaDC.

of limiting slope will be scattered on the plot. However, an estimate of the limiting slope can be drawn. Based on this line, new values of x and M_w can be found to fit the data to the limiting slope. Utilizing these new values of x and M_w, the data are reanalyzed until a consistent set of association constants is obtained.

The analysis results are shown in Table 8. As can be seen from Table 8, the nature of self association of dihydroxy bile salts is remarkably different from that of trihydroxy bile salts. First of all, dihydroxy bile salts form a tetramer as well as dimer and trimer. As an example, the plots for the values of K_2, K_3, K_4, and K_5 of sodium deoxycholate in 0.15M NaCl are shown in Figures 28-30. As can be seen from Figure 30, the limiting zero slope appeared on the plot for association constant of the pentamer. Also, the slope at higher values of $(\frac{xc}{M})$ of the plot is shown to increase abruptly as an indication of the existence of large aggregates.

At the same time, the values of K_2 and K_3 are significantly higher than those in the trihydroxy bile salts. Also the aggregation numbers of large aggregates formed by dihydroxy bile salts are substantially higher than those formed by the trihydroxy bile salts. The greater tendency toward self association of the dihydroxy bile salts compared to trihydroxy bile salts can be attributed to the greater hydrophobicity of these bile salts.

The comparisons between the calculated results and the experimental values of the above systems are shown in Figures 31-33. In the calculation, the equilibrium constants, 2×10^{47}, for sodium deoxycholate, 8×10^{52} for sodium glycodeoxycholate and 1.2×10^{95}

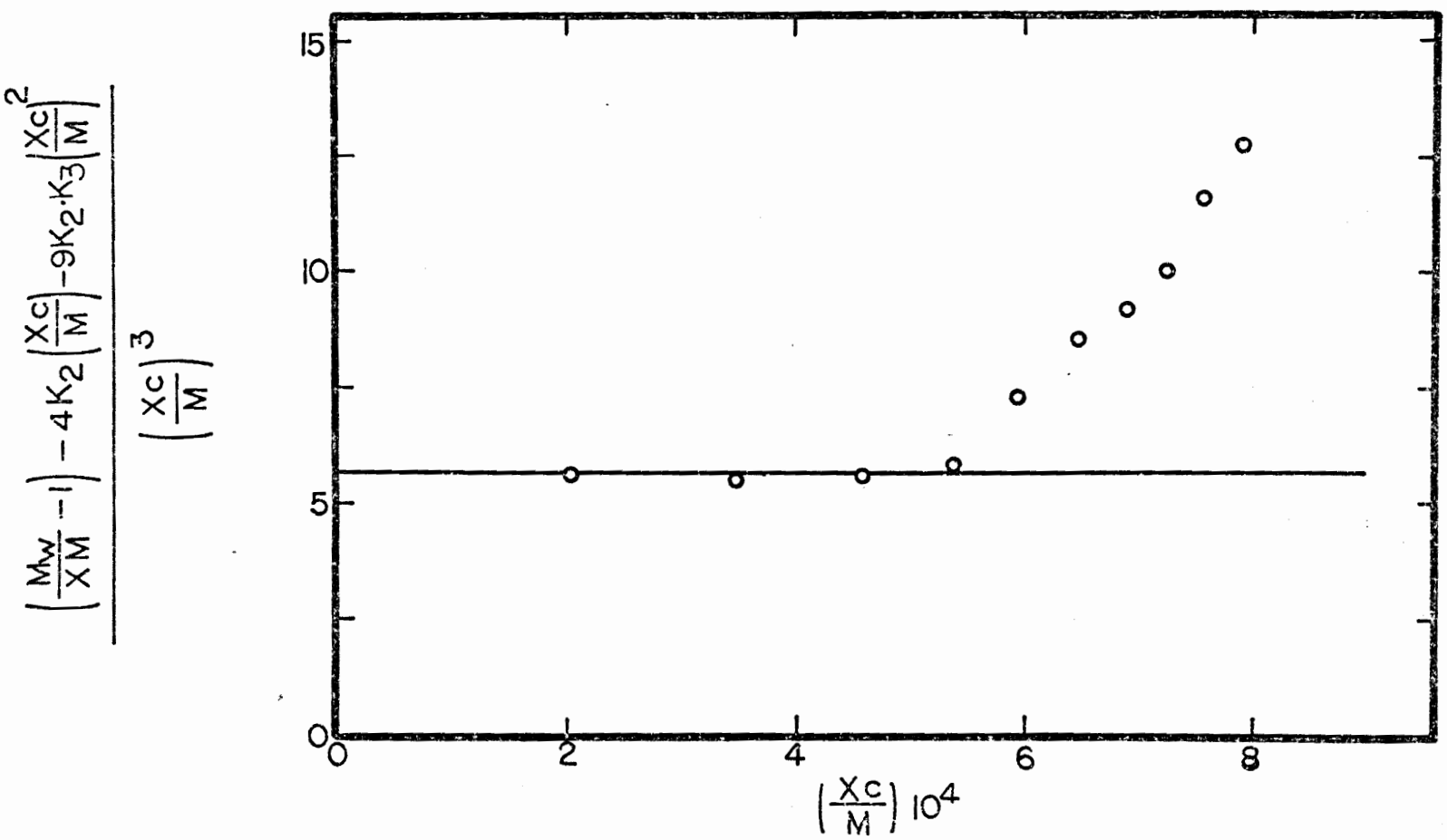

Figure 30. Plot of $[(M_w/xM - 1) - 4K_2(xc/M) - 9K_2K_3(xc/M)^2]/(xc/M)^3$ vs. xc/M for NaDC in 0.15M NaCl

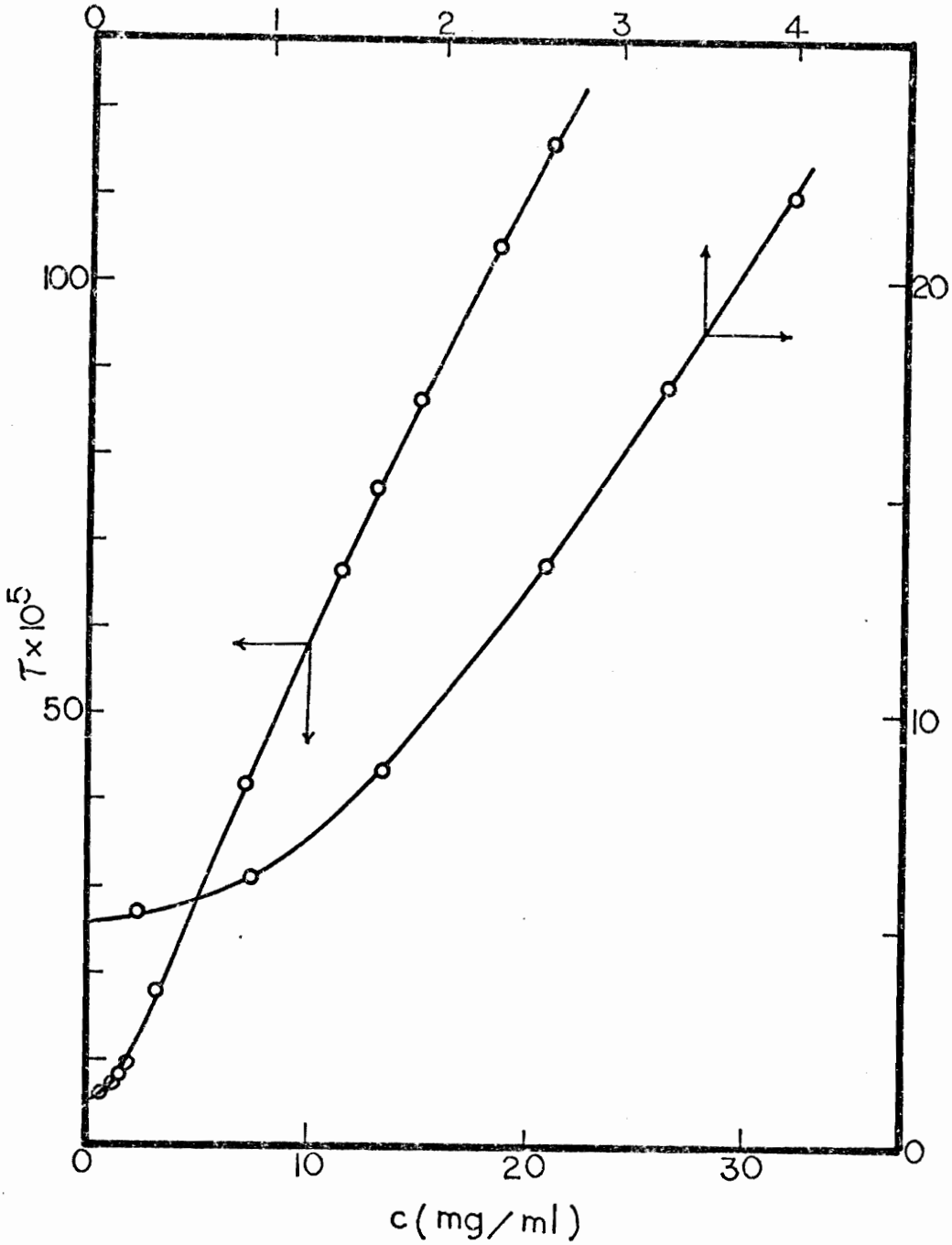

Comparison of the experimental turbidity of NaDC in 0.15M NaCl with the results calculated from stepwise association model. The symbols are the same as Figure 25.

Figure 31. Comparison of the Experimental Turbidity of NaDC with the Results Calculated Based on Stepwise Association Model.

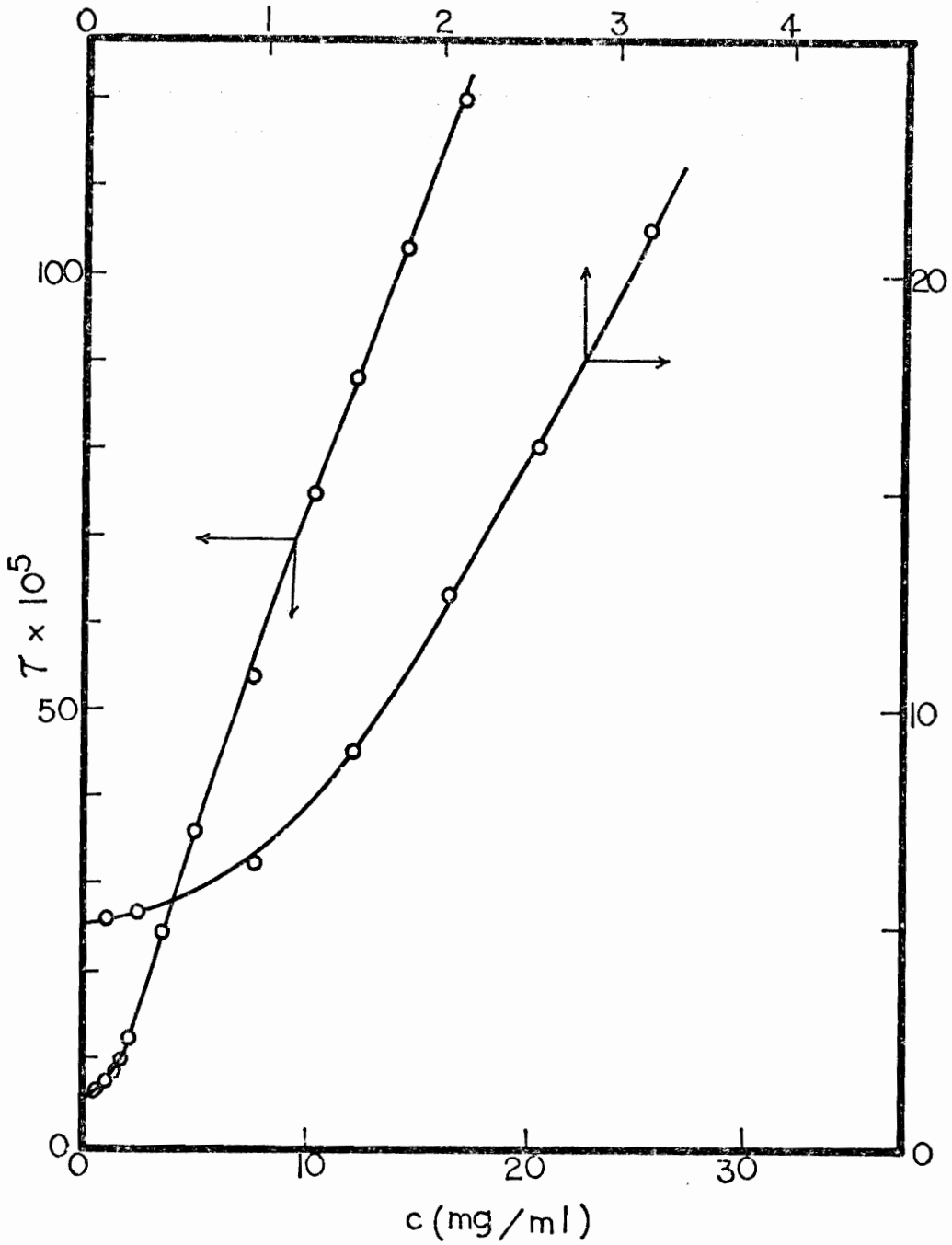

Comparison of the experimental turbidity of NaGDC in 0.15M NaCl with the results calculated from stepwise association model. The symbols are the same as Figure 25.

Figure 32. Comparison of the Experimental Turbidity of NaGDC with the Results Calculated Based on Stepwise Association Model.

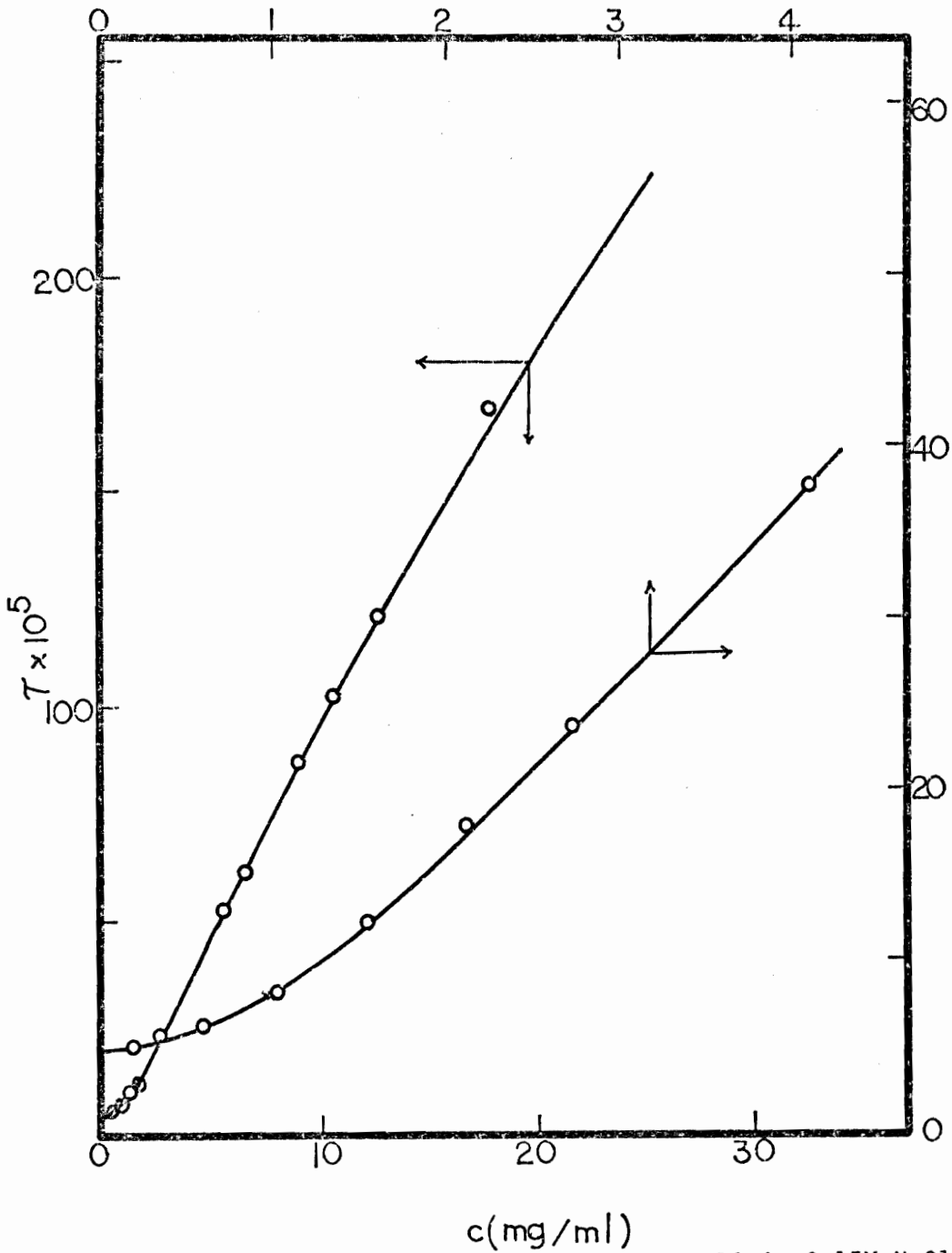

Comparison of the experimental turbidity of NaTDC in 0.15M NaCl with the results calculated from stepwise association model. The symbols are the same as Figure 25.

Figure 33. Comparison of the Experimental Turbidity of NaTDC with the Results Calculated Based on Stepwise Association Model.

for sodium taurodeoxycholate were used, which had been obtained by fitting experimental curves at 9 mg/ml. Similar correlations between experimental results and calculated values were obtained (Figures 31, 32, 33) as was observed from the trihydroxy bile salts.

To further investigate the validity of this model for the self-association of the bile salts, some of the light scattering data were analyzed by correcting for the effects of negative adsorption. Since all the results are qualitatively the same, only the analysis of sodium taurocholate in 0.15M NaX will be discussed in detail. In order to correct for the effect of negative adsorption on the large aggregates as outlined by Vrij and Overbeek (66), all low aggregates were assumed to be a part of the supporting electrolyte in the same way as the monomers are assumed to be a part of the supporting electrolyte in the treatment of the micellar model (18). This assumption seems to be reasonable since the small aggregates carry the same charge as the large aggregates and therefore, should be excluded from the electrical double layer of the large aggregates. This means that the fluctuations of the small aggregates should be independent of the large aggregates. Based on this assumption, the plot $\sqrt{M^*}$ versus $M_2(\partial n/\partial c_2)_{c_1}$ was made by the same procedure as described for the micellar model to determine the true molecular weight of large aggregates formed by sodium taurocholate. For this plot, the values of $\sqrt{M^*}$ was obtained by Equation (9). Figure 34 shows the plot. From the intercept of the plot, the true molecular

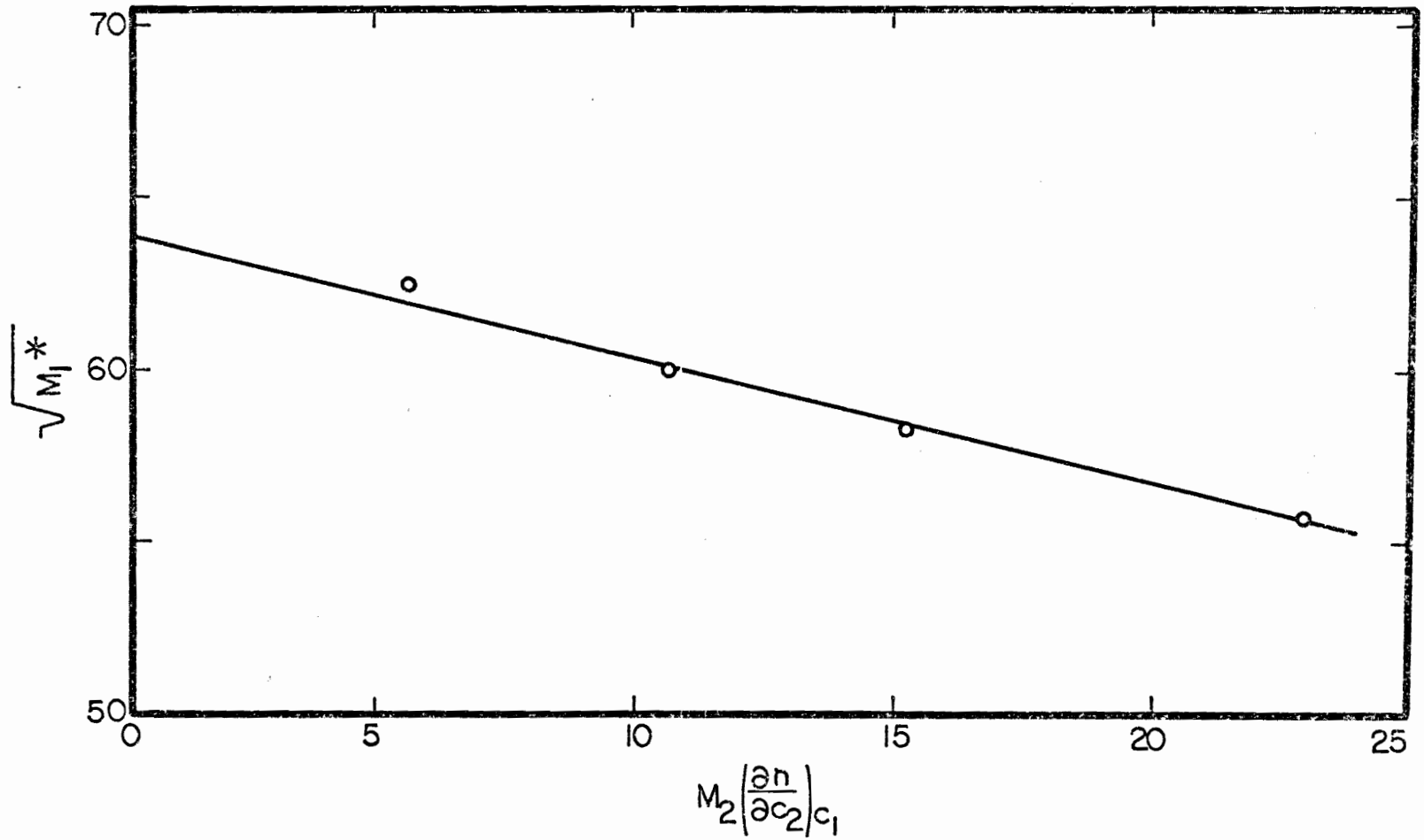

Figure 34. Plot of $\sqrt{M^*}$ vs. $M_2(\partial n/\partial c_2)_{c_1}$ for NaTC Obtained by Stepwise Association Model.

weight was found to be 4120, which corresponds to the aggregation number 7.7.

In order to see the agreement between the curves obtained by experiment and calculation, the total turbidity as a function of concentration will be calculated. In the calculation of total concentration according to Equation (28), average values of the association constants obtained from four sodium halide solutions were used. The value $q K_{\beta}$ in Equation (28) was found to be 5.5×10^{14} by fitting the experimental value of the sodium chloride system at 10 mg/ml. The turbidity due to monomer, dimer, trimer were obtained by the same procedure described above. The turbidity due to large aggregates were calculated by using different H' values obtained by Equations (10-12) as described in the monomer-micelle equilibrium model. The average second virial coefficient obtained from four sodium halide solutions was used. All the results are summarized in Table 9. Figures 35 and 36 show the comparison of the calculated values with the experimental curves. The results calculated based on only the different values of H' for four systems show the excellent correlation of this model with the experimental results.

Based on the same procedure, the light scattering data obtained from sodium cholate, sodium glycocholate and sodium deoxycholate in 0.15M NaX were analyzed. The results including the overall equilibrium constant values obtained by fitting one of the experimental curves are shown in Tables 10-12. Figures 37-42 show the comparison

between the calculated results and experimental curves. These figures show the excellent agreement between the calculated results and the experimental curves. This is further proof of the validity of the present model for the nature of self-association of bile salts.

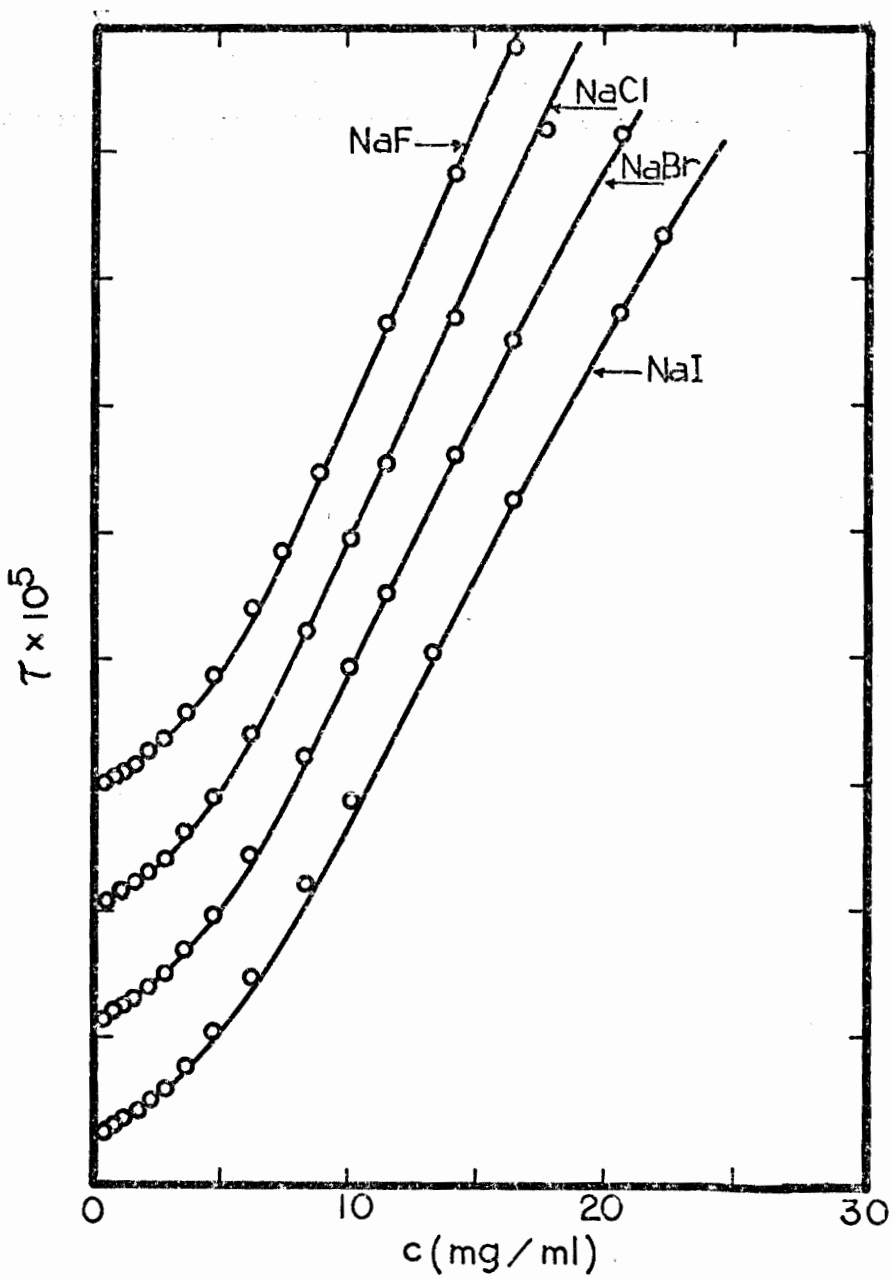

Comparison of the experimental turbidity of NaTC in 0.15M NaX with the results calculated from stepwise association model. The division and intercepts are the same as Figure 15. Solid lines represent experimental values and circles are the calculated values.

Figure 35. Comparison of the Experimental Turbidity of NaTC with the Results Calculated by Vrij-Overbeek Treatment of Stepwise Association Model.

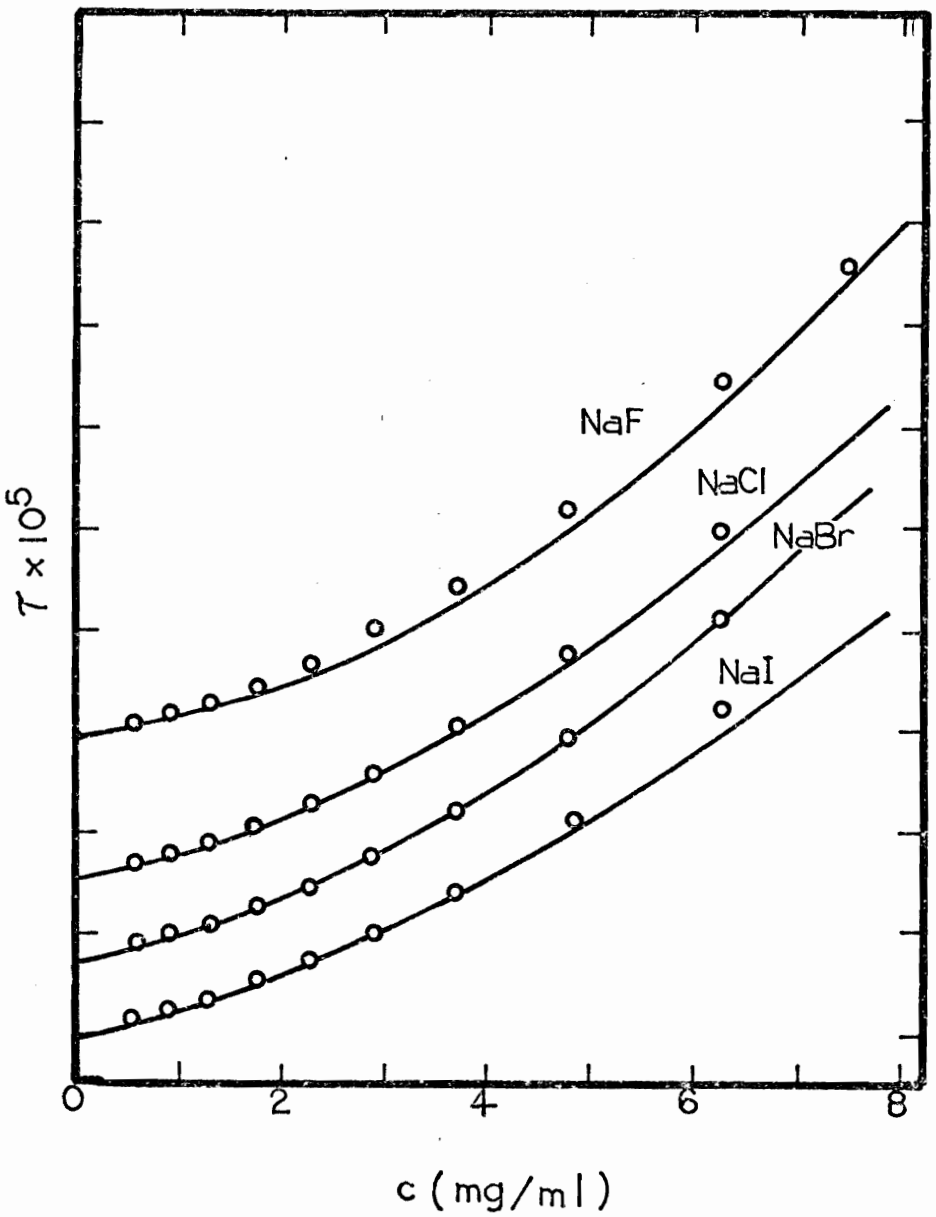

Expanded plot of Figure 35 at low concentrations. The division and intercepts are the same as Figure 16.

Figure 36. Comparison of the Experimental Turbidity in Low Concentration of NaTC with the Results Calculated by Vrij-Overbeek Treatment of Stepwise Association Model.

Table 9. Sodium Taurocholate Results from the Vrij-Overbeek-Huisman Treatment Based on Stepwise Association Model

0.15 M Salt	K_2	K_3	B	M_w^*	Agg.#	$(\partial n/\partial c_1)_\mu$	H'
NaF	20	244	1.21×10^{-3}	3946	7.4	0.162	7.24×10^{-6}
NaCl	35	312	1.18×10^{-3}	3617	6.7	0.158	6.86×10^{-6}
NaBr	33	350	1.18×10^{-3}	3370	6.3	0.154	6.48×10^{-6}
NaI	31	239	1.32×10^{-3}	3190	5.9	0.146	5.89×10^{-6}
Average or Extrapolated Values	30	286	1.22×10^{-3}	4121	7.7		

Table 10. Sodium Cholate Results from the Vrij-Overbeek-Huisman Treatment Based on Stepwise Association Model

0.15 M Salt	K_2	K_3	B	M_w^*	Agg.#	$(\partial n/\partial c_1)_\mu$	H'
NaF	8.5	294	4.00×10^{-3}	3174	7.4	0.188	9.66×10^{-6}
NaCl	6.9	256	5.39×10^{-3}	3113	7.2	0.184	9.26×10^{-6}
NaBr	7.0	302	3.53×10^{-3}	2594	6.0	0.180	8.85×10^{-6}
NoI	6.5	319	4.61×10^{-3}	2781	6.5	0.173	8.2×10^{-6}
Average or Extrapolated Values	7.2	293	4.38×10^{-3}	3286	7.6		

Table 11. Sodium Glycocholate Results from the Vrij-Overbeek-Huisman Treatment Based on Stepwise Association Model

0.15 M Salt	K_2	K_3	B	M_w^*	Agg.#	$(\partial n/\partial c_1)_\mu$	H'
NaF	34	243	2.38×10^{-3}	3896	8.0	0.184	9.26×10^{-6}
NaCl	34	201	2.15×10^{-3}	3486	7.2	0.181	8.95×10^{-6}
NaI	35	191	2.32×10^{-3}	3369	6.9	0.172	8.18×10^{-6}
Average or Extrapolated Values	34	212	2.28×10^{-3}	3925	8.1		

Table 12. Sodium Deoxycholate Results from the Vrij-Overbeek-Huisman Treatment Based on Stepwise Association Model

0.15 M Salt	K_2	K_3	K_4	B	M_w^*	Agg. #	$(\partial n/\partial c_1)_\mu$	H'
NaF	300	815	1364	1.05×10^{-3}	7351	17.7	0.187	9.64×10^{-6}
NaCl	313	871	1286	7.82×10^{-4}	6940	16.7	0.183	9.16×10^{-6}
NaBr	314	708	1125	8.41×10^{-4}	6617	16.0	0.178	8.69×10^{-6}
Average or Extrapolated Values	309	798	1258	8.91×10^{-4}	7779	18.8		

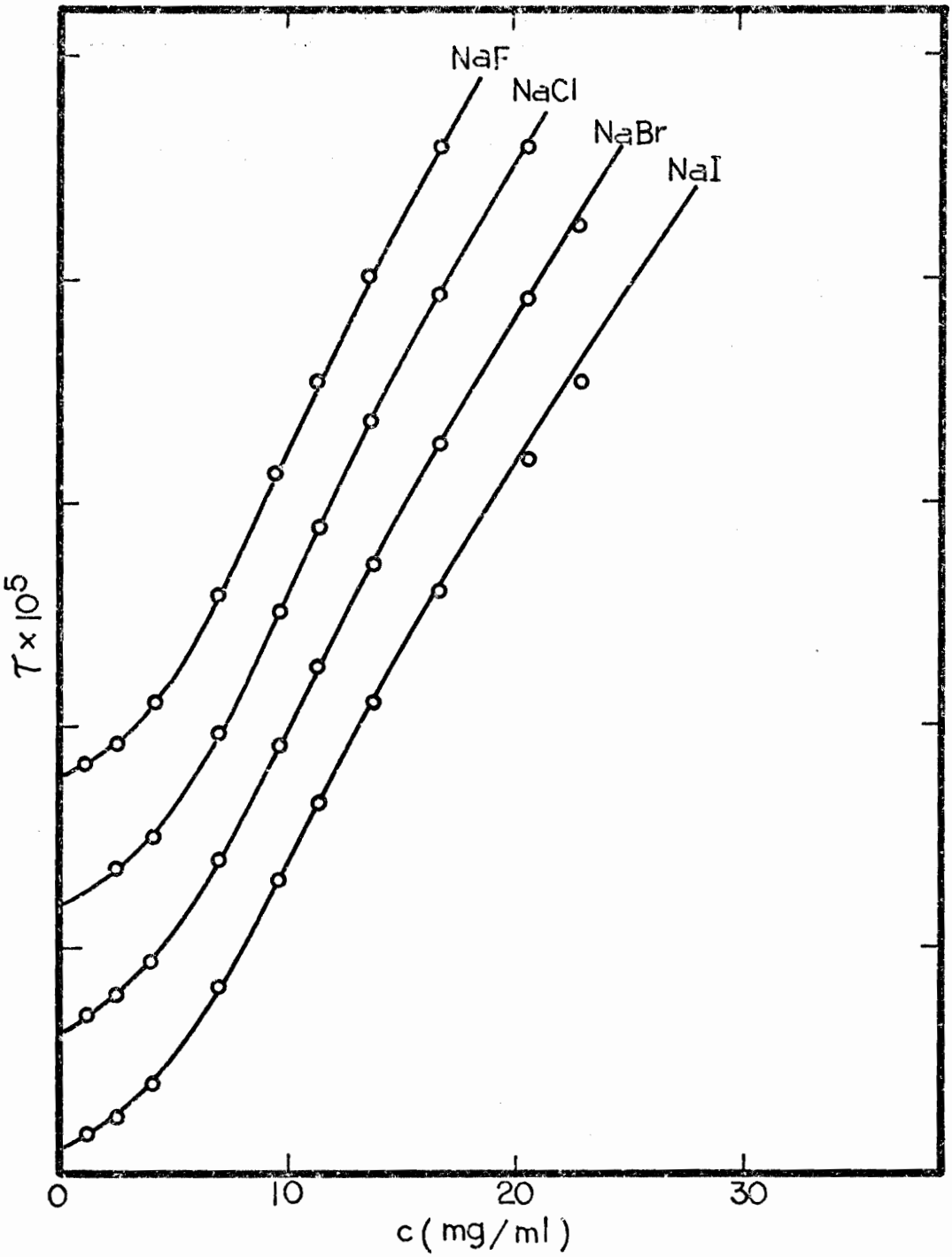

Comparison of the experimental turbidity of NC in 0.15M NaX with the results calculated from stepwise association model. The division and intercept are the same as Figure 1. The symbols are the same as Figure 25.

Figure 37. Comparison of the Experimental Turbidity of NaC with the Results Calculated by Vrij-Overbeek Treatment of Stepwise Association Model.

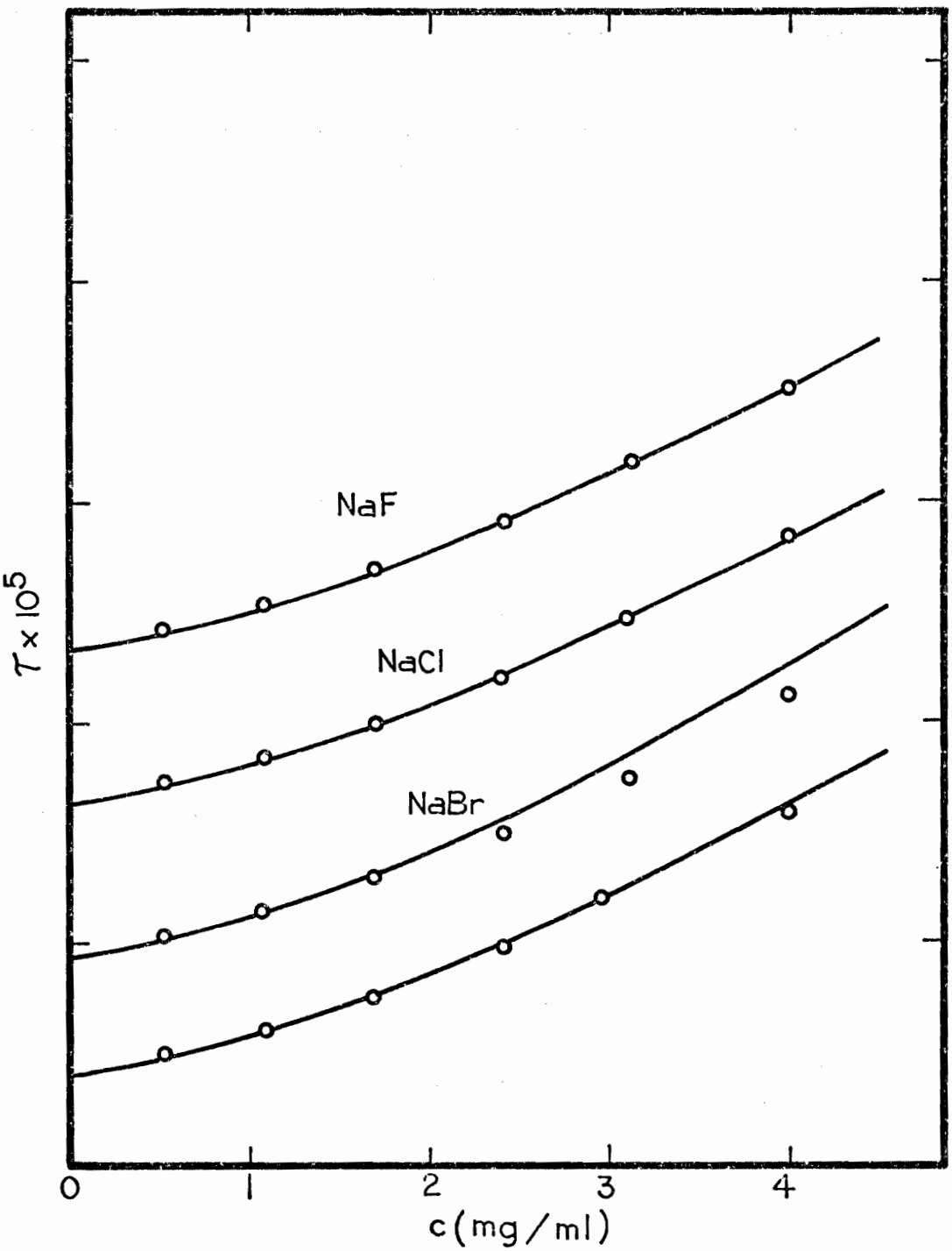

Expanded plot of Figure 37 at low concentrations. For τ, each division represents 1 x 10^{-5} cm^{-1}.

Figure 38. Comparison of the Experimental Turbidity in Low Concentration of the NaC with the Results Calculated by Vrij-Overbeek Treatment of Stepwise Association Model.

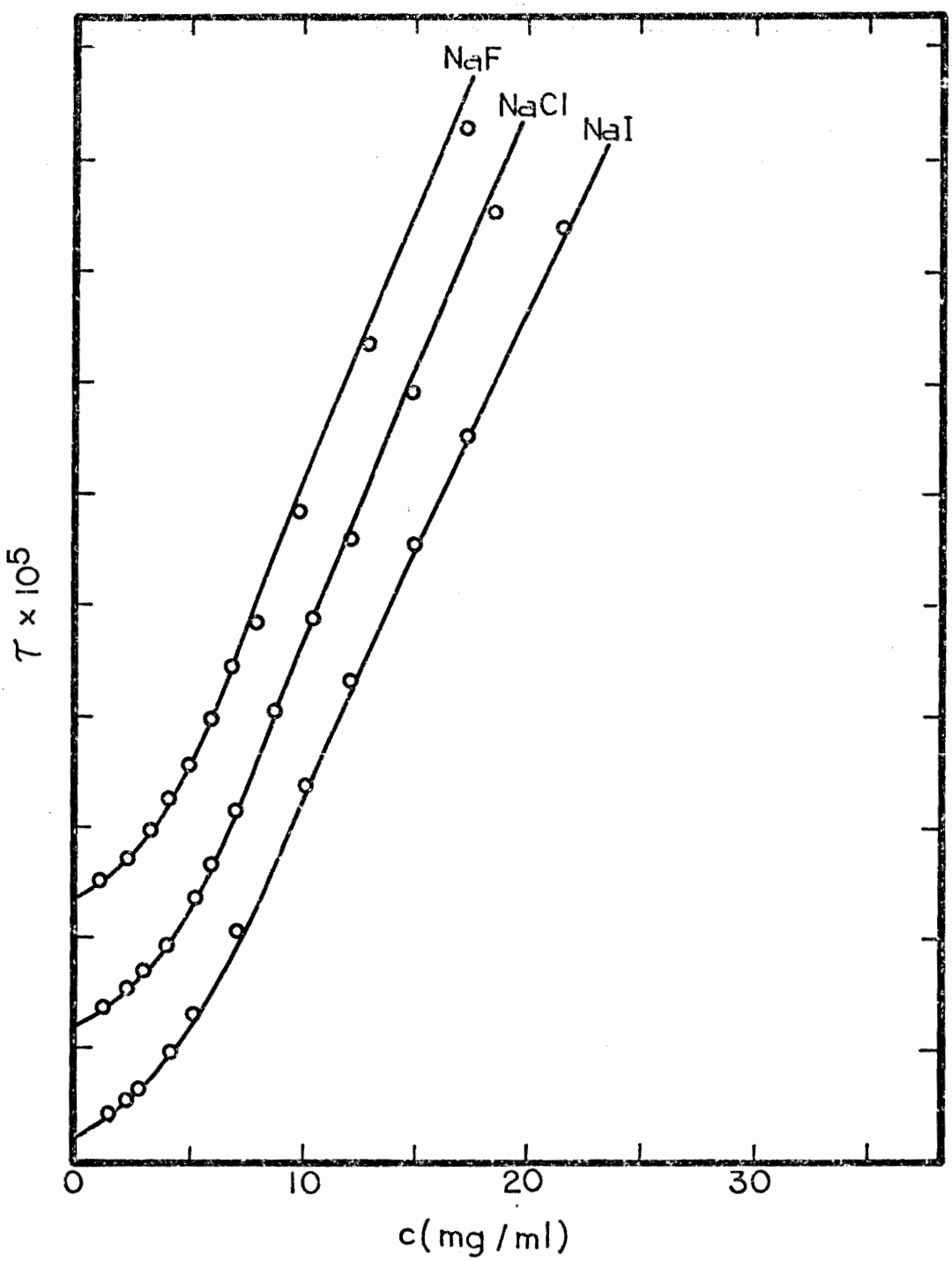

Comparison of the experimental turbidity of NaGC in 0.15M NaX with the results calculated from stepwise association model. The division and intercept are the same as Figure 15. The symbols are the same as Figure 35.

Figure 39. Comparison of the Experimental Turbidity of NaGC with the Results Calculated by Vrij-Overbeek Treatment of Stepwise Association Model.

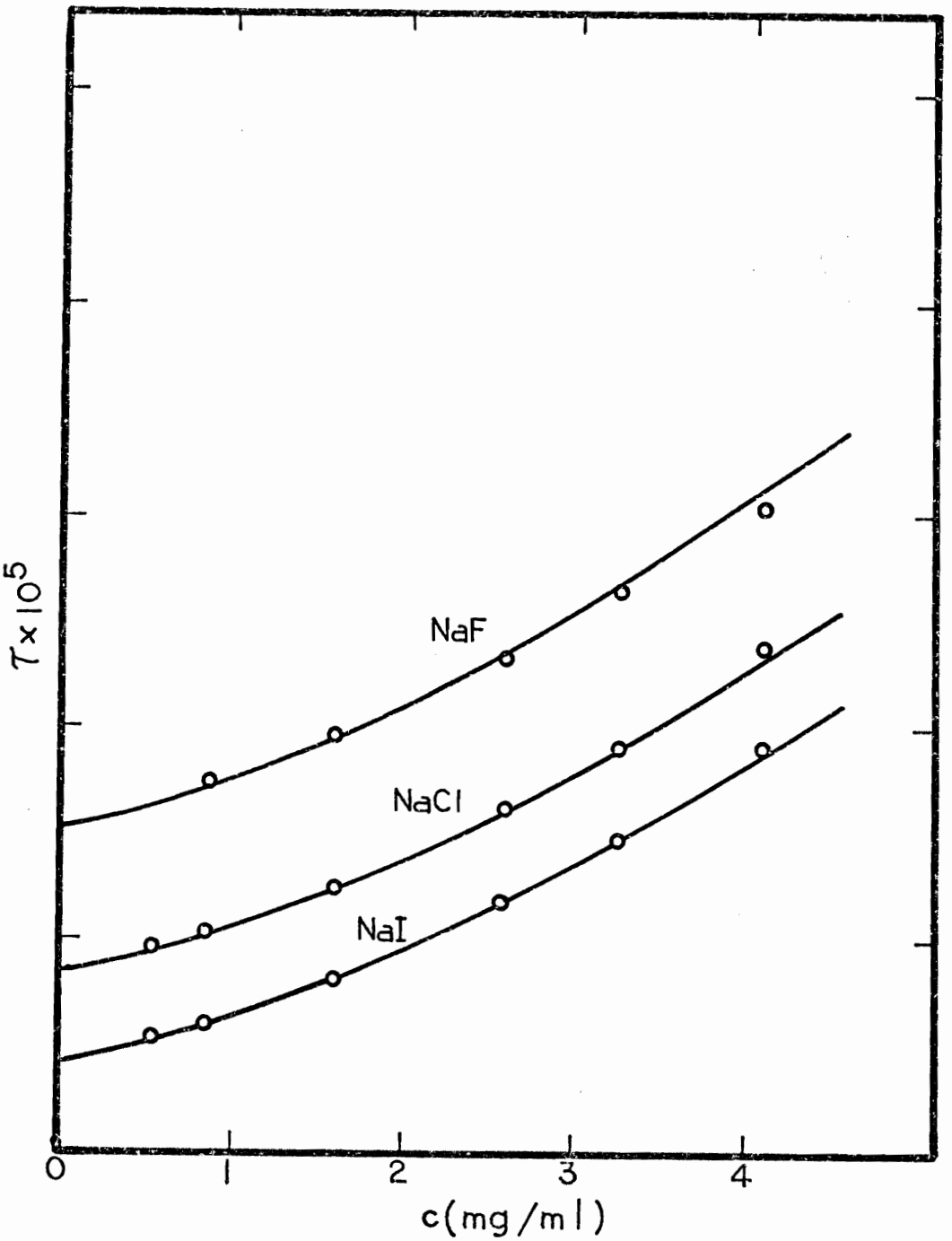

Expanded plot of Figure 39 at low concentrations. The division and intercepts are the same as Figure 38.

Figure 40. Comparison of the Experimental Turbidity in Low Concentrations of NaGC with the Results Calculated by Vrij-Overbeek Treatment of Stepwise Association Model.

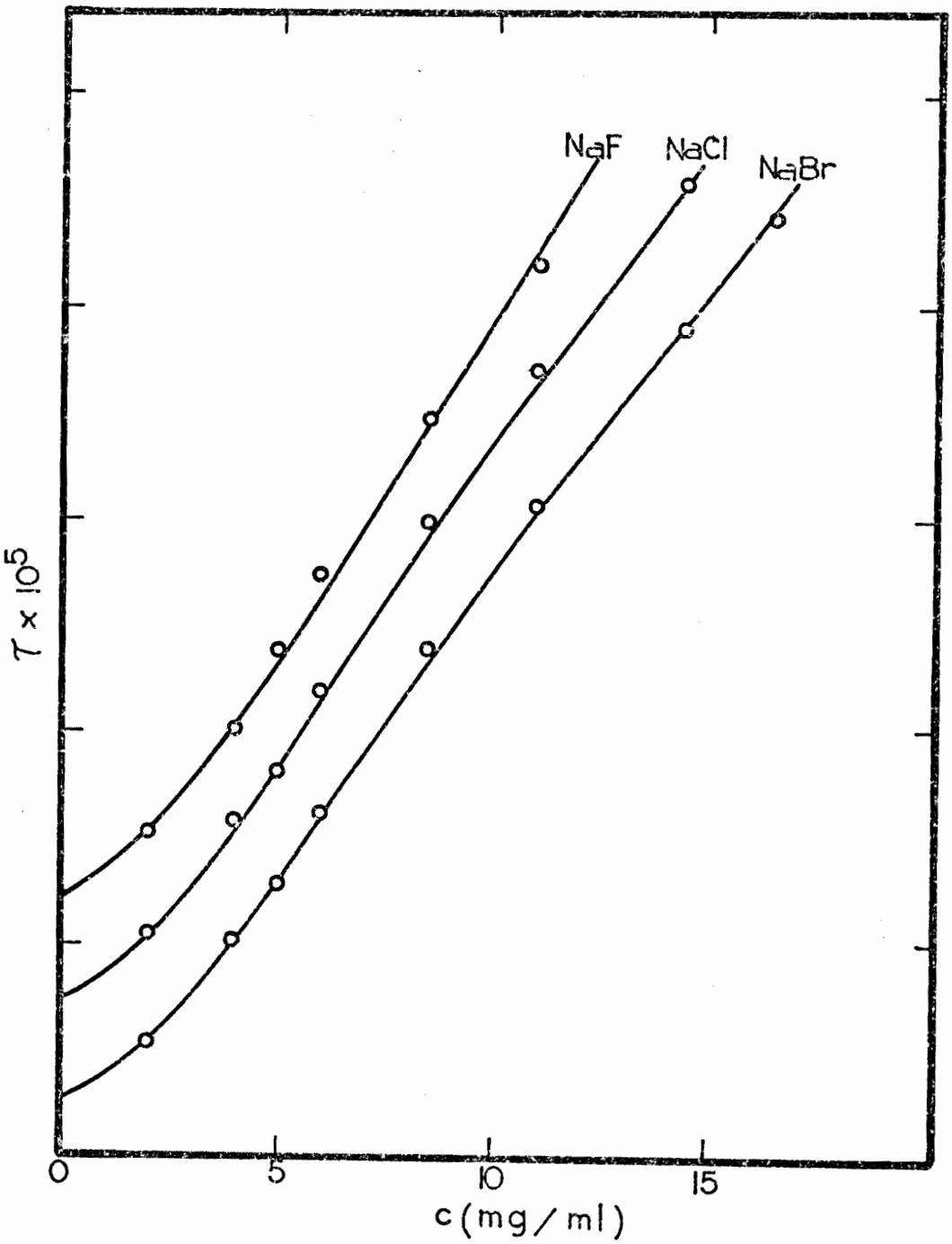

Comparison of the experimental turbidity of NaDC in 0.15M NaX with the results calculated from stepwise association model. The division and intercepts are the same as Figure 4. The symbols are the same as Figure 35.

Figure 41. Comparison of the Experimental Turbidity of NaDC with the Results Calculated by Vrij-Overbeek Treatment of Stepwise Association Model.

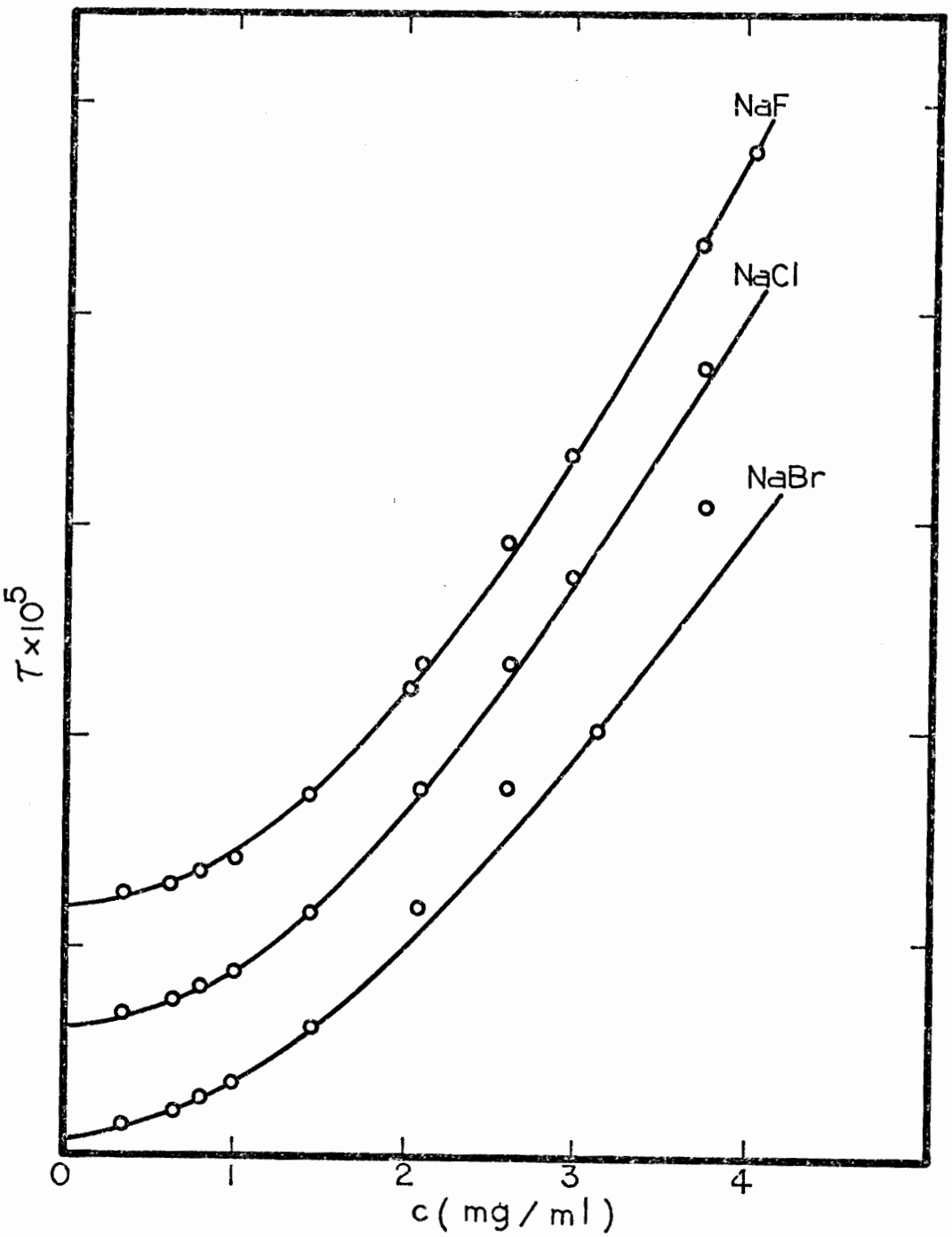

Expanded plot of Figure 41 at low concentrations. The division and intercepts are the same as Figure 20.

Figure 42. Comparison of the Experimental Turbidity at Low Concentrations of NaDC with the Results Calculated by Vrij-Overbeek Treatment of Stepwise Association Model.

C. Effects of Ionic Strength

The ionic strength effects on the nature of self-association of sodium cholate will be discussed based on the light scattering results obtained from sodium cholate in the absence of salt and in 0.15M NaCl, 0.3M NaCl and 0.5M NaCl. Figures (1, 6, 7) show the turbidity as a function of concentration of sodium cholate in the above systems. These data have been analyzed based on the stepwise association model described in the previous section. Figures (26, 43, 44, 45) show the comparison between the calculated values and the experimental curves. As can be seen from these figures, all the calculated curves show excellent agreement with the experimental values except in the absence of salt system. In the absence of salt, the calculated values show a reasonable agreement with the experimental curve at low concentration range. In the high concentration range, the calculated turbidity is much lower than the experimental values. This disagreement may be due to non-ideality effects in the system.

The non-ideality affect on the pattern of the self-association of sodium cholate have been discussed previously by Cardinal (30). For the case of dimerization, he has shown that non-ideality effects arise primarily from two sources: namely, i) the effects arising from the variations in the degree of overlap of the ionic atmospheres of the charges of the cholate dimer as the ionic strength of the medium increases, and ii) the effects arising from the variations in the degree of overlap of the ionic atmospheres of the charge

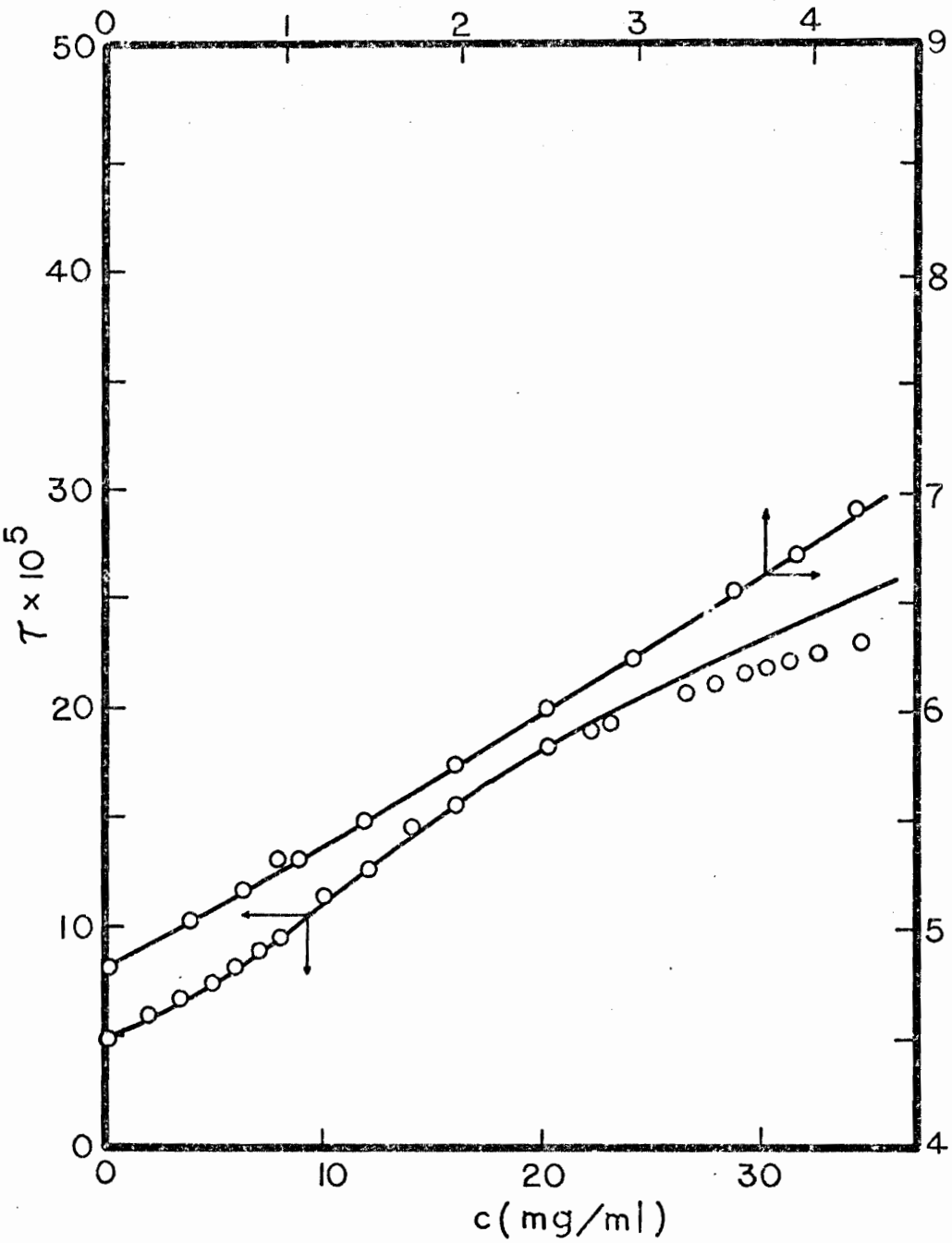

Comparison of experimental turbidity of NaC in the absence of salt with the results calculated from stepwise association model. The symbols are the same as Figure 35.

Figure 43. Comparison of the Experimental Turbidity of NaC in the Absence of Salt with the Results Obtained Based on Stepwise Association Model.

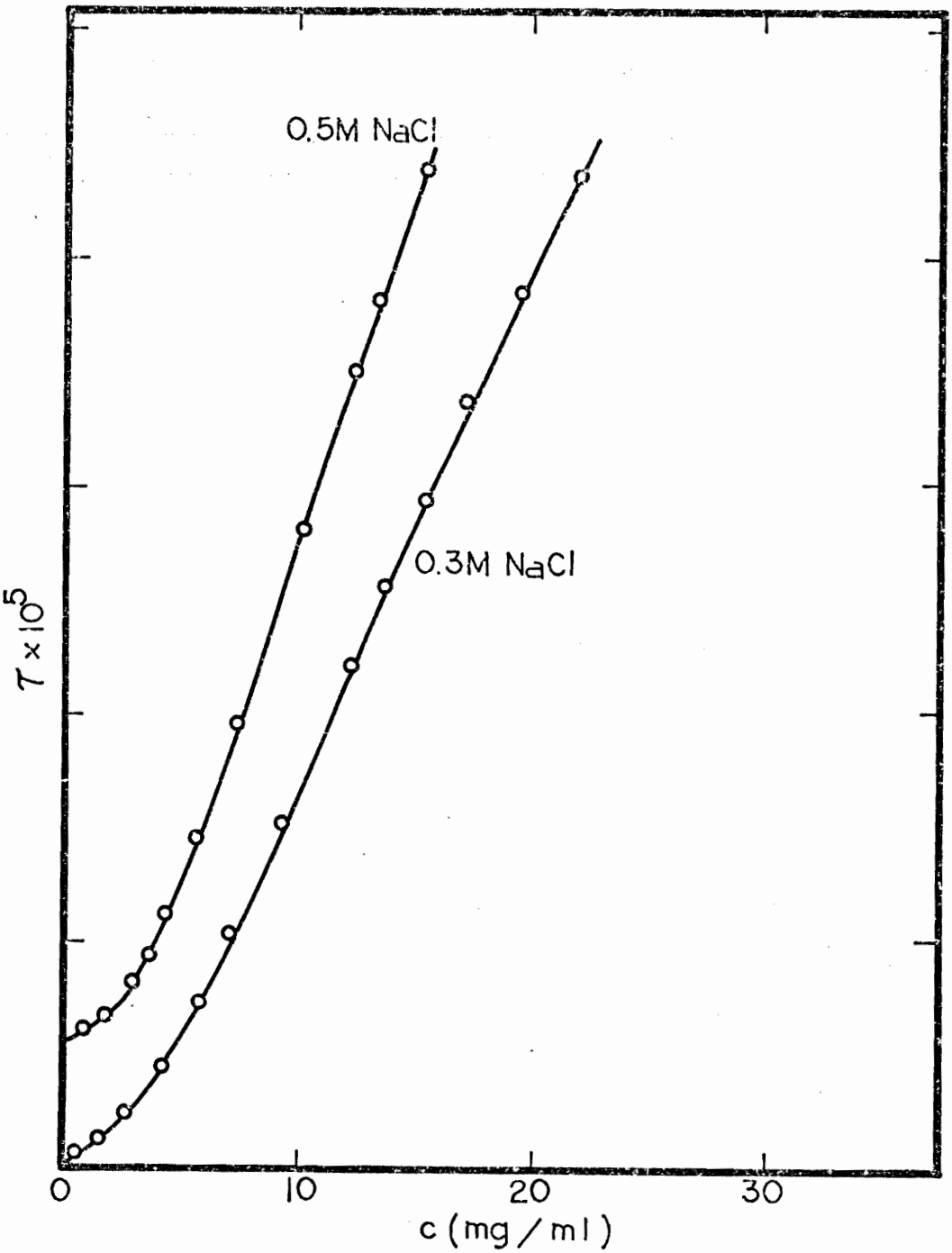

Comparison of experimental turbidity of NaC in 0.3 and 0.5 M NaCl with the results calculated from stepwise association model. The division and intercepts are the same as Figure 20. The symbols are the same as Figure 35.

Figure 44. Comparison of the Experimental Turbidity of NaC in 0.3M and 0.5M NaCl with the Results Obtained Based on Stepwise Association Model.

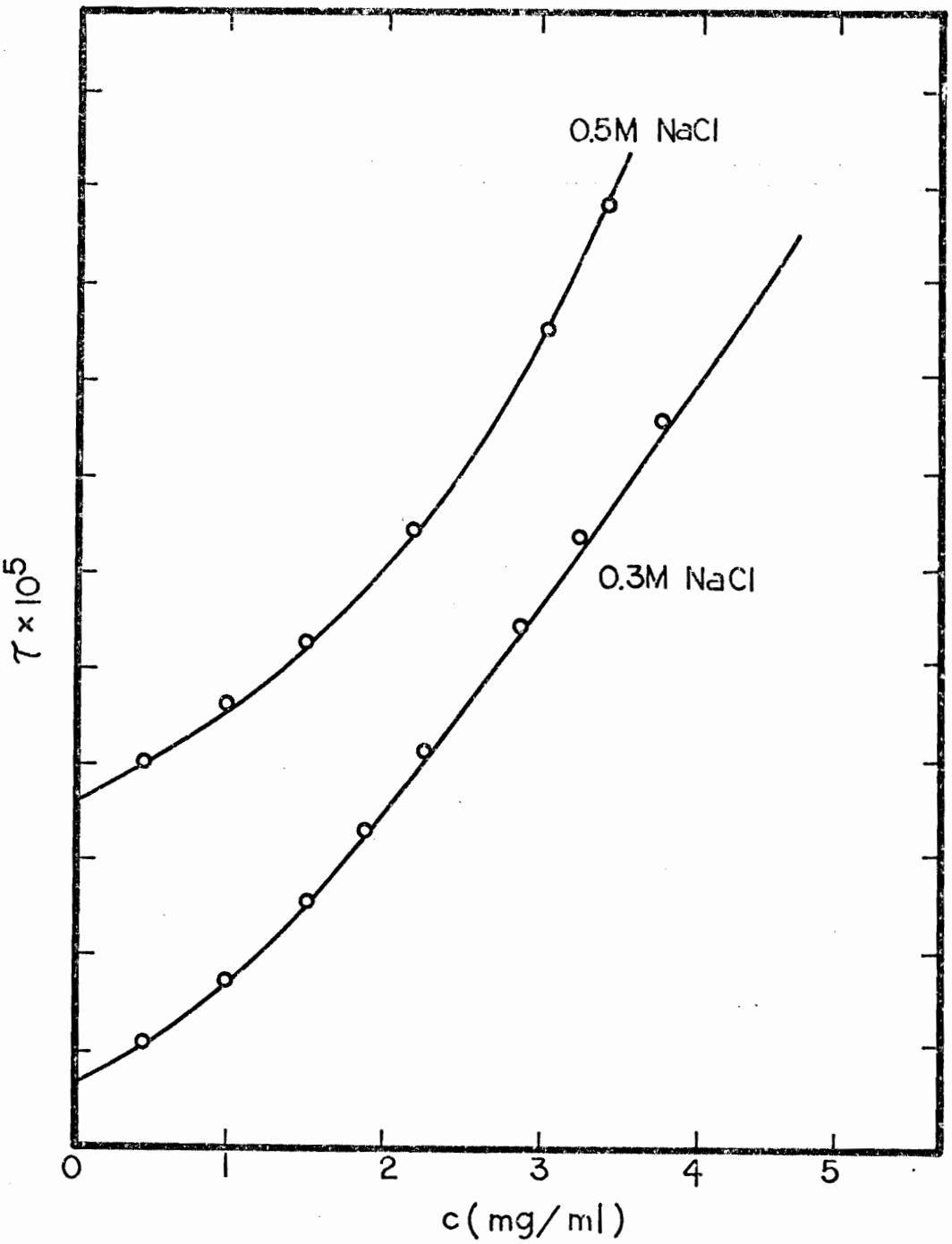

Expanded plot of Figure 44 at low concentrations. For τ, each division represents 5×10^{-6} cm^{-1}. The symbols are the same as Figure 35.

Figure 45. Comparison of the Experimental Turbidity in Low Concentrations of NaC in 0.3M and 0.5M-NaCl with the Results Obtained Based on Stepwise Association Model.

of the cholate dimer as a function of ionic strength. For this second effect he has shown that as the ionic strength decreases, the size of ionic atmosphere will increase according to the usual Debye-Hückel treatment (72). This will create an additional repulsive force to dimerization at low ionic strengths. Based on this analysis, he predicted that these two effects could lead to an increase in the dimerization constant by as much as a factor of 10 on-going from an ionic strength of about 0.01 to about 0.25. By comparison of the values given for K_2 for the absence of salt case and for a 0.15M NaCl in Table 13, it would appear that this estimate of about 10 for increase of K_2 is not unreasonable. The arguments for the variation in K_3 as a function of ionic strength would probably be similar although somewhat more difficult to quantitate because of the unknown geometry of the trimer.

For the case of the high aggregate, it is expected that two effects may be dominant. i) Based on the observed result that the aggregation number for cholate increases with ionic strength, Table 13, it might be anticipated that the average size of the high aggregate in the absence of salt would increase somewhat as the total cholate concentration increases. ii) In all of the prior calculations of K_β the somewhat idealized Equation (28) has been utilized. This equation was also utilized to calculate the values shown in Figure 43. However, for the current system it cannot be assumed that counter-ion effects on the association process are constant. If the variation in the counter-ion concentration is included in Equation (28), it would be anticipated that K_β would increase with an increase in c_T.

Table 13. Summary of Analysis Results Obtained from Sodium Cholate in Various Concentrations of Sodium Chloride Solution

Concentration of NaCl (mol/l)	K_2	K_3	K_x	B	M_w	Agg.#
0	0.8	77.8	6.0×10^{6}	8.82×10^{-2}	2460	5.7
0.15	6.9	256	5.2×10^{11}	5.40×10^{-3}	3110	7.2
0.30	15.6	405	8.3×10^{11}	1.41×10^{-3}	2760	6.4
0.50	10.3	325	7.2×10^{16}	2.0×10^{-3}	3820	8.9

As a result of all the above mentioned effects it is expected that the contributions of all higher aggregates to the total turbidity have been somewhat underestimated. Thus, for the overall calculations of turbidity as shown in Figure 43, the contribution of all aggregates including dimers, trimers, and the high aggregates have been underestimated, especially at high ionic strengths. That the calculated curve falls below the experimental curve is, therefore, an expected result. Much further work would be necessary before a complete analysis of this system could be accomplished.

Table 13 shows the results obtained for cholate at all ionic strengths studied. The molecular weight of high aggregates are the apparent values uncorrected for the effect of negative adsorption. From Table 13, it can be seen that the values of the association constants and the aggregation numbers show a tendency to increase with an increase in the ionic strength of the medium. This tendency may arise from the fact that the charge repulsive interactions between the monomeric units decrease as a result of a decrease in the charge effects with increases in the ionic strength. Similar tendencies have also been shown by Kushner (70) and Emerson and Holtzer (71) in the investigation of ionic strength effects on the micelle aggregation number of long chain hydrocarbon surfactants. For the present results, however, this effect is hard to confirm, since the aggregation number in 0.3M NaCl is lower than the value in 0.5M NaCl. On the other hand, the association constant values in 0.3M NaCl are significantly higher than the values in 0.5M NaCl. The latter results may be the reason why the aggregation number in 0.3M NaCl

is lower than the value in 0.15M NaCl. The exact reason for this is uncertain. For better understanding of the ionic strength effects on the nature of self-association of sodium cholate, further study on the other halides is necessary.

D. Solubility Studies

It has been shown previously (44) that data on the variation in the solubility of naphthalene as a function of total cholate concentration can be utilized to obtain information about the pattern of the association of cholate. In this study, the variation is the naphthalene solubility as a function of cholate concentration in 0.15M NaCl has been obtained in an effort to determine whether the results of the light scattering study can be verified by this method.

In the present study, the equilibrium solubility of naphthalene as a function of sodium cholate concentration in 0.15M NaCl was obtained and is shown in Table 3 and Figure 10. The variation of naphthalene solubility as a function of sodium cholate concentration is qualitatively the same as in the case of the absence of the salt system studied by Mukerjee and Cardinal (44). The solubility of naphthalene increases slowly at low concentrations of sodium cholate followed by rapid increases in the solubility at high concentrations of sodium cholate. It is a smooth curve with no distinct "break" as the indication of the CMC.

Based on the method described by Mukerjee and Cardinal (44), the present naphthalene solubility data were analyzed by making a plot of log ΔN versus log c. Figure 46 shows this plot. As can be seen from Figure 46, the slope at the low concentration range is about 2. This implies that the naphthalene solubility at low concentrations of sodium cholate is mainly due to the cholate dimers (44). On the other hand, the light scattering results obtained

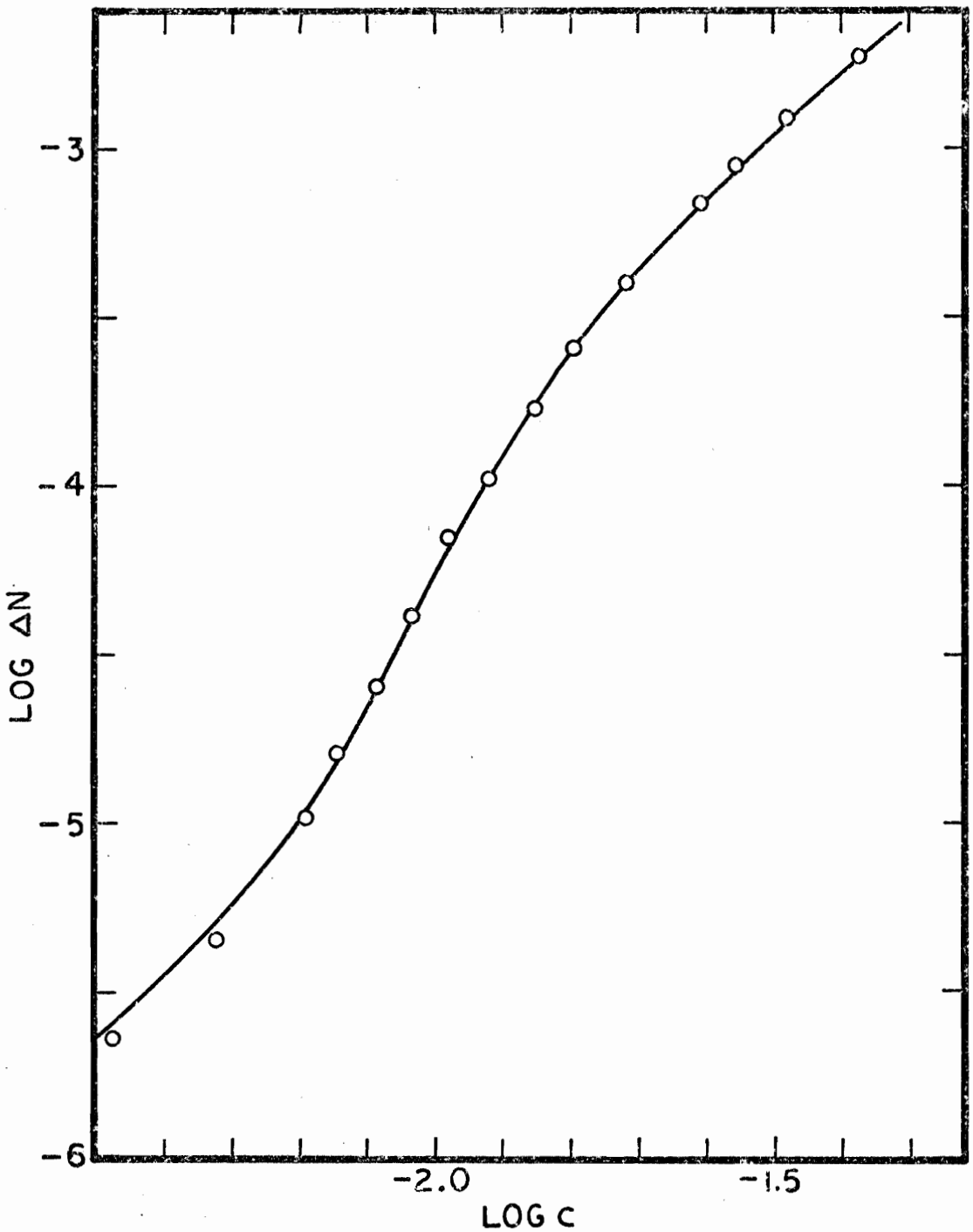

Comparison of the plots of log ΔN vs. log c. The symbols are the same as Figure 35.

Figure 46. Plot of log ΔN vs. c for naphthalene in NaC in 0.15M NaCl.

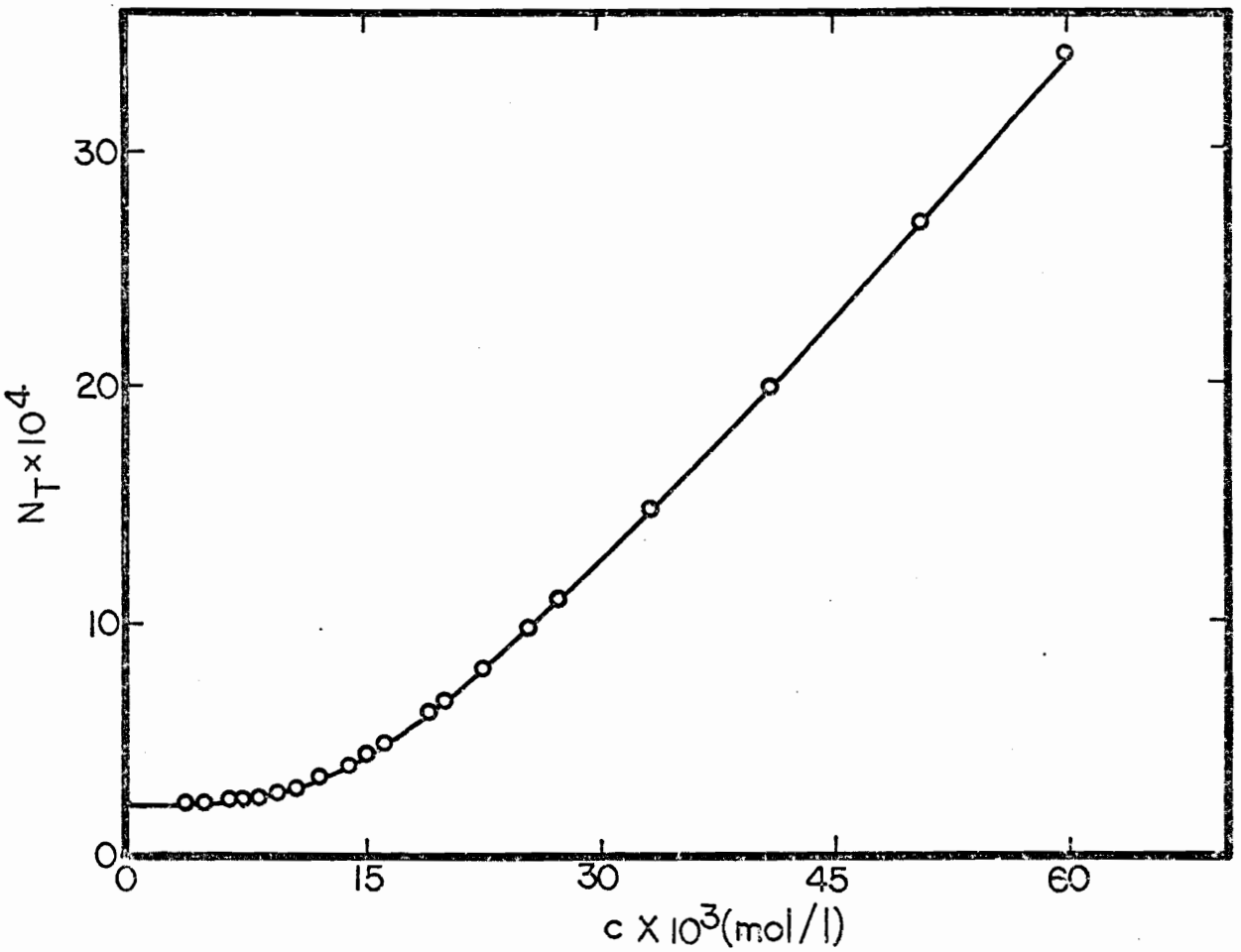

Comparison of the experimental solubility of naphthalene in NaC with the results calculated by light scattering results. The symbols are the same as Figure 35.

Figure 47. Comparison of Naphthalene Solubility in NaC with the Results Calculated Based on the Model Obtained from Light Scattering Results.

from sodium cholate in 0.15M NaCl, it was found that sodium cholate associates to form dimers, trimers and a high aggregate containing an average of 7.63 monomeric units. Based on this result, it was assumed, as an initial approximation, that the solubility of naphthalene as a function of total cholate concentration might be represented by a model such as the following.

$$N_T = N_o + A_2N + A_{7.63}N$$

$$= N_o + N_oK_2'K_2[A_1]^2 + N_oK_{7.63}' K_\beta[A_1]^{7.63} \qquad (32)$$

where $A_{7.63}N$ represents the total concentration of naphthalene solubilized by the aggregate of cholate and $K_{7.63}'$ is defined as

$$K_{7.63} = \frac{[A_{7.63}N]}{[A_{7.63}][N_o]} \qquad (33)$$

and K_β is the overall association constant for the 7.63-mer.

In order to see the degree of agreement of light scattering results with the naphthalene solubility curve, the naphthalene solubility as a function of cholate concentration will be calculated according to Equation (32). The values of K_2 and K_β were obtained from the light scattering results as shown in Table 9. The value of K_2' can be obtained by fitting the solubility data (Figure 46) in the very low concentration region. The value of $K_{7.63}'$ can then be obtained by fitting the high concentration region through Equation (32). Using this method a value of 115 was obtained for K_2',

while a value of 6.5×10^3 was obtained for $K_{7.63}$.

Figure 10 shows the comparison between the experimental curve and the calculated results. As can be seen from this figure, the calculated results show excellent agreement with the experimental curve.

For further analysis of the results, the comparison between calculated results and experimental curve was made on the plot of log ΔN versus log c. Figure 47 shows this comparison. As can be seen from Figure 47, the calculated results again show excellent agreement with experimental curve at high concentrations. In the intermediate range of log c, the calculated values are slightly higher than the experimental curve. As can be seen from Equation (32), the calculated values do not include the possible concentration of naphthalene solubilized by the trimers existing in the system. Since the calculated results are already higher than the experimental values, further calculation including the trimer contribution in the naphthalene solubility could only lead to a greater deviation in this region. At low values of log c, there is small disagreement between the curves obtained by calculations and experiments. This disagreement may arise from the experimental difficulties. Based on the above considerations, it is assumed that the naphthalene solubility in trimer is negligible. Since the calculated naphthalene solubility is in excellent agreement with the experimental curve as shown in Figures 46 and 47, these solubilization results offer further proof of the validity of the light scattering results.

VI. SUMMARY AND CONCLUSIONS

The nature of the self-association of trihydroxy and dihydroxy bile salts in aqueous electrolyte solutions has been investigated by the light scattering technique. The turbidities obtained as a function of concentration have been examined in terms of a monomer-micelle equilibrium model and a model based on a more complex pattern of the self-association by comparing the experimental curves with the calculated results. It has been shown that the values calculated based on the monomer-micelle equilibrium model are in qualitative agreement with the experimental curves. The shape of calculated curves follows the same general trend as the experimental curves in that the turbidity increases slowly at low concentrations followed by a rapid increase in turbidity in the high concentration range. However, it is impossible to find a consistent set of parameters which permit the calculation of values that fit the experimental curve quantitatively throughout the concentration range studied. These variations between calculated and experimental curves are more significant in the case of the dihydroxy bile salts than in the case of trihydroxy bile salts. Such deviations between the calculated results and experimental curves suggest that the monomer-micelle equilibrium model may not be an appropriate model for the self-association of the bile salts.

In contrast to the monomer-micelle equilibrium model, it has been shown that qualitative as well as quantitative agreement

between the experimental curves and the calculated values can be obtained based on a more complex pattern of the self-association of bile salts. This model assumes the existence of monomers, dimers, trimers and a high aggregate for trihydroxy bile salts and the above species plus a tetramer for the dihydroxy bile salts.

In the case of trihydroxy bile salts, the aggregation number of high aggregate is about 8. The size of high aggregate does not vary significantly with conjugation of the free bile salts. However, the value of the association constant for dimers was increased somewhat by conjugation.

As compared to the trihydroxy bile salts, the dihydroxy bile salts show a greater tendency toward self-association. All the values of the association constants obtained from dihydroxy bile salts are markedly higher than the values of trihydroxy bile salts. Also, the aggregation numbers of the high aggregates formed by dihydroxy bile salts are substantially higher than in the case of trihydroxy bile salts.

With an increase in the ionic strength, the values of the association constants and the size of high aggregates for sodium cholate showed an increasing tendency. However, this effect is hard to confirm from the present study.

On comparison of light scattering results obtained from sodium cholate in 0.15M NaCl with the naphthalene solubility data obtained from the same system, excellent agreement between two different systems was obtained. This agreement is a further proof of the validity of the light scattering results.

From the naphthalene solubility results, it was found that at low concentrations of sodium cholate, naphthalene is mainly solubilized by dimers while at high concentrations, both the dimer and the high aggregate are responsible for the increase in solubility of naphthalene. It appears that the naphthalene solubilization by trimers is negligible.

REFERENCES

1. Hofmann, A. F., and Small, D. M., Ann. Rev. Med., 18, 333, (1967).

2. Nair, P. P., and Kritchevsky, D., "The Bile Acids," Vol. II, Chapter

3. Mattson, F. H., and Volgenheim, R. A., J. Biol. Chem., 239, 2772, (1964).

4. Hofmann, A. F., Biochem. J., 89, 57, (1963).

5. Lutton, E. S., J. Amer. Oil Chemists' Soc., 42, 1068, (1965).

6. Borgström, B., Lundh, G., and Hofmann, A. F., Gastroenterology, 45 229, (1963)

7. Small, D. M., Gastroenterology, 52, 607, (1967).

8. Snall, D. M., Bourges, M., and Dervichian, D. G., Biochem. Biophys. Acta, 144, 189, (1967).

9. Isaksson, B., Thesis, University of Lunc I-VI (1954).

10. Maki, T., Ann. Surg., 164, 90, (1966).

11. Isselbacher, K. J., N. Engl. J. Med., 286, 40, (1972).

12. Small, D. M., "The Physical Chemistry of Cholanic Acids," Plenum Press, New York, Chapter 3, p. 249,(1971).

13. Mukerjee, P., Advan. Colloid. Interface Sci., 1, 241, (1967).

14. Williams, R. J., Phillips, J. N., and Mysels, K. J., Trans. Farsday Soc., 51, 728, (1955).

15. Mukerjee, P., Mysels, K. J., and Dulin, C. I., J. Phys. Chem., 62, 1390, (1958).

16. Goodman, D. S., J. Am. Chem. Soc., 80, 3887, (1958).

17. Hutchinson, E., Z. physik. Chem. (Frankfurt), 21, 38, (1959).

18. Huisman, H. F., Konikl. Ned. Akad. Wetenschap. Proc. Ser., B67, 367, 376, 388, 407, (1964).

19. Mysels, K. J., and Abu-Hamdiyyah, M., J. Phys. Chem., 71, 418, (1967).

20. Elworthy, P. H., and Mysels, K. J., J. Colloid. Interface Sci., 21 331, (1966).

21. Mukerjee, P., J. Pharm. Sci., 63, 972, (1974).

22. Jencks, W. P., "Catalysis in Chemistry and Ezymology," Chapter 8, McGraw-Hill Co., (1969).

23. Mukerjee, P., J. Phys. Chem., 73, 2054, (1969).

24. Mukerjee, P., and Ghosh, A. K., J. Amer. Chem. Soc., 92, 6419, (1970).

25. Mukerjee, P., and Ghosh, A. K., ibid., 92, 6408, (1970).

26. Mukerjee, P., and Ghosh, A. K., ibid., 92, 6403, (1970).

27. Mukerjee, P., and Ghosh, A. K., ibid., 92, 6408, (1970).

28. Florence, A. T., and Parfitt, R. T., J. Pharm. Pharmac., 22, 1215, (1970).

29. Florence, A. T., and Parfitt, R. T., J. Phys. Chem., 75, 3554, (1971).

30. Cardinal, J. R., "Micellar Systems in Aqueous Solutions," Ph.D. Thesis, Univ. of Wisconsin, (1973).

31. Attwood, D., and Udeala, K. D., J. Pharm. Pharmac., 26, 854, (1974).

32. Attwood, D., and Udeala, K. D., ibid., 27, 395, (1975).

33. Attwood, D., and Udeala, K. D., J. Pharm. Sci., 65, 1053, (1976).

34. Attwood, D., and Udeala, K. D., J. Phys. Chem., 79, 889, (1975).

35. Ekwall, P., Ekholm, R., and Norman, A., Acta Chem. Scan., 11, 693, (1957).

36. Ekwall, P., Ekholm, R., and Norman, A., Acta Chem. Scan., 11, 693, (1957).

37. Roepke, R. R., and Mason, H. L., J. Biol. Chem., 133, 103, (1940).

38. Small, D. M., in "Molecular Association in Biological and Related Systems," (R. F. Gould, Ed.), Advances in Chemistry Series, 84, 31, (1968).

39. DeMoerloose, P., and Ruysson, R., J. Pharm. Belg., 14, 95, (1959).

40. Kratohvil, J. P., and DelliColli, H. T., Can. J. Biochem., 46, 943, (1968).

41. Kratohvil, J. P., and DelliColli, H. T., Fed. Pro., 29, 1335, (1970).

42. Fontell, K., Kolloid - Z.Z. Polymer, 244, 253, (1971).

43. Vitello, L. B., Ph.D. Thesis, Clarkson College of Technology, Potsdam, New York, (1973).

44. Mukerjee, P., and Cardinal, J. R., J. Pharm. Sci., 65, 882, (1976).

45. McBain, J. W., Merrill, R. C., and Vinograd, J. R., J. Am. Chem. Soc., 63, 670, (1941).

46. Norman, A., Acta Chem. Scand., 14, 1295, (1960).

47. Fontell, K., Kolloid - Z.Z. Polymer, 250, 333, (1972).

48. Carey, M. C., and Small, D. M., J. Colloid. Interface Sci., 31, 382, (1969).

49. Fontell, K., Kolloid - Z.Z. Polymer, 246, 614, (1971).

50. Small, D. M., Penkett, S. A., and Chapman, D., Biochem. Biophys. Acta, 176, 178, (1969).

51. Leibfritz, D., and Roberts, J. D., J. Am. Chem. Soc., 95, 4996, (1973).

52. Fontell, K., Kolloid - Z.Z. Polymer, 246, 710, (1971).

53. Kosower, E. M., J. Am. Chem. Soc., 80, 3253, (1958).

54. Ekwall, P., Fontell, K., and Sten, A., Proc. Intern. Cong. Surface Activity, 2nd, London, 1957, p. 357, Butterworths, London, 1957.

55. Fontell, K., Kolloid - Z. Z. Polymer, 244, 246, (1971).

56. Broom, A. D., Schweizer, M. P., and Tso, P. O. P., J. Am. Chem. Soc., 89, 3612, (1967).

57. Plesiewica, E., Stepień, E., and Wiarzchowski, K. L., Studia Biophysics, Berlin, 48, 93, (1975).

58. Hofmann, A. F., Acta Chem. Scand., 17, 173, (1963).

59. Sobotka, H., and Goldberg, A., Biochem. J., 26, 555, (1932).

60. Lack, L., Singletary, G. D., Walker, T., and Dorrity, F. O., J. Lipid. Res., 14, 367, (1973).

61. Hofmann, A. F., J. Lipid Res., 3, 127, (1962).

62. Shipmann, R. H., and Farber, E., J. Polymer Sci., B1, (1963).

63. Krahtovil, J. P., Dezelic, G., Kerker, M., and Matijevic, E., J. Polymer Sci., 57, 59, (1962).

64. Utiyama, H., "Light Scattering from Polymer Solutions," Chapter 4, p. 78, Academic Press, (1972).

65. Smoluchowski, M., Von. Ann. Physik, 25, 205, (1908).

66. Vrij, A., and Overbeek, J. Th., J. Colloid. Sci., 17, 570, (1962).

67. Ooi, T., J. Polymer Sci., 28, 459, (1958).

68. Debye, P., J. Phys. and Colloid. Chem., 51, 18, (1947).

69. Steiner, R. F., Arch. Biochem. Biophys., 39, 333, (1952).

70. Kushner, L. M., Hubbard, W. D., and Parker, R. A., J. Res. Natl. Bur. Stand., 59, 113, (1957).

71. Emerson, M. F., and Holtzer, A., J. Phys. Chem., 71, 1898, (1967).

72. Robinson, R. A., and Stokes, R. H., "Electrolyte Solutions," 2nd ed., Butterworths, London, (1968).

73. Mysels, K. J., and Princen, L. H., J. Phys. Chem., 63, 1696, (1959).

VITA

Personal Data

Yunik Chang
Date of Birth: July 6, 1942
Marital Status: Married

Education

B.S. in Pharmacy, Chung-Ang University
Seoul, Korea, 1964
M.S. in Physical Pharmacy, Seoul National University
Seoul, Korea, 1966
Ph.D. in Pharmacy, The University of Utah
Salt Lake City, Utah, 1977

Work Experience

Research Assistant. June 1974. College of Pharmacy,
The University of Utah
Teaching Assistant, 1974. Student Physical Pharmacy
Laboratory, College of Pharmacy,
The University of Utah
Research Assistant, 1974 to present. College of Pharmacy,
The University of Utah